(2)

SRI International

AD-A217 768

AFOSR-TR- 90-0003

Final Report • January 1990

ELECTRONICALLY METASTABLE MOLECULES OF HIGH SYMMETRY

Hanspeter Helm

SRI Project 2915
MP 90-001

Prepared for:

The Air Force Office of Scientific Research
Building 410
Bolling Air Force Base
Washington, DC 20332-6448

Attn: Major L. Davis, Program Manager
Chemical and Atmospheric Sciences

Contract No. F49620-87-K-0002

Approved:

Donald C. Lorents, Laboratory Director
Molecular Physics Laboratory

G. R. Abrahamson
Senior Vice President
Sciences Group

[illegible] • Menlo Park, CA 94025-3493 • (415) 326-6200 • FAX (415) 326-5512 • Telex: 334486

UNCLASSIFIED
SECURITY CLASSIFICATION OF THIS PAGE

REPORT DOCUMENTATION PAGE

Form Approved OMB No. 0704-0188

1a. REPORT SECURITY CLASSIFICATION UNCLASSIFIED	1b. RESTRICTIVE MARKINGS NONE
2a. SECURITY CLASSIFICATION AUTHORITY N/A	3. DISTRIBUTION/AVAILABILITY OF REPORT UNRESTRICTED DISTRIBUTION
2b. DECLASSIFICATION/DOWNGRADING SCHEDULE N/A	
4. PERFORMING ORGANIZATION REPORT NUMBER(S) MP 90-001	5. MONITORING ORGANIZATION REPORT NUMBER(S) AFOSR-TR- 90-0003
6a. NAME OF PERFORMING ORGANIZATION SRI INTERNATIONAL 6b. OFFICE SYMBOL (If applicable)	7a. NAME OF MONITORING ORGANIZATION AIR FORCE OFFICE OF SCIENTIFIC RESEARCH
6c. ADDRESS (City, State, and ZIP Code) 333 Ravenswood Avenue Menlo Park, CA 94025	7b. ADDRESS (City, State, and ZIP Code) Building 410 Bolling AFB, Washington, DC 20332-6448
8a. NAME OF FUNDING/SPONSORING ORGANIZATION AFOSR 8b. OFFICE SYMBOL (If applicable)	9 PROCUREMENT INSTRUMENT IDENTIFICATION NUMBER F49620-87-K-0002
8c. ADDRESS (City, State, and ZIP Code) Building 410 Bolling AFB, DC 20332-6448	10. SOURCE OF FUNDING NUMBERS PROGRAM ELEMENT NO. 61102F; PROJECT NO. 2303; TASK NO. B1; WORK UNIT ACCESSION NO.

11. TITLE (Include Security Classification)
Electrically Metastable Molecules of High Symmetry

12. PERSONAL AUTHOR(S)
Hanspeter Helm

13a. TYPE OF REPORT	13b. TIME COVERED	14. DATE OF REPORT (Year, Month, Day)	15. PAGE COUNT
~~Annual Technical~~ FINAL	FROM 861101 TO 891101	900101	69

16. SUPPLEMENTARY NOTATION

17. COSATI CODES			18. SUBJECT TERMS (Continue on reverse if necessary and identify by block number)
FIELD	GROUP	SUB-GROUP	
20	8		Photoionization, Photodissociation, Lasers, H_3, HD, H_2, Metastable Molecules

19. ABSTRACT (Continue on reverse if necessary and identify by block number)

The origin of metastability in high symmetry molecules was studied by photoionization and photodissociation techniques. We have studied one- and two-photon ionization processes in the H_3 molecule and photodissociation of H_3. We have also observed photoionization of He_2, N_3, and D_3O and performed a background study of metastable HD, H_2, and He_2. A new source for formation of H_3 and H_5 has been developed.

20 DISTRIBUTION/AVAILABILITY OF ABSTRACT ☐ UNCLASSIFIED/UNLIMITED ☐ SAME AS RPT ☐ DTIC USERS	21 ABSTRACT SECURITY CLASSIFICATION UNCLASSIFIED
22a. NAME OF RESPONSIBLE INDIVIDUAL DR. L. DAVIS	22b TELEPHONE (Include Area Code) (202) 767-4963 22c OFFICE SYMBOL AFOSR/NC

DD Form 1473, JUN 86 Previous editions are obsolete.

SECURITY CLASSIFICATION OF THIS PAGE
UNCLASSIFIED

CONTENTS

INTRODUCTION AND SUMMARY

In this research, we studied of the metastable electronic states of small molecules such as H_3. Our goal was to obtain precise information on the origin of metastability in molecular systems of high symmetry and on structural, spectroscopic, and dynamic properties of such species.

The research was performed in two experimental setups, both using fast neutral molecular beams that we form by charge transfer of an electron from a suitable donor gas to a mass selected ion. In one set of experiments we illuminate the neutral species by using laser light and detect the appearance of photoions so that we can study photoionization events. In the other we photodissociate the molecule and detect the neutral photofragments by using a position- and time-sensitive detector.

This study focused on photodissociation and photoionization processes of triatomic hydrogen. A detailed account of the results obtained on triatomic hydrogen is given below. We also obtained new experimental data on the metastable species of H_2, He_2, H_3O, and D_3O.

SPECIFIC TASKS

1. High-Pressure Ion Source

A new ion source was developed for this project. The source is a hollow cathode glow discharge operating at pressures above 1 torr between a cooled cylindrical stainless steel cathode (5 cm in diameter) and a cooled cylindrical anode made of copper. At a discharge current of 5-20 mA, a bright negative glow approximately 1 cm in diameter develops along the axis of the 4-cm-long cathode. Ions are extracted from the negative glow through a 300-μm hole in a stainless steel electrode opposite the anode.

This source delivers H_3^+ beams of up to 8×10^{-7} A collimated to 1 mm diameter 80 cm from the source. With a 1-torr gas pressure and water cooling, the ratio H_3^+/H_2^+ is typically 5:1. This beam is stable over weeks, with drifts in the ion beam current being less than 10%.

An added benefit of this source is that the ions produced have low internal energy. For example, at room temperature the source can provide an intense beam of the helium molecular ion and the trialomic nitrogen ion; when cooled to the temperature of liquid nitrogen, it provides copious amounts of H_5^+. Clustering of D_3O^+ and H_3O^+ ions is also observed. In the following discussion we describe results obtained for the triatomic hydrogen molecule that we form by charge transfer of the fast H_3^+ beam in a cesium vapor cell.

2. Photodissociation of H_3

Photodissociation of metastable H_3 allows direct access into the ground repulsive state of H_3 under conditions in which all relevant quantum numbers of the system, the total energy, and the geometry of the ground state are defined within the uncertainty principle limit. The half-collision of this laser-selected transition state is mapped by measuring the translational and internal energy content of the dissociation products.

We find that minute changes in the initial starting conditions of the half-collision on the ground state surface lead to drastic variations in the fragment distribution. Some of the results obtained in this work have been published in *Physical Review Letters* (see Appendix A).

3. Proton Affinity of H_2

The photodissociation work described above provided a direct measurement of the absolute energy of the H_3 Rydberg states above the dissociation limit H(1s) + H_2(v = 0, J = 0). This energy can be combined with the previously measured ionization potential of H_3 and the well-known ionization potential of atomic hydrogen to yield, in a thermodynamic cycle, the dissociation energy of H_3^+.

This constitutes the first direct measurement of the H_3^+ bond dissociation energy. Previous experiments defined brackets for this value from relative proton affinity measurements. Our value, 4.373 + 0.021 eV, is more precise than any previous measurement and compares favorably with the best theoretical value for this quantity: $4.303 \,^{+0.059}_{-0.006}$ eV. A publication describing the thermodynamic cycle has appeared in *Chemical Physics Letters* (see Appendix B).

4. Two-photon Ionization of H_3

One-photon-resonant two-photon ionization was used to determine the vibrational energy spacings in the n=3 Rydberg states of H_3. Both the symmetrical stretch and bending mode vibrational quanta were determined. A description of this work has been published in the *Journal of Chemical Physics* (see Appendix C).

5. Depletion Spectroscopy of H_3

A novel experimental technique was used to explore the energy of the lowest Rydberg states of H_3. A tunable laser is scanned in the energy region where transitions to low-lying excited states of H_3 are expected. In the event of photoexcitation, the laser depletes the population of molecules in the metastable state. This depeletion is sensed by a second laser that is fired after the first laser. This second laser is tuned to the transition

$$H_3(2p) + h\nu \rightarrow H_3(40d) \qquad (1)$$

Because the (40d) Rydberg state can be monitored with 100% efficiency by field ionization spectroscopy, excitation step (1) permits monitoring of the metastable population. Depletion of the metastable population when the first laser photoexcites the triatomic hydrogen population can thus be monitored with very high sensitivity. These

spectra provide information about the vibrational and rotational energies of the low-lying Rydberg states of triatomic hydrogen. An account of this work has been published in *Chemical Physics Letters*.(see Appendix D).

6. Rotational Excitation of H_3

Photoexcitation of triatomic hydrogen primarily affects the unpaired Rydberg electron of the molecule. However, the interaction of the electron with the rotational motion of the core permits energy interchange between them and thus makes possible photoexcitation processes in which both the electron orbital and the core motion change.

We have studied one class of such transitions that involve excitation of core rotation concurrent with excitation of the Rydberg orbital: photoexcitation from the 2p state to the various 3d states. To prove that specific rotational core excitation can be achieved in the excitation to the 3d states, we determine the core rotation by using photoionization of the resulting 3d state. The results obtained for two selected 3d state cores are shown in Figure 1.

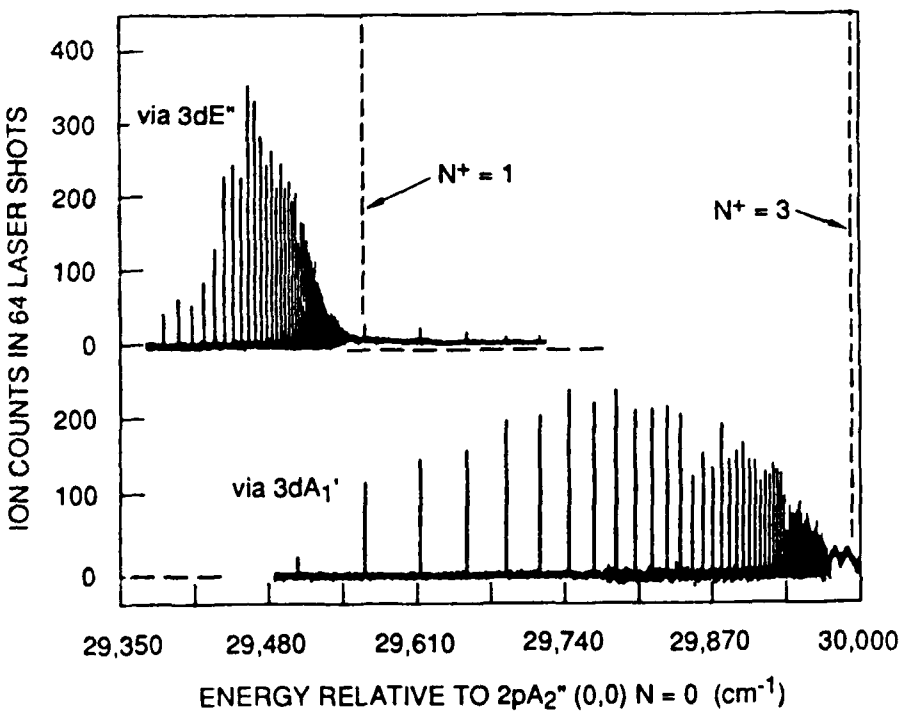

Figure 1. Photoionization spectra of laser-prepared H_3 molecules.

The top trace gives the photoionization spectrum of the 3d $A_1'(N = 1)$ state. We see that this spectrum consists of a regular Rydberg series converging to the energy limit of the $N^+ = 3$, $K^+ = 0$ core of H_3^+. The continuum portion of the ionization spectrum does not appear with any significant strength below the $N^+ = 3$ limit. This very clearly indicates that the molecule in the 3d A_1' state is well described by a 3d orbital attached to a core that tumbles with angular momentum, $N^+ = 3$. On the other hand, the photoionization spectrum of the 3dE"(N = 1) state (second trace from the top in Figure 1) shows that the continuum portion sets in just at the $N^+ = 1$ threshold, which indicates that the molecule in the 3d E" state is in fact a 3d orbital on a core rotating with the tumbling motion $N^+ = 1$, $K^+ = 0$.

These results, together with those given in Appendix C, show that we have now learned how to selectively prepare the tumbling rotational motion as well as the vibrational motion in isolated H_3 molecules. A first account of these data has been published in *Lecture Notes of Physics* (see Appendix E).

7. Doubly Excited States in H_2 and HD

As a background study to the work on H_3, we investigated the metastable H_2 employing optical-optical double-resonance studies. That is, we use one laser to mark a photoionization transition; keeping its wavelength fixed, we monitor the ion signal from this laser. Then we tune a second laser that illuminates the same molecules. Whenever the second laser excites the same molecules that the first laser photoionizes, a dip in the photoionization signal from the first laser occurs. In this fashion a correlated spectrum of transitions results, originating from the same rovibrational level of the metastable species. These double-resonance studies revealed the following novel results.

The intense transitions involved in photoionization originate in high vibrational levels of the metastable state (v = 9-12), and they terminate in Rydberg levels of similar v, which autoionize into the ionic state with v = 2 and v = 3. This ionization process accomplishes changes in nuclear configuration of up to 10 vibrational quanta. To our knowledge, such a dramatic exchange between nuclear and electronic energy has never been observed before. The origin for this exchange is attributed to the presence of the lowest doubly excited triplet state of H_2, whose effects are observed here for the first time in an experiment.

In a diabatic picture the repulsive state has the electron configuration $2p\sigma 2p\pi$, whereas the autoionizing Rydberg states have the configuration $1s\sigma nd\lambda$ ($\lambda = \sigma,\Pi,\delta$).

Excitation from the c-state, which is $1s\sigma 2p\pi$, can follow two paths that involve excitation of one of the electrons. We have either

$$1s\sigma 2p\pi + h\nu \rightarrow 1s\sigma nd\lambda \qquad (1)$$

or

$$1s\sigma 2p\pi + h\nu \rightarrow 2p\sigma 2p\pi \qquad (2)$$

In case (1), a bound Rydberg state is excited, the nuclear wavefunction being unaffected in the excitation event. The high vibrational wavefunction in the Rydberg ($v \sim 10$) has very poor overlap with the ionic state wavefunction ($v^+ = 2$), and the molecule, excited in a pure case (1) transition, is unwilling to autoionize. In the second case, a repulsive doubly excited state is accessed; that is, as a consequence of the electron rearrangement, the nuclei start to separate in space. In other words, the dilution of bonding character that was brought about by the electron excitation (2) allows Coulomb forces between the protons to become active. Then the system develops in time along the continuum wavefunction of separating atoms H + H. Configuration interaction (induced by exchange and Coulomb interaction) couples the configurations

$$2s\sigma 2p\pi \leftrightarrow 1s\sigma\varepsilon d \qquad (3)$$

where εd denotes a free electron with kinetic energy ε and orbital angular momentum $\ell = 2$. In this fashion, process (2) allows absorption of the photon and process (3) permits autoionization, the large change in internuclear distance being facilitated by the presence of the repulsive, doubly excited intermediate. Needless to say, this separation into two distinct excitation sequences, (1) and (2), is superficial; in reality the two cases are indistinguishable because the mixing (3) couples the ionization continuum, the bound Rydberg state, and the repulsive doubly excited state. As an added consequence, competition between autoionization and dissociation occurs; indeed, we discovered this competition in the double-resonance experiment.

To date we have analyzed the effects in some detail in the H_2 case and prepared two papers describing these results (see Appendices F and G). Note that this doubly excited state is in part responsible for the inverse process of dissociative recombination and that complementary configurations to this molecule should exist also in the case of H_3. All these experiments on H_2 were initially performed at SRI in collaboration with two visiting

scientists from Denmark, who received funding from NSF and a NATO travel grant. During two short visits by the Principal Investigator (funded through NSF and a NATO travel grant), some of the experiments were repeated at the University of Aarhus.

8. Review for Antimater Condensation Concept

In December 1986, H. Helm was asked by J. T. Bahns from Edwards AFRPL to present an overview of molecular hydrogen work with specific emphasis on possible applications in antimatter molecule formation concepts. This overview was presented at the CCSHCL meeting in January, and a paper was written for publication in the conference proceedings of this meeting.

CUMULATIVE LIST OF PUBLICATIONS

The following publications acknowledge AFOSR support under Contract No. F49620-87-K-0002.

1. "Autoionization of H_2 Induced by a Doubly-Excited Triplet State," N. Bjerre, S. R. Keiding, L. J. Lembo, and H. Helm, *Phys. Rev. Lett.* **60**, 2465 (1988).

2. "Double-Resonance Study of Predissociation of the $j^3\Delta_g$ State of H_2," L. J. Lembo, D. L. Huestis, N. Bjerre, S. R. Keiding, and H. Helm, *Phys. Rev.* A **38**, 3447 (1988).

3. "Photodissociation of Triatomic Hydrogen," P. C. Cosby and H. Helm, *Phys. Rev. Lett.* **61**, 298 (1988).

4. "Experimental Determination of the H_3^+ Bond Dissociation Energy," P. C. Cosby, and H. Helm, *Chem. Phys. Lett.* **152**, 71 (1988).

5. "Measurement of Vibrational Frequencies of the H_3 Molecule Using Two-Step Photoionization," L. J. Lembo, H. Helm, and D. L. Huestis, *J. Chem. Phys.* **90**, 5299 (1989).

6. "Observation of Low-Lying Rydberg States of the Triatomic Hydrogen Molecule" *Chem. Phys. Lett.* **163**, 425 (1989).

7. "Photoionization and Dissociation of the Triatomic Hydrogen Molecule," H. Helm, L. J. Lembo, P. C. Cosby, and D. L. Huestis. *Lecture Notes of Physics, Fundamentals of Laser Interactions* **339**, 264 (1989).

8. "Photon-Assisted Formation and Cooling of Molecular Hydrogen," H. Helm, *Proc. Workshop on Cooling Condensation and Storage of Hydrogen Cluster Ions.* (Ed. J. T. Bahns) **1987**, 97 (1987).

PROJECT SUMMARY

TITLE: METASTABLE MOLECULES OF HIGH SYMMETRY

PRINCIPAL INVESTIGATOR: Dr. Hanspeter Helm
Molecular Physics Department
SRI International
333 Ravenswood Avenue
Menlo Park, CA 94025-3493

INCLUSIVE DATES : 1 November 1986 - 1 November 1989

CONTRACT NUMBER: F49620-87-K-0002

COSTS: $326,552

RESEARCH PERSONNEL: Dr. Hanspeter Helm
Dr. Larry J. Lembo
Dr. Philip C. Cosby
Dr. David L. Huestis

Appendix A

PHOTODISSOCIATION OF TRIATOMIC HYDROGEN

P. C. Cosby and H. Helm

Phys. Rev. Lett. 61, 298 (1988)

Photodissociation of Triatomic Hydrogen

P. C. Cosby and H. Helm

Molecular Physics Department, SRI International, Menlo Park, California 94025

(Received 2 May 1988)

We report the first observation of photodissociation of H_3. Predissociation of the optically prepared $3s^2A_1'$ and $3d^2E''$ states by the $\tilde{X}^2E'$ ground state is detected by monitoring of the production of rovibrationally excited H_2 molecules and H atoms. Product excitation is found to be highly dependent on H_3 electronic and nuclear configuration.

PACS numbers: 33.80.Gj, 34.50.Lf, 34.50.Pi

The unstable ground-state potential surface of H_3 has served as prototype for the development of bimolecular reaction-rate theory,[1] and is still largely territory only of theoretical chemistry. While the ground electronic state of H_3 is dissociative, electronically excited states of this molecule are tightly bound.[2-4] These states are described in terms of a Rydberg electron bound by the field of the stable, triangular H_3^+ core. Since the first experimental indication[5] of a stable H_2 molecule was obtained in 1968, rapid progress has been made in the characterization of its bound excited states.[6-11]

We report here a study of photodissociation of the H_3 molecule with high-resolution kinetic-energy analysis of the H_2+H fragments. Using optical excitation of predissociated states of H_3, we gain selective access to the unstable ground-state surface, under conditions where all relevant quantum numbers of the system, the total energy, and the geometry of the transition state are defined within the uncertainty principle limit. The half-collision of the selected transition state is mapped out by measurement of the translational and internal energy content of the $H_2(v,J)+H$ fragments.

The experiments were performed in the SRI fast-neutral-beam photofragment spectrometer, which has been described recently.[12] H_3 molecules are formed by near-resonant charge transfer[13] of H_3^+ in a Cs vapor cell. Approximately 1.4 μs after formation the H_3 beam intersects at right angles the intracavity beam of a cw dye laser. Photodissociation fragments are detected on a position-sensitive detector for correlated particles. This detector explicitly measures the distance between the fragments (R) and their temporal separation (Δt). From these quantities[14] the center-of-mass energy release W with which the molecule ejected two fragments with masses M and m is determined for each fragment pair H_2+H. The separation of the fragments R is the sum of the individually measured radial distances of each fragment from the center of the detector: $R=R_m+R_M$. The ratio R_m/R_M for the photodissociations reported here was peaked at 2, as expected for the reaction:

$$H_3+h\nu \rightarrow H+H_2.$$

Approximately 10% of the observed photofragments yielded ratios in a broad distribution centered at unity. These fragments reflect photodissociation of H_3 into three H atoms (two of which are observed by the detector), but we will not consider this process further here.

In the absence of the laser, a small fraction of the neutral beam is observed to fragment by spontaneous decay within the 8.7-cm interval between the beam defining slit and the beam terminating flag (see Fig. 3 of Ref. 12). When the laser is turned on, no variation in this dissociation rate is observed except at six discrete wavelengths in the range of 577–603 nm. A plot of the observed fragment flux (for fragments produced with $W \geq 4$ eV) as the laser is tuned over this wavelength range is shown in Fig. 1. The two strong transitions labeled $3dv_0$ and $3sv_0$ in this figure occur at the wavelengths reported by Herzberg and co-workers[6-10] for transitions between the long-lived,[13] vibrationless H_3 $2_p^2A_2''(N=K=0)$ level and the $(N=1)$ levels of the H_3 $3d^2E''$ and $3s^2A_1'$ states, respectively.

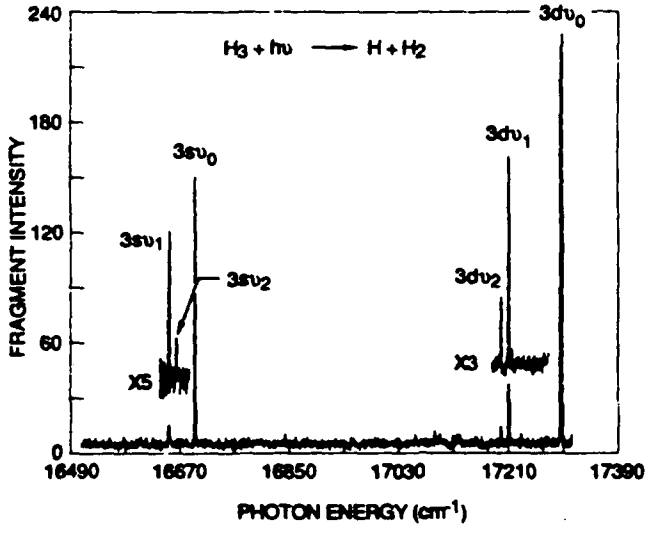

FIG. 1. Observed production of photofragments from H_3 as a function of the photon energy of the exciting laser. Only photofragments produced with $W \geq 4$ eV are recorded for this spectrum. The spectrum at other energy releases is similar, but with a substantial background due to spontaneous dissociation fragments.

TABLE I. Observed photodissociation transitions in H_3.

Label	Observed line[a] (cm^{-1})	Identification Upper state (v_1', v_2', N', K')	Lower state (v_1'', v_2'', N'', K'')	Reported line[b] (cm^{-1})	Measured upper state energy[c] (eV)
$3dv_0$	17297.6	$3d^2E''(0,0,1,1)$	$2p^2A_2''(0,0,0,0)$	17296.982	7.706 ± 0.028
$3dv_1$	17211.6	$3d^2E''(1,0,1,1)$	$2p^2A_2''(1,0,0,0)$		8.115 ± 0.024
$3dv_2$	17199.1	$3d^2E''(0,1,1,1)$	$2p^2A_2''(0,1,0,0)$		8.011 ± 0.028
$3sv_0$	16695.6	$3s^2A_1'(0,0,1,0)$	$2pA_2''(0,0,0,0)$	16694.972	7.634 ± 0.020
$3sv_2$	16665.7	$3s^2A_1'(0,1,1,0)$	$2p^2A_2''(0,1,0,0)$		
$3sv_1$	16653.6	$3s^2A_1'(1,0,1,0)$	$2p^2A_2''(1,0,0,0)$		8.042 ± 0.028

[a]Estimated accuracy $\pm 1.5\ cm^{-1}$.
[b]References 7 and 10.
[c]Relative to $H(1s)+H_2\ X^1\Sigma_g^+(v=0, J=0)$.

The remaining four lines that appear in Fig. 1 are identified as transitions from the $2p^2A_2''(N=K=0)$ level with one quantum of vibration in the symmetric stretch v_1 and bending v_2 vibrational modes into the corresponding levels of the $3d$ and $3s$ states. The measured transition energies and identifications of all six lines are given in Table I. These assignments are based on the energy and angular distributions measured for their photofragments.

The production of photofragments can be understood from the radiative and dissociative pathways that exist for the H_3 molecule (see Fig. 2). The energies of the relevant H_3 states have been established in the work of Herzberg and co-workers,[6-10] Watson,[15] and Vogler.[16] Transitions observed in the present work are denoted by the solid vertical arrows, and radiative transitions connecting the states are denoted by the dashed arrows. The six possible dissociation channels, denoted by horizontal arrows and labeled I–VI, are indicated, together with their expected fragment energies (W) for dissociation to the lowest-energy products $H(1s)+H_2\ X(v=0, J=0)$.

The center-of-mass kinetic-energy releases (W) observed from the dissociation of H_3 into $H+H_2$ products

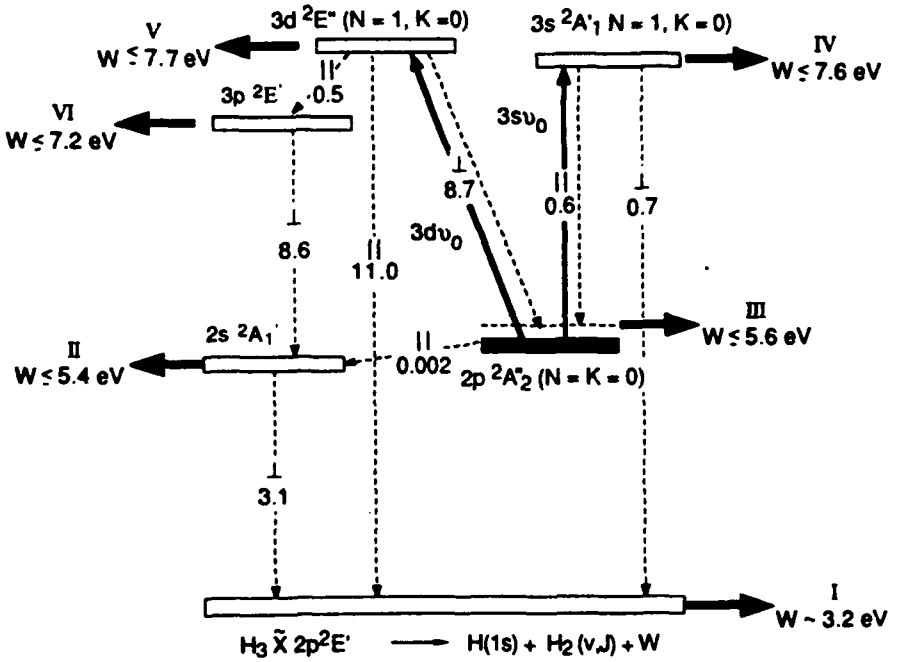

FIG. 2. Radiative connections among the H_3 electronic states access from the $2p^2A_2''(N=K=0)$ metastable level. Photoabsorption transitions are shown by the two solid vertical arrows, spontaneous emission by the dashed arrows. Theoretical transition rates (in units of $10^7\ s^{-1}$) and the orientation of the transition moment relative to the C_3 axis of H_3 are given for each. Predissociation channels are labeled by I–VI, with expected maximum fragment energy releases given for each.

are shown in Fig. 3. The two upper spectra refer to photodissociation via the $3s$ and $3d$ states of the vibrationless molecule. The lower part is the energy-release spectrum observed in the absence of photons, or with the laser not tuned to one of the six transitions. A major contribution to this spontaneous dissociation arises from the very slow ($\tau \sim 50$ μs) radiative decay of the $2p^2A_2''(N=K=0)$ molecules into the $2s^2A_1'(N=1,K=0)$ level. The latter is rapidly predissociated,[7,10] producing fragments in channel II (Fig. 2).

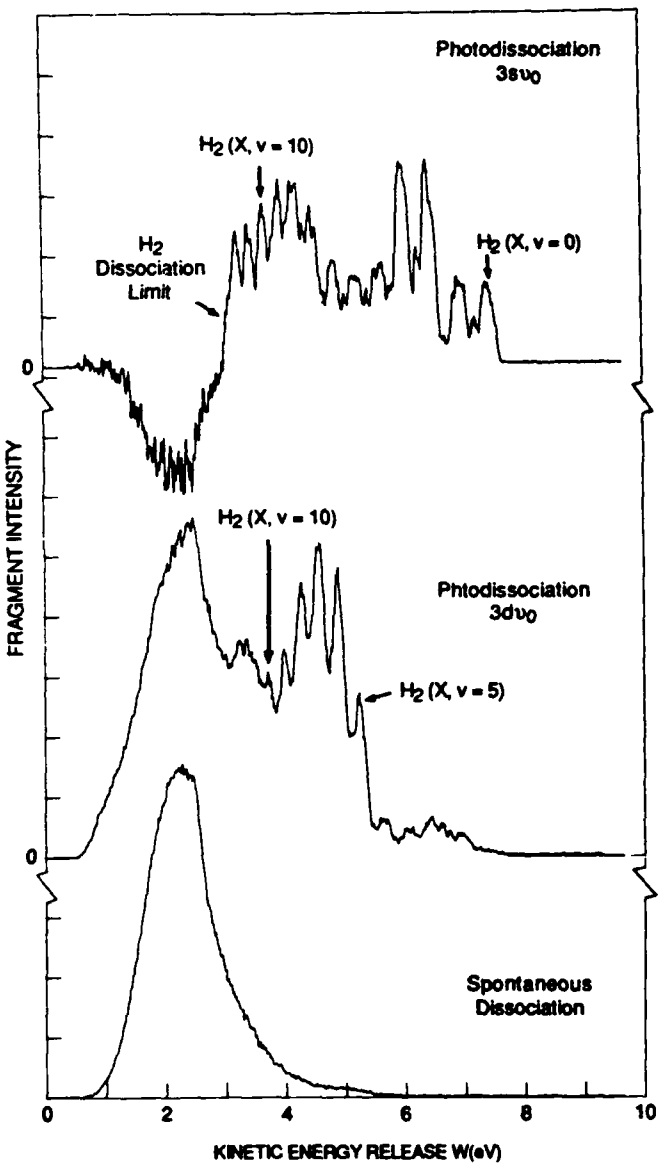

FIG. 3. Fragment kinetic-energy releases (W) accompanying the production of $H+H_2$ from H_3. Fragmentation observed as a result of spontaneous dissociation is shown in the lower portion of the figure, while that observed to accompany absorption in the $3d\nu_0$ and $3s\nu_0$ transitions is shown in the center and upper portions of the spectrum, respectively. Selected vibrational levels of the H_2 $X^1\Sigma_g^+$ photofragments are identified in the figure. All spectra have been corrected for the collection efficiency of the apparatus.

The photodissociation-fragment energy spectra in the center and top portions of Fig. 3 show considerable structure. For both spectra, the laser was chopped and fragments observed with the laser off were subtracted from those observed with the laser irradiating the beam. In the $3s\nu_0$ spectrum (top), the structure is clearly assignable to the production of H_2 photofragments in vibrational levels $v=0$–10 via channel IV. The anharmonicity of the H_2 molecule makes the assignment completely unique. Moreover, subsidiary rotational structure is resolved in a number of the vibrational levels, most notably $J=7$ in $v=0$, 2, 4, 5, and 7. Preliminary modeling of the rotational contributions within each vibrational peak suggests a highly nonequilibrium distribution peaking at $J=5$ in the lower vibrational levels. Only two peaks appear in the spectrum with energy releases below that corresponding to H_2 ($v=10$), whereas there are fifteen bound vibrational levels[17] in the nonrotating molecule. We tentatively assign these two peaks to H_2 ($v=11, J=7$) and ($v=12, J=9$), suggesting a higher propensity for strong rotational excitation when the H_2 photofragment is produced near its dissociation limit. This is consistent with the lack of photofragments corresponding to $v=13$ and 14, since both these vibrational levels are unbound for this degree of rotational excitation.

Structure also appears in the kinetic-energy spectrum of $H+H_2$ produced when the $3d^2E''(N=1,K=0)$ level is excited, as shown in the center of Fig. 3. This structure is uniquely identified as predissociation of the $3d$ state via channel V (Fig. 2). The H_2 fragments are produced with a distribution of vibrational levels quite different from those observed when $3s\nu_0$ is pumped. The H_2 fragments produced in a given v,J level are found to have higher translational energies by 0.072 ± 0.010 eV when those produced from predissociation of the $3s^2A_1'$ level. This is consistent with the $3d^2E''(N=1,K=1)$-$3s^2A_1'(N=1,K=0)$ energy separation of 0.07464 eV established by Herzberg and co-workers.[6-10]

At lower kinetic-energy releases ($W \leq 3$ eV), below the kinematic limit for dissociation into $H+H_2$ via channels IV and V, the spectra from $3s^2A_1'$ and $3d^2E''$ excitation are also dramatically different. When the $3s^2A_1'$ state is excited, fewer fragments are produced in this energy range when the laser is tuned to the $3s\nu_0$ transition than when it is turned off. Since the $2p^2A_2''(N=K=0)$ level is the ultimate parent in both the spontaneous-dissociation process II and the photofragment process IV, depletion of population in this level by photodissociation will produce a corresponding decrease in the number of spontaneous dissociations occurring while the laser is irradiating the H_3 beam. From Fig. 2, it is clear that in order for such a depletion to be observed, the rate for radiative decay of the $3s^2A_1'$ state must be slower than its direct predissociation.

In contrast, photoexcitation of the ground vibrational

level of the $3d^2E''$ state, shown in the center of Fig. 3, gives rise to an *increase* in the low-energy photofragments. This suggests that the rate for radiative decay of $3d^2E''$ into the ground state or into $2p^2A_2''(N=2,K=0)$ is comparable with its rate of predissociation.

The measured fragment energies establish the energies of the photoexcited H_3 levels absolutely with respect to the $H(1s)+H_2$ $X^1\Sigma_g^+(v=0,J=0)$ dissociation limit. These energies are given in the last column of Table I. The energy of the absorbing $2p^2A_2''(N=K=0)$ level relative to this same limit is obtained from these values by subtraction of the photon energy that produced the transition. This places the ground vibrational level of the H_3 $2p^2A_2''(N=K=0)$ state 5.563 ± 0.020 eV above this dissociation limit.

The $3s^2A_1'$ and $3d^2E''$ levels which are observed to predissociate here are, at least superficially, quite similar. Each state has a total angular momentum $J=1$ and is described by an *ortho* H_3^+ core tumbling end over end as characterized by the quantum numbers $N^+=1$, $K^+=0$. Both states predissociate by vibronic coupling and access the ground-state surface at nearly the same energy: The $3s^2A_2''$ at an energy 7.634 eV above the $H+H_2$ dissociation limit and the $3d^2E''$ at an energy only 0.074 eV higher. Nevertheless, the two states produce dramatically different dissociation product distributions, suggesting that the evolution into continuum states is greatly influenced and by the instantaneous distribution of momenta in this six-particle system and the topography of the ground state. We anticipate that quantitative rovibrational populations for the H_2 fragment can be derived from the photofragment data to provide a detailed probe into the dynamical properties[18] of the ground-state potential surface of H_3.

We gratefully acknowledge many helpful discussions during the course of this work with Dr. David L. Huestis, Dr. Roberta P. Saxon, and numerous other coworkers at SRI International. This research was supported by U.S. Air Force Office of Scientific Research Contract No. F49620-87-K-0002.

[1]H. Eyring, H. Gershinowitz, and C. E. Sun, J. Chem. Phys. 3, 786 (1935).
[2]H. F. King and K. Morokuma, J. Chem. Phys. 71, 3213 (1979).
[3]M. Jungen, J. Chem. Phys. 71, 3540 (1979).
[4]R. L. Martin, J. Chem. Phys. 71, 3541 (1979).
[5]F.-M. Devienne, C. R. Acad. Sci. Paris B 267, 1279 (1968).
[6]G. Herzberg, J. Chem. Phys. 70, 4806 (1979).
[7]I. Dabrowski and G. Herzberg, Can. J. Phys. 58, 1238 (1980).
[8]G. Herzberg and J. K. G. Watson, Can. J. Phys. 58, 1250 (1980).
[9]G. Herzberg, H. Lew, J. J. Sloan, and J. K. G. Watson, Can. J. Phys. 59, 428 (1981).
[10]G. Herzberg, J. T. Hougen, and J. K. G. Watson, Can. J. Phys. 60, 1261 (1982).
[11]H. Helm, Phys. Rev. Lett. 56, 42 (1986).
[12]H. Helm and P. C. Cosby, J. Chem. Phys. 86, 6813 (1987).
[13]G. I. Gellene and R. F. Porter, J. Chem. Phys. 79, 5975 (1983).
[14]D. P. deBruijn and J. Los, Rev. Sci. Instrum. 53, 1020 (1982).
[15]J. K. G. Watson, Phys. Rev. A 22, 2279 (1980).
[16]M. Vogler, Phys. Rev. A 19, 1 (1979).
[17]P. R. Bunker, C. J. McLarnon, and R. E. Moss, Mol. Phys. 33, 425 (1977).
[18]K. C. Kulander and J. C. Light, J. Chem. Phys. 85, 1938 (1986).

Appendix B

EXPERIMENTAL DETERMINATION OF THE H_3^+ BOND DISSOCIATION ENERGY

P. C. Cosby and H. Helm

Chem. Phys. Lett. 152, 71 (1988)

EXPERIMENTAL DETERMINATION OF THE H_3^+ BOND DISSOCIATION ENERGY

P.C. COSBY and H. HELM
Molecular Physics Department, SRI International, Menlo Park, CA 94025, USA

Received 10 August 1988

The results of recent photoionization and photodissociation studies of the H_3 molecule are used to establish an experimental value for the H_3^+ ion bond dissociation energy of $D_0^\circ(H_3^+) = 4.373 \pm 0.021$ eV. Comparison is made with the theoretical value and with previous measurements.

The H_3^+ ion is the simplest, stable triatomic molecule. This ion is believed to be the most abundant charged species in interstellar clouds [1,2] and is a major charge carrier in hydrogen discharges [3], where it is formed by the highly exothermic reaction

$$H_2^+ + H_2 \rightarrow H_3^+ + H. \quad (1)$$

Recent advances in infrared spectroscopy [4,5] have allowed experimental determination of many of the physical properties of H_3^+ and its isotopomers in the region of its equilibrium configuration (for a recent review of H_3^+, see ref. [6]). However, an accurate experimental determination of the bond dissociation energy of this ion, or its related heat of formation, has been more elusive. Traditional spectroscopic techniques have been frustrated by the lack of low-lying bound excited electronic states [7,8] in this ion and the repulsive character of the ground electronic state [9] in neutral H_3. Laser photofragment spectroscopy has observed numerous H_3^+ levels in the region of its dissociation limit [10], but the energies of these levels have yet to be established. Careful measurements of the collision-induced dissociation [11–13] of H_3^+, the relative rates of proton transfer reactions [14–16], and the translational [17] and internal [18] energies of the products of reaction (1) have allowed progressively tighter experimental limits to be placed on the possible value of the H_3^+ dissociation energy. Nevertheless, the theoretical value for the total binding energy of three protons and two electrons established by ab initio molecular structure calculations [19,20] remains the most accurate estimate for the H_3^+ dissociation energy.

It has been found that a long-lived H_3 molecule can be produced in a molecular beam [21–26]. This has allowed several recent optical absorption studies [27–31] of the molecule, including both photodissociation [29] and photoionization [27,30,31]. The combined results of these latter studies, together with current knowledge of the rotational structure of the H_3^+ ground electronic state, permit a precise value for the H_3^+ bond dissociation energy to be established in a spectroscopic cycle. We discuss this cycle below, and compare the experimental bond dissociation energy obtained thereby with the theoretical value and with related experimental measurements.

The long-lived H_3 molecule in its lowest vibrational level is the $N=0$, $K=0$ level of the $2p\,^2A_2''$ electronic state [25,27–29]. The dominant one-photon excitation transitions are to the $ns\,^2A_1'$ and $nd\,^2E''$ Rydberg states with no change in vibrational quantum number (see fig. 1). Following excitation into the $n=3$ levels at low laser fluence, we observed [29] predissociation of the excited H_3 molecules. Using position and time-sensitive detection of the correlated H_2+H fragments from isolated molecular dissociations we have determined the translational and internal energy distribution of $H_2(v, J)+H$ fragments. Analysis of these distributions yielded the absolute energies of the $3s\,^2A_1'$ ($N=1$, $K=0$) level and the $3d\,^2E''$ ($N=1$, $K=1$) level with respect to the dissociation limit $H_2\ X\,^1\Sigma_g^+$ ($v=0$, $J=0$) + H(1s). For the vibrationless molecule these energies are meas-

0 009-2614/88/$ 03.50
(North-Holland Physics Publishing Division)

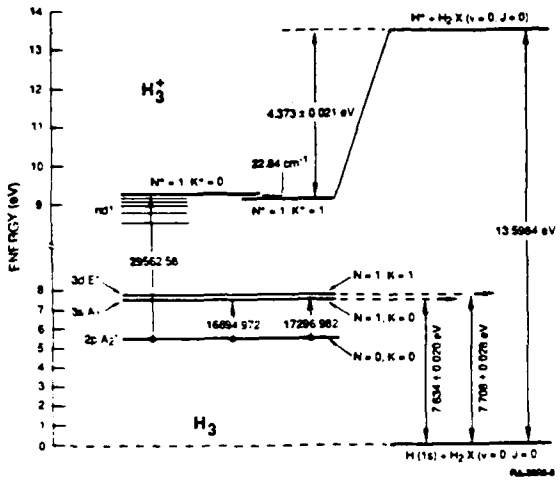

Fig. 1. Schematic diagram of the H_3^+ and H_3 energy levels and dissociation limits relevant to the determination of the H_3^+ bond dissociation energy.

ured to be 7.634 ± 0.020 and 7.706 ± 0.028 eV respectively. Since the photo-excitation energy to predissociated levels is known precisely, the absolute energy of the long-lived H_3 level is determined as 5.563 ± 0.021 eV [29].

The actual lowest bound level of H_3 is the $N=1$, $K=1$ level of the $2s\,^2A_1'$ state, which is rapidly predissociated [32]. This level lies 923.6 cm^{-1} below the long-lived 2p level [33,34]. Subtracting this energy from 5.563 eV, we obtain a value of 5.449 ± 0.021 eV for the lowest bound level of H_3. For comparison, we note that Watson [35] has obtained a value of 5.52 ± 0.05 eV for the energy of the $2s\,^2A_1'$ state from a reanalysis of Vogler's [36] dissociative charge-transfer data. This energy does not refer to a discrete rotational level in the 2s state, but rather to the mean of an unresolved (thermal) distribution of rotational levels in the ground vibrational level [35]. His value is therefore expected to be somewhat higher than that reported here.

Predissociation of the 3s and 3d levels is a consequence of vibrational and rotational coupling of the Rydbergs to the repulsive ground state surface of H_3, $2p\,^2E'$. The rate of predissociation is therefore related to the wavefunction overlap of the Rydberg electron with the 2p ground state orbital. As the principal quantum number increases, this overlap diminishes and hence the rate of predissociation of the Rydbergs is expected to become exceedingly small for large values of n. This fact permits photoexcitation of the higher Rydbergs in a field free region, followed by field ionization and detection of the product ion. In the ionization experiment [30], the photon energies were measured for absorption from the long-lived H_3 $2p\,^2A_2''$ ($N=K=0$) level into the lowest d-Rydberg series converging to the ground vibrational level of the ion. This series, labeled $nd/$ in fig. 1, converges to the lowest rotational level of ortho-H_3^+, $N^+=1$, $K^+=0$. It was observed for n values ranging from $n=30$ to $n=100$ and extrapolated a very short distance to obtain [30] an ionization energy of 29562.58 ± 0.5 cm^{-1}. A value of 29561 ± 1 cm^{-1} has been reported by Dodhy et al. [31] for similar measurements at $n=15$ to $n=50$.

By combining the photofragment kinetic energy data and the photoionization result, it is possible to compute a precise experimental value for the dissociation energy of H_3^+ in a spectroscopic cycle. The photoionization data establish the energy difference between the metastable $2p\,^2A_2''$ ($N=K=0$) level of H_3 and the lowest existing ortho level of H_3^+, $X\,^1A_1'$ ($N^+=1$, $K^+=0$) as 29562.58 cm^{-1} (3.6653 eV). Combining this value with the measured absolute energy of the $2p\,^2A_2''$ ($N=K=0$) level, we obtain the energy of the lowest ortho level of H_3^+ to be $E_o=9.228 \pm 0.021$ eV above $H(1s)+H_2(X,\ v=0,\ J=0)$. The lowest allowed rotational level of H_3^+ is the $N^+=1$, $K^+=1$ level of para-H_3^+. This level lies $\Delta E_{o-p}=22.846$ cm^{-1} (0.0028 eV) lower in absolute energy [37] and is thus the appropriate level from which to calculate the dissociation energy of H_3^+:

$$D_0^0(H_3^+) = IP(H) - E_o + \Delta E_{o-p}$$
$$= 4.373 \pm 0.021 \text{ eV}, \quad (2)$$

where IP(H) is the spectroscopic ionization potential [38] of the hydrogen atom.

Comparison can be made with the value of $D_0^0(H_3^+)$ derived from ab initio molecular structure calculations of this simplest triatomic molecule. The absolute energy required to form H_3^+ from three protons and two electrons is calculated [20] to be $\epsilon = -1.342784$ hartree with a stated absolute (variational) error of 0.0022 hartree (0.059 eV). This energy is related to the dissociation energy by

$$D_0(H_3^+)_{\text{theo}} = \epsilon - 2R_\infty - D_0^0(H_2) - \text{ZPE}(H_3^+), \quad (3)$$

where R_∞ is the Rydberg constant[#1], $D_0^0(H_2)$ is the dissociation energy [40] of H_2 (4.4781 ± 0.0001 eV), and ZPE(H_3^+) is the zero-point energy [41] of H_3^+ in its lowest existing level (0.5410 eV). This latter value is from theory; we estimate its accuracy to be within ±0.005 eV. Eq. (3) leads to the value $D_0^0(H_3^+)_{theo} = 4.309^{+0.060}_{-0.005}$ eV. This lies only 0.064 eV below the present measurement of 4.373 ± 0.021 eV and within the combined error range.

Three experimental values for the dissociation energy of H_3^+ have been derived in collision-induced dissociation measurements. A value of 4.23 ± 0.15 eV was reported by Harris et al. [11] obtained from the translational threshold for the production of H^+ in collisions of H_3^+ with He. Goh and Swan [12] have measured the translational energy of the fragments produced in the production of H_2^+ in collisions of H_3^+ on He to find an energy of 6.3 ± 0.3 eV for dissociation to this higher limit. Martinez et al. [13] have studied this same reaction, additionally observing the angular distribution of the fragments, to find an energy of 6.3 ± 0.5 eV. From the difference in ionization potentials of H_2 and H, their values imply a dissociation energy of H_3^+ of 4.47 ± 0.3 eV. All of these measurements presume that the reactant ions are in their lowest state and that the products are produced without internal excitation. From the agreement with the present measurement, these presumptions appear to have been largely correct.

Additional experimental information on the dissociation energy of H_3^+ is found in the proton affinity of H_2, PA(H_2). Its value is measured [14–16] to lie in the range $4.2 \leqslant PA(H_2) \leqslant 4.9$ eV with a recommended [42] value of 101.3 kcal/mol (4.393 eV). In comparing these values with the present measurement of $D_0^0(H_3^+)$, it should be remembered that PA(H_2) represents the difference in energy (enthalpy) between the products $H^+ + H_2$ and the ion H_3^+, both at thermal (298 K) equilibrium. Payzant et al. [43] estimate that this differs from the dissociation energy by ≈0.05 eV.

In conclusion, we report a fully characterized experimental value for the H_3^+ dissociation energy $D_0^0(H_3^+) = 4.373 \pm 0.021$ eV. This value is in agreement with and greatly improves upon the accuracy of, previous experimental measurements. The new value is also consistent with that predicted by ab initio calculations of this ion's molecular structure.

This research was supported by US Air Force Office of Scientific Research Contract No. F49620-87-K-0002.

[#1] Values for the fundamental constants and energy conversions are from the 1986 CODATA values [39].

References

[1] A Dalgarno and J.H. Black, Rept. Progr. Phys. 39 (1976) 573.
[2] W.D. Watson, Rev. Mod. Phys. 48 (1976) 513.
[3] R.N. Varney, Phys. Rev. Letters 5 (1960) 559.
[4] J.-T. Shy, J.W. Farley, W.E. Lamb and W.H. Wing, Phys. Rev. Letters 45 (1980) 535.
[5] T. Oka, Phys. Rev. Letters 45 (1980) 531.
[6] T. Oka, in: Molecular ions: spectroscopy, structure and chemistry, eds. T.A. Miller and V.E. Bondybey (North-Holland, Amsterdam, 1983) p. 73.
[7] K. Kawaoka and R.F. Borkman, J. Chem. Phys. 54 (1971) 4234.
[8] L.J. Schaad and W.V. Hicks, J. Chem. Phys. 61 (1974) 1934.
[9] R.N. Porter, R.M. Stevens and M. Karplus, J. Chem. Phys. 49 (1968) 5163.
[10] A. Carrington and R.A. Kennedy, J. Chem. Phys. 81 (1984) 91.
[11] H.H. Harris, M.G. Crowley, T.R. Grossheim, P.J. Woessner and J.J. Leventhal, J. Chem. Phys. 59 (1973) 6181.
[12] S.C. Goh and J.B. Swan, Phys. Rev. A 24 (1981) 1624.
[13] H. Martinez, I. Alvarez, J. de Urquijo, C. Cisneros and A. Amaya-Tapia, Phys. Rev. A 36 (1987) 5425.
[14] W.A. Chupka, M.E. Russell and K. Refaey, J. Chem. Phys. 48 (1968) 1518.
[15] J.A. Burt, J.L. Dunn, M.J. McEwan, M.M. Sutton, A.E. Roche and H.I. Schiff, J. Chem. Phys. 52 (1970) 6062; P.F. Fennelly, R.S. Hemsworth, H.I. Schiff and D.K. Bohme, J. Chem. Phys. 59 (1973) 6405.
[16] R.J. Cotter, R.W. Rozett and W.S. Koski, J. Chem. Phys. 57 (1972) 4100.
[17] J. Durup and M. Durup, J. Chim. Phys. 40 (1967) 603.
[18] D.L. Smith and J.H. Futrell, J. Phys. B 8 (1975) 803.
[19] M.E. Schwartz and L.J. Schaad, J. Chem. Phys. 47 (1967) 5325.
[20] C.E. Dykstra, A.S. Gaylord, W.D. Gwinn, W.C. Swope and H.F. Schaefer III, J. Chem. Phys. 68 (1978) 3951.
[21] F.-M. Devienne, Compt. Rend. Acad. Sci. (Paris) B 267 (1968) 1279.
[22] C.F. Barnett and J.A. Ray, Phys. Rev. A 5 (1972) 2120.
[23] T. Nagasaki, H. Doi, K. Wada, K. Higashi and F. Fukuzawa, Phys. Letters A 38 (1972) 381.
[24] M.J. Gaillard, A.G. de Pinho, J.C. Poizat, J. Remillieux and R. Saoudi, Phys. Rev. A 28 (1983) 1267.

[25] G.I. Gellene and R.F. Porter, J. Chem. Phys. 79 (1983) 5975.
[26] J.F. Garvey and A. Kuppermann, Chem. Phys. Letters 107 (1984) 491.
[27] H. Helm, Phys. Rev. Letters 56 (1986) 42.
[28] S.F. Selgren and G.I. Gellene, Chem. Phys. Letters 146 (1988) 485.
[29] P.C. Cosby and H. Helm, Phys. Rev. Letters 61 (1988) 298.
[30] H. Helm, Phys. Rev. A, to be published.
[31] A. Dodhy, W. Ketterle, H.-P. Messmer and H. Walther, Chem. Phys. Letters 151 (1988) 133.
[32] I. Dabrowski and G. Herzberg, Can. J. Phys. 58 (1980) 1238.
[33] G. Herzberg and J.K.G. Watson, Can. J. Phys. 58 (1980) 1250.
[34] G. Herzberg, H. Lew, J.J. Sloan and J.K.G. Watson, Can. J. Phys. 59 (1981) 428.
[35] J.K.G. Watson, Phys. Rev. A 22 (1980) 2279.
[36] M. Vogler, Phys. Rev. A 19 (1979) 1.
[37] J.K.G. Watson, S.C. Foster, A.R.W. McKellar, P. Bernath, T. Amano, F.S. Pan, M.W. Crofton, R.S. Altman and T. Oka, Can. J. Phys. 62 (1984) 1875.
[38] C.E. Moore, NSRDS-NBS 34 (1970).
[39] E.R. Cohen and B.N. Taylor, Phys. Today 40 (1987) BG11.
[40] K.P. Huber and G. Herzberg, Molecular spectra and molecular structure, Vol. 4. Constants of diatomic molecules (Van Nostrand Reinhold, New York, 1979) p. 241.
[41] S. Miller and J. Tennyson, J. Mol. Spectry. 126 (1987) 183.
[42] S.G. Lias, J.F. Liebman and R.D. Levin, J. Phys. Chem. Ref. Data 13 (1984) 695.
[43] J.D. Payzant, H.I. Schiff and D.K. Bohme, J. Chem. Phys. 63 (1975) 149.

Appendix C

MEASUREMENT OF VIBRATIONAL FREQUENCIES OF THE H_3 MOLECULE USING TWO-STEP PHOTOIONIZATION

L. J. Lembo, H. Helm, and D. L. Huestis

J. Chem. Phys. 90, 5299 (1989)

Measurement of vibrational frequencies of the H_3 molecule using two-step photoionization

L. J. Lembo, H. Helm, and D. L. Huestis
Molecular Physics Laboratory, SRI International, Menlo Park, California 94025

(Received 15 November 1988; accepted 20 January 1989)

A two-step photoionization scheme is used to determine vibrational frequencies of the $n = 3$ Rydberg states of triatomic hydrogen. Symmetric-stretch frequencies in orthotrihydrogen of 3212.1 and 3168 cm^{-1} are measured for the $N = 1$ levels of the states $3s\,^2A_1'$ and $3d\,^2E''$, respectively. Transitions to bending-mode excited levels in the $3d$ states and overtone levels of the $3p\,^2E'$ state are observed also.

I. INTRODUCTION

The triatomic hydrogen molecule is the simplest of all neutral triatomics and is, therefore, of significant fundamental interest. Serious spectroscopic studies of H_3 began approximately ten years ago with the experiments of Herzberg and co-workers.[1-5] These observations provided the first example of a discrete Rydberg spectrum of a polyatomic molecule that is unstable in its ground state. Figure 1 shows a rudimentary level diagram for some of the low Rydberg states in H_3, along with emission bands observed by Herzberg's group.

With the exception of the rotationless levels of the electronic state designated $\tilde{B}$ in Fig. 1, all levels of H_3 will either predissociate (rotationally or vibrationally) to the ground $\tilde{X}$ state, or will promptly radiate to predissociating states. The electronic $\tilde{B}$ state cannot vibrationally predissociate to $\tilde{X}$; therefore, the rotationless levels of this state are stable with respect to predissociation. The lifetime of the rotationless levels is limited by the slow infrared radiative emission to the $2s\,^2A_1'$ state. This metastability has permitted observation of "stable" H_3 molecules in a variety of experiments.[6-11] Definitive spectroscopic characterization of metastable H_3 has come about through photoionization techniques.[12,13] A fast-beam experiment[12] has shown that the rotationless $\tilde{B}$-state molecules are long lived in the vibrationless level as well as in vibrationally excited cores.

We have recently exploited the metastability of the rotationless $\tilde{B}$ level to perform high-resolution laser spectroscopy of neutral H_3. Using one- and two-photon excitation schemes, we have observed the excitation of the *np*, *nd*, and *nf* Rydberg series converging to the vibrationless state of the H_3^+ ion.[14,15] We have also studied series of autoionizing transitions converging to vibrationally excited states of the H_3^+ core.[12] In addition, predissociation of the Rydberg states belonging to the $n = 3$ manifold have been studied using photofragment spectroscopy.[16] In each case, the transitions are purely electronic in the sense that they involve no vibrational excitation; all the transitions take place from some vibrational level of the rotationless $\tilde{B}$ state to an upper level with the same vibrational quantum numbers. The same applies to Herzberg's emission studies.

The equilibrium geometry of the H_3^+ ion is that of an equilateral triangle; the bound states of H_3 are predicted to be close to this geometry.[17] The vibrational frequencies for such an object are two: one corresponding to a symmetric-stretch, or "breathing" mode, and another corresponding to a twofold degenerate asymmetric stretch, or a "bending" mode. Some theoretical effort has been devoted to calculating these vibrational frequencies in H_3^+, an ion of significant astrophysical importance. The bending mode of H_3^+ is infrared active by virtue of a distortion-induced dipole moment, and measurements by Oka[18] and by Watson, *et al.*[19] are in good agreement with the calculations of Miller and Tennyson.[20] The pure breathing mode of H_3^+ is infrared inactive and cannot be excited optically, since it is a purely symmetric excitation. On the other hand, we show here that the addition of an electron to H_3^+ allows excitation of the breathing and/or the bending mode of the H_3^+ core simultaneously with electronic transitions to certain of the Rydberg states shown in Fig. 1. We have observed these off-diagonal transitions for excitation of the $n = 3$ Rydberg manifold as well as for excitation of vibrationally autoionizing[21] resonances. In this paper, we discuss the off-diagonal transitions to the low-lying $n = 3$ states.

The process upon which we rely to detect these transitions is two-step photoionization. One laser photon induces

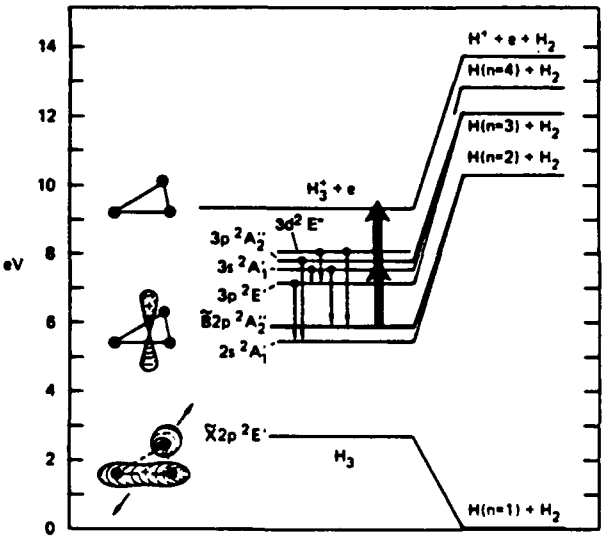

FIG. 1. Level diagram for low-lying Rydberg states of H_3. Emission bands observed by Herzberg and co-workers are shown; double arrow represents two-step photoionization scheme employed in our experiments.

transitions from the metastable level of the $\tilde{B}$ state to the intermediate levels of interest. This excitation is detected by bound–free photoionization of the intermediates by a second laser photon. This process is represented in Fig. 1 by the bold double arrows. Using this technique, we have observed symmetric-stretch, bending, and overtone levels in the $n = 3$ manifold of triatomic hydrogen.

EXPERIMENTAL SETUP AND RESULTS

The experiment was performed using the SRI fast-neutral-beam spectrometer (Fig. 2), which has been described in detail previously.[12,14] A beam of H_3^+ ions is extracted from a hollow-cathode hydrogen discharge operated at pressures between 2 and 10 Torr, accelerated to an energy of 1.5 keV, and mass selected in a Wien filter. The H_3^+ ions are directed into a cesium-vapor cell, where near-resonant charge transfer populates a distribution of (neutral) H_3 energy levels. 20 cm after the charge–transfer cell, the resulting fast neutral beam enters a 120 cm ultrahigh vacuum region with a flight time of approximately 4 μs. The predissociation rates of all but the rotationless $\tilde{B}$ levels are very fast in comparison with this, thereby leaving the H_3 beam prepared in a well-defined manner. The high ion source pressure chosen for the current experiment ensures[16] that the vibrationless $\tilde{B}$ level is the dominant ($>90\%$) H_3 species present in the beam. All transitions reported here are attributed to this lower-state level. This beam is excited coaxially with pulsed laser beams of 10 ns duration and pulse energies <4 mJ. H_3^+ ions created as a result of the optical interaction are energy analyzed and detected by a channel-electron multiplier.

The laser was scanned in the wavelength range 480–600 nm. Spectra were recorded with the laser operating in a low-resolution ($\Delta\nu = 0.2$ cm^{-1}) mode. Each of the transitions discovered in the low-resolution spectra were subsequently scanned under higher resolution ($\Delta\nu = 0.04$ cm^{-1}) along with an I_2 reference spectrum whenever possible. Since the H_3 beam velocity is a substantial fraction ($\sim 10^{-3}$) of the speed of light, each H_3 molecule will experience a substantial first-order Doppler shift of the laser frequency (~ 20 cm^{-1}). In order to account for this effect, high-resolution spectra were taken with the laser and H_3 beams in both the counterpropagating and copropagation configurations. The geometric mean the two transition frequencies so recorded equals the actual H_3 "rest-frame" transition frequency. This procedure eliminates the need for precise measurements of the neutral-beam energy.

Figures 3(a) and 3(b) are broadband (0.2 cm^{-1}) spectra showing the number of H_3^+ ions created in 256 laser shots as a function of excitation wavelength. No background subtraction is necessary to exhibit the spectral features which appear in Fig. 3; the typical number of background ion counts is less than 0.02 per laser shot. Since the spectra seen in Figs. 3(a) and 3(b) were taken under different neutral-beam and laser conditions, the intensities of the peaks in Fig. 3(a) relative to those in Fig. 3(b) are not meaningful; however, the relative intensities in each figure are.

Features (A) and (B) in Fig. 3(a) correspond to transitions assigned previously.[2,5] Their frequencies are thus well known and were easy to identify in the two-step ionization spectra. These transitions involve no vibrational excitation and are expected to be strong. The linewidths seen in Fig. 3(a) are attributable to power broadening; this was verified by repeating these scans using different laser intensities. The feature labeled (B′) is a fortuitous yet dramatic illustration of this point. The broadband spectra in Figs. 3(a) and 3(b) were accumulated with the laser and neutral beams in the counterpropagating configuration, and the photon-energy scale is calibrated on this assumption. Inadvertently, apertures along the beam line and the exit window for the laser beam reflect a small portion of the laser beam into the copropagating direction. Features (B) and (B′) occur at laser fre-

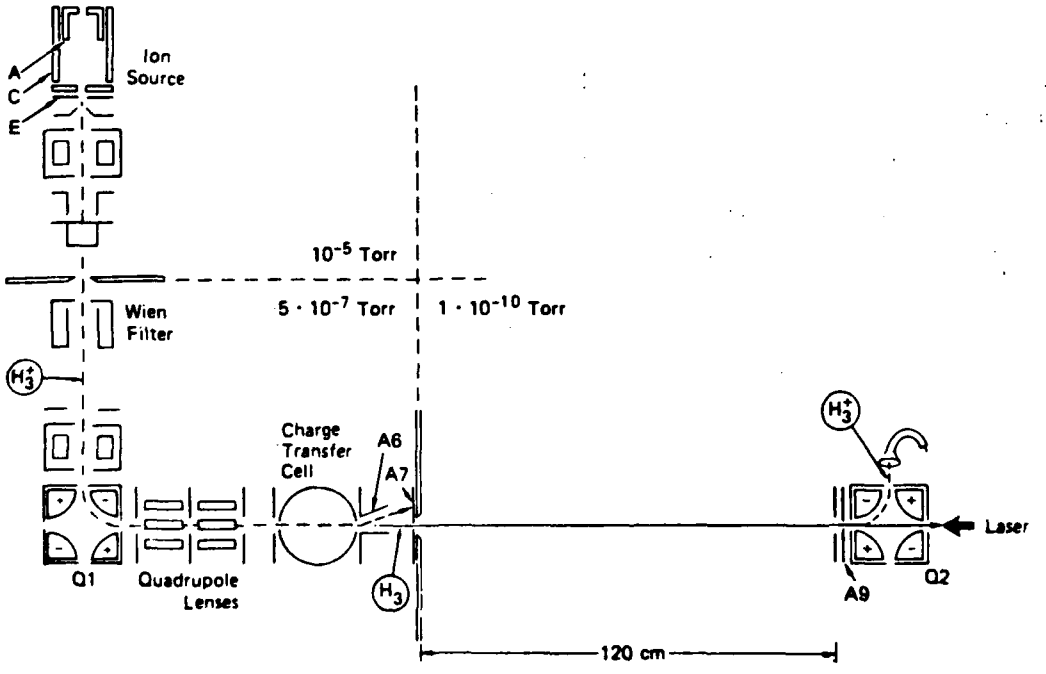

FIG. 2. Schematic view of the fast–neutral–beam photoionization spectrometer.

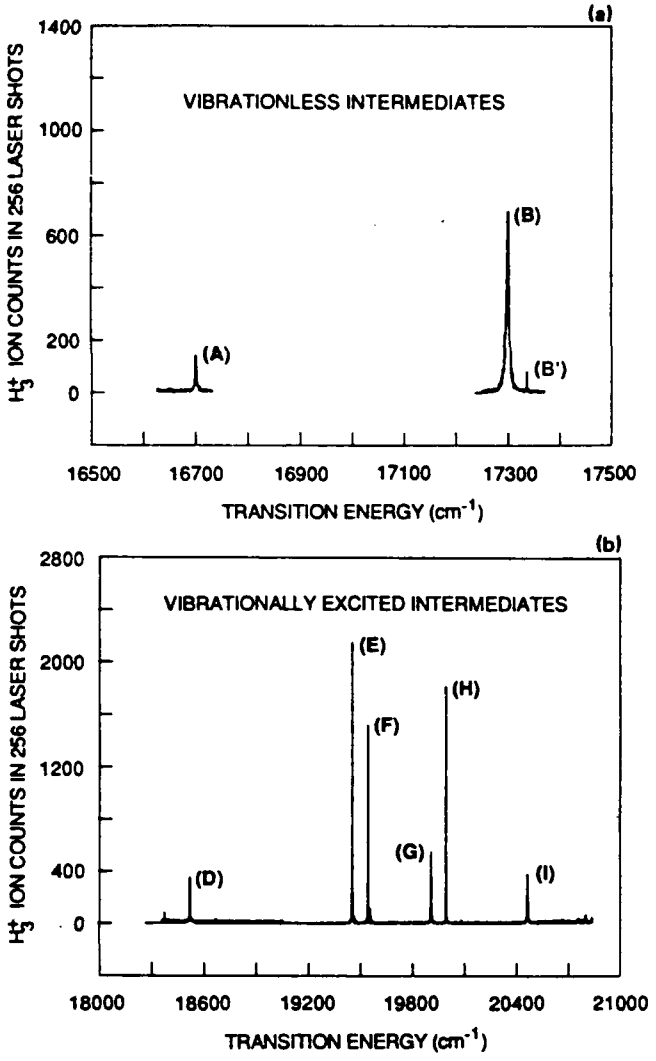

FIG. 3. (a) and (b): Low-resolution two-step photoionization spectra.

quencies which are Doppler shifted into resonance with the same intermediate level of H_3 for the counter- and copropagating laser beams, respectively. Since we are dealing with a very strong transition, the weak copropagating beam will have a strength sufficient to cause some excitation to the intermediate level. The strong counterpropagating beam then provides the intensity needed to ionize the intermediate [feature (B')], without causing the broadening apparent when it is in resonance with the first excitation step [feature (B)].

Figure 4 shows high-resolution spectra of the features labeled (D)–(I) in Fig. 3(b). These were taken with the laser and neutral beams in the counterpropagating configuration. The lower traces in each portion show the number of H_3^+ ion counts collected in 256 laser shots, as before. Four of the ion spectra are accompanied by their corresponding I_2 calibration spectra, recorded in fluorescence from a commercial room-temperature cell. Several of the I_2 reference lines are labeled according to the numerical indexing used in the standard iodine reference atlas.[22] Two of the H_3 resonances occur at wavelengths beyond the spectral range of the I_2 reference [peaks (H) and (I)]. These spectra were calibrated by feeding a small portion of the laser into a monochromator and recording the laser wavelength at several points during the scans.

Spectra analogous to those shown in Fig. 4 were taken in the copropagating configuration. The resulting rest-frame frequencies are listed in the final column of Table I. The uncertainty limits for the four I_2-calibrated H_3 lines are estimates based on the experimental linewidths, while the uncertainty limits for the two remaining lines are based on the precision of the monochromator measurements. In order to glean some impression of the neutral-beam energy stability, each pair of I_2-calibrated frequencies were used to determine the requisite Doppler shifts. These ranged from $v/c = 1.046\times10^{-3}$–1.055×10^{-3}. This scatter is equivalent to a frequency uncertainty of 0.1 cm^{-1}, which is smaller than the observed spectral linewidths.

The linewidths seen in Fig. 4 are all significantly larger than the laser bandwidth (0.04 cm^{-1}). In addition, three of these lines show a definite splitting. The three peaks which show splitting in the high-resolution spectra [peaks (D), (G), and (I)] appear relatively weak in the broadband scan [Fig. 3(b)]. We have been able to show that both the splitting and broad linewidths are associated with the high optical intensity required by the photoionization step. This has been accomplished by conducting an additional set of experiments where ionization was accomplished with a two-color scheme. The intensity of a laser tuned through the resonant excitation step can be made small, while the nonresonant second laser has the intensity sufficient to photoionize the excited intermediate. This resulted in $n = 3$ resonances showing no structure and peak widths equal to the laser bandwidth. An interpretation of these results appears in the Discussion.

SPECTRAL ASSIGNMENT

The transitions shown in Figs. 3 and 4 are depicted on the energy-level diagram of Fig. 5; the proposal assignments for these levels are listed in Table I, along with the measured transition energies and estimated transition energies based upon two models to be explained in due course. The levels shown in Fig. 5 are labeled according to the state designation describing the Rydberg-electron orbital, with its D_{3h} electronic-symmetry label in Hund's case (b), followed by a pair of numbers in parentheses (v_1,v_2) indicating the number of vibrational quanta in the symmetric-stretch and bending modes, respectively. In Table I we use four quantum numbers in parentheses (v_1,v_2,N,G), where N is the angular momentum excluding spin, and G is Hougen's "convenient quantum number."[23] It is defined as $G = \lambda + l_2 - K$, where λ and K are, respectively, the projections of electronic and total angular momentum onto the H_3 (body-fixed) principal symmetry axis. The projection of vibrational angular momentum in the degenerate bending mode l_2 is related to the number of bending quanta by $l_2 = v_2, v_2 - 2,..., -v_2$. The quantum number G thus indicates the amount of angular momentum associated with the mechanical rotation of the H_3 frame about the principal-symmetry axis; it is therefore related to the nuclear-exchange symmetry of a level. For

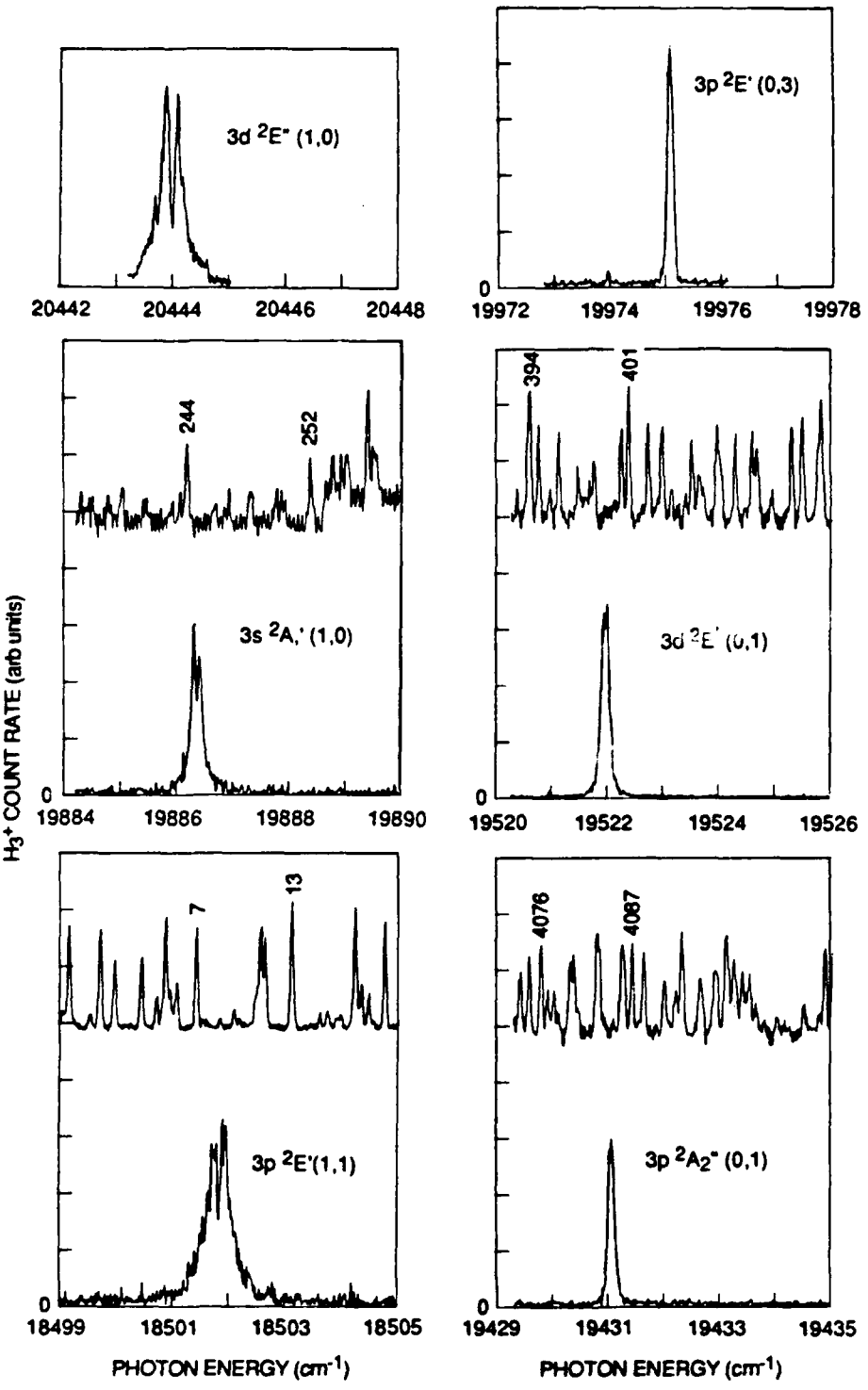

FIG. 4. High-resolution spectra of the features labeled D–I in Fig. 3(b). Lower traces show H_3^+ ion production, upper traces show I_2 reference spectrum whenever possible. Laser and H_3 beams in counterpropagating configuration. The photon-energy scale refers to the stationary iodine target.

ortho (total nuclear spin = 3/2) levels, $G = 0, 3, 6, \ldots$, while for para (nuclear spin = 1/2) levels, $G = 3t \pm 1$, where t is an integer. With only a few transitions to assign, without a recognizable pattern, we have made our assignment in two ways: (1) by identifying the transitions that are allowed by symmetry and (2) by estimating the transition energies from the available spectroscopic information on H_3^* and H_3^+.

Symmetry considerations

The "overall symmetry" classification of rovibronic wave functions for symmetric-top molecules has been discussed extensively[23–25] and used to label the rotational levels of the vibrationless excited states of H_3 and D_3 (see, e.g., Fig. 6 of Ref. 5). The overall-symmetry labels are the same as for the representations of the normal symmetry group of the nonrotating molecule, but the rotational wave function also makes a contribution, since changing the numbering of the nuclei requires a reanalysis of the Euler angles.

In the present case we have a single initial state, ($N = 0$ $2p^2A_2''$), an ortho level with $G = 0$ and overall symmetry label A_2''. One-photon electric-dipole transitions are possible only to $N = 1$ levels with the opposite parity and the same

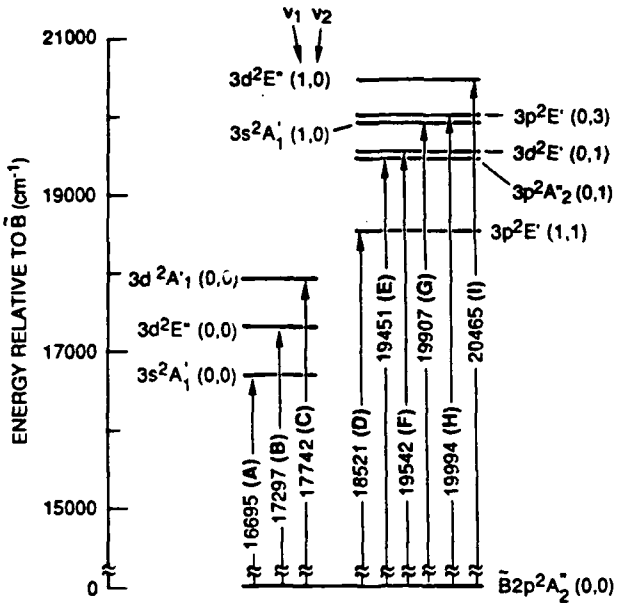

FIG. 5. Energy-level diagram showing observed transitions and proposed level assignments.

nuclear–spin configuration. Since the upper levels must be ortho, they will have $G = 0, 3, \ldots$; and since the dipole operator transforms as A_1'', the overall symmetry label of the upper levels must be $A_2' = A_2'' \otimes A_1''$.[23] To assign overall symmetry labels to the states of vibrating H_3^*, we find it simplest to use a Hund's case (d) model, and take the direct product of the overall symmetry representation of the rovibrational wave function of the underlying H_3^+ core (containing all the nuclear permutational symmetry information) with the overall symmetry representation of the Rydberg electron uncorrelated with the nuclear frame. The latter is just A_1' for $3s$ and $3d$ and A_1'' for $3p$ (i.e., for even and odd l, respectively).

The vibrational wave functions for all levels of the symmetric stretch mode are classified as A_1', the completely symmetric representation, and thus the value of v_1 does not change the overall symmetry label. In contrast, addition of an odd number of bending quanta to a level of fixed l, λ, and G changes the parity of that level. This means that $p \leftarrow p$ transitions are now expected, $s \leftarrow p$ transitions are forbidden, and $d \leftarrow p$ transitions are still allowed, but only for rotational levels that were forbidden in the vibrationless or symmetric-stretch cases.

Energy-level estimates

To estimate the upper-state energies, we use two similar methods, hereafter referred to as models I and II. In model I, an "electronic energy", derived from the energy separations observed by Herzberg' group[1-5] for the vibrationless electronic states, is added to a "vibrational energy," derived either from the experimental energies of the vibrationless and bending-excited levels of H_3^+ (see Ref. 19) or from the accurate theoretical calculations of the symmetric-stretch excited and overtone vibrational levels of H_3^+.[20,26] These vibrational energies are listed in Table II. In model II, we make an additional rather ad hoc adjustment for the rotational energy content of the term values we are subtracting. Such an adjustment is significant because the rotational constant is so large. The results of models I and II for our proposed level assignments are summarized in Table I, and further explicated in the remainder of this section.

The first conclusion of either model is that in the wavelength range scanned, from 16 500 to 21 000 cm^{-1}, we expect to find the $3s$, $3p$, and $3d$ Rydberg states of H_3 with various amounts of vibrational excitation. The lowest allowed transitions to the $n = 4$ manifold are estimated to be at 22 423 and 22 673 cm^{-1} for the vibrationless $4s^2A_1'$ and $4d\,^2E''$ states, respectively, and at 23 498 for the bending-excited

TABLE I. Comparison of estimated and observed transition frequencies. The rovibrational label is (v_1, v_2, N, G).

Proposed assignment		Estimated transition frequency cm^{-1}		Observed transition Frequency (cm^{-1})	
Electronic	Rovibration	Model I[a]	Model II[b]		
$3d\,A_1'$	(1,0,1,0)	20 920	20 918	...	
$3d\,E''$	(1,0,1,0)	20 475	20 473	20 465.4 ± 1	(I)
$3p\,E'$	(0,3,1,0)	20 009	20 056 ± 48	19 994.0 ± 1	(H)
$3d\,E''$	(0,1,1,3)	19 818	20 012 ± 44		
$3s\,A_1'$	(1,0,1,0)	19 873	19 871	19 907.1 ± 0.3	(G)
$3dE'$	(0,1,1,3)	19 717	19 536 ± 44	19 542.4 ± 0.2	(F)
$3pA_2''$	(0,1,1,0)	19 317	19 473 ± 49	19 451.5 ± 0.2	(E)
$3p\,E'$	(1,1,1,0)	18 553	18 604 ± 48	18 521.4 ± 0.4	(D)
$3d\,A_1'$	(0,0,1,0)		17 741.732[c]	17 742 ± 1	(C)
$3d\,E''$	(0,0,1,0)		17 296.982[c]	17 297 ± 1	(B)
$3sA_1'$	(0,0,1,0)		16 694.972[c]	16 695 ± 1	(A)
$3p\,E'$	(0,1,1,0)	15 520	15 576 ± 50	15 548.8 ± 1[d]	

[a]Model I consists of adding vibrational band origins to the energy of the lowest ortho level in each electronic state.
[b]Model II estimates the rotational energy of the pertinent term values.
[c]Measurements from Refs. 2 and 5.
[d]See *Note added in proof.*

TABLE II. Rovibrational energies (cm^{-1}) of ortho levels of H_3^+ relative to the hypothetical level $N^+ = 0$, $G = 0$.

(v_1, v_2, N^+, G)	Energy[a]	Overall symmetry	Parity
0, 0, origin	0.00		
0, 0, 1, 0	86.96	A_2'	+
0, 0, 2, 2	169.27	E'	+
0, 0, 3, 0	516.88	A_2'	+
0, 0, 3, 3	315.29	A_2''	−
0, 1, origin	2521.31		
0, 1, 1, 0	2616.69	A_2''	−
0, 1, 2, 0	2812.86	A_2''	−
0, 1, 2, 3	2614.22	A_2'	+
0, 1, 3, 0	3025.96	A_2''	−
0, 1, 3, 3	2876.78	A_2'	+
1, 0, origin	3178.35		
1, 0, 1, 0	3263.21	A_2'	+
1, 1, origin	5554.07		
1, 1, 1, 0	5644.4	A_2''	−
1, 1, 2, 0	5834.77	A_2''	−
0, 3, origin[b]	7010.49		
0 3 1 0[b]	7101.0[c]	A_2''	−
0, 3, 2, 0[b]	7291.0[c]	A_2''	−

[a] Energies for $(0,0,N^+,G)$ and $(0,1,N^+,G)$ taken from Ref. 19; higher levels taken from Ref. 20.

[b] $l_2 = 1$.

[c] This number is computed by taking the (0,3,0,0) band origin cited in Ref. 20 and adding estimated rotational energies taken from the (1,1,1,0) and (1,1,2,0) levels.

$4p^2E'$ state (assuming that the $4l$ levels have the same quantum defects as the corresponding $3l$ level). By adding the theoretical vibrational energies to the spectroscopically known energies of the $3l$ states, we conclude that we might observe the $3s\,^2A_1'$, $3p\,^2A_2''$, $3d\,^2E'$, and $3d\,^2E''$ states with zero or one quantum of vibrational excitation. For the lower lying $3p\,^2E'$ state, we expect to see only levels with two or three quanta of vibrational excitation.

Vibrationless and symmetric-stretch excited levels

As mentioned above, the transitions labeled (A) and (B) were previously assigned in emission studies.[2,5] These transitions take place from the vibrationless metastable $(N=0)\tilde{B}\ 2p\,^2A_2''$ level to the vibrationless $N=1$ levels of the $3s\,^2A_1'$ and $3d\,^2E''$ states. Although not shown in Fig. 3, we have also used our two-step ionization technique to observe the vibrationless $N=1$ level of the $3d\,^2A_1'$ state, shown as transition (C) at 17 742 cm^{-1} in Fig. 5 and listed in Table I.

Corresponding to each allowed vibrationless transition [e.g., (A) and (B) in Fig. 3] we expect to find additional transitions at shorter wavelength, separated by approximately the symmetric-stretch frequency in H_3^+; Miller and Tennyson[20] calculate a value of 3178.3 cm^{-1} for this frequency. This allows us to assign peaks (G) and (I) as transitions to the $v_1 = 1$ levels of the $3s\,^2A_1'$ and $3d\,^2E''$ states, respectively. The differences between the transitions to the $v_1 = 1$ and $v_1 = 0$ levels give directly the symmetric-stretch frequencies of 3212.1 ± 0.3 cm^{-1} for the $3s\,^2A_1'$ and 3168.4 ± 1 cm^{-1} for the $3d\,^2E''$ state. These frequencies refer to the energy differences between the lowest ortho levels in each state [for these two electronic states, the $(N=1,G=0)$ levels]. The $v_1 = 1$ levels of the $3s\,^2A_1'$ and $3d\,^2E''$ states have also been observed recently[16] in photopredissociation transitions from the $v_1 = 1$ level of the $2p\,^2A_2''$ state, at 16 653.6 and $17\,211.6 \pm 1.5$ cm^{-1}, respectively. The difference between these two values, 558.0 ± 2 cm^{-1} agrees with the separation of 558.3 ± 1 cm^{-1} between our peaks (G) and (I), in support of our assignment. Combining these independent measurements allows us to infer a value of 3253.6 ± 1.2 cm^{-1} for the symmetric-stretch frequency of the $\tilde{B}\ 2p\,^2A_2''$ state.

Bending-excited levels

Consider first the case of the $3p$ states. To deduce the number of bending-excited levels that satisfy all symmetry requirements, consider building a Hund's case (d) representation by attaching a $3p$ electron to the various low-lying ortho $v_2 = 1$ $l_2 = 1$ states of H_3^+ with core angular momentum $N^+ < 2$. Referring to Table II, these are the states $(N^+ = 1, G = 0)$, $(N^+ = 2, G = 0)$, and $(N^+ = 2, G = 3)$. These three core states give rise to three $N = 1$ states of H_3 when combined with the $l = 1$ $3p$ orbital. The $3p$ orbital contributes an overall symmetry of A_1' (in the direct product sense). The two resulting H_3 levels with $G = 0$ will have overall symmetry A_2', while the $G = 3$ H_3 level will have overall symmetry A_2''. These A_2' levels correspond, in the Hund's case (b) limit, to the electronic states designated $3p\,^2E'$ and $3p\,^2A_2''$. Since the $3p\,^2E'$ state lies about 3800 cm^{-1} lower in energy than the $3p\,^2A_2''$ state, Hund's case (b) is likely to be a good approximation.

The symmetry of any level is determined by the parity of N and the combination $v_2 + l - G$; the foregoing construction is therefore also valid for the $v_2 = 3$, $l_2 = 1$ levels listed in Table II. This results in two more bending-excited A_2' levels. The selection rules will allow transitions to the A_2' levels we have so constructed, as well as other A_2' levels obtained from these by the addition of any amount of symmetric-stretch excitation. Energy considerations limit the candidate $3p$ levels to the once-excited $3p\,^2A_2''$ ($v_1 = 0$, $v_2 = 1$) and multiply excited $3p\,^2E''$ (1,1) and $3p\,^2E'$ (0,3) levels. [A transition to the $3pE'$ (0,1) level is allowed by symmetry, but for this level, the second photon has insufficient energy to reach the H_3^+ (0,1) threshold. We have also foregone discussion of $l_2 > 1$ levels. For example, the $3p\,^2E'$ ($v_1 = 0, v_2 = 3, l_2 = 3$) level would be energetically accessible; however, for the $N = 1$, $l_2 = 3$ p-state level, angular momentum requires that $G = 3$, and this level has the wrong symmetry.]

The expected Hund's case (d) bending-excited $3d$ states with $N = 1$ can be constructed by adding a $3d$ electron to each of the five states of $v_2 = 1$ ortho H_3^+ with $N^+ < 3$: $(N^+ = 1, G = 0)$, $(N^+ = 2, G = 0)$, $(N^+ = 2, G = 3)$, $(N^+ = 3, G = 0)$, and $(N^+ = 3, G = 3)$. Since the $3d$ orbital contributes overall symmetry A_1', only the $(N^+ = 2, G = 3)$ and $(N^+ = 3, G = 3)$ core states survive as candidate par-

TABLE III. Estimated rotationless level energies.

State	(v_1, v_2, N, G)	Overall symmetry label	Hund's Case (b) ion-core parentage	E_{Herz}[a]	Core rotational energy	Rotationless energy
$3dA_1'$	(0,0,1,0)	A_2'	40% $(N^+=1, G=0)$ 60% $(N^+=3, G=0)$	17 741.73	431 ± 86	17301 ± 86
$3dE''$	(0,0,0,1)	E''	100% $(N^+=2, G=1)$	17 415.86	237.35	17178.5
$3dE''$	(0,0,1,0)	A_2'	60% $(N^+=1, G=0)$ 40% $(N^+=3, G=0)$	17 296.75	172 ± 85	$17\,125 \pm 85$
$3dE'$	(0,0,1,3)	A_2''	100% $(N^+=3, G=3)$	17 196.38	315.29	16881.1
$3dE'$	(0,0,0,2)	E'	100% $(N^+=2, G=2)$	17 043.74	169.27	16874.5
$3dE'$	(0,0,2,0)	A_2'	80% $(N^+=1, G=0)$ 20% $(N^+=3, G=0)$	17 001.17	130 ± 43	16871 ± 43
$3pA_2''$	(0,0,0,0)	A_2''	100% $(N^+=1, G=0)$	16 796.2	86.96	16709.2
$3sA_1'$	(0,0,1,0)	A_2'	100% $(N^+=1, G=0)$	16 694.97	86.96	16608.0
$3pE'$	(0,0,1,0)	A_2''	100% $(N^+=1, G=0)$	12 998.69	86.96	12911.7

[a] From the data in Refs. 2, 4, and 5.

ents. In Hund's case (b), the resulting H_3 states would be designated $3d\,^2E'$ and $3d\,^2E''$.

At this point in our analysis we have four peaks to assign [(D), (E), (F), and (H)] and five candidate levels: the $3p\,^2E'(v_1=1, v_2=1)$, $3p\,A_2''(0,1)$, $3d\,^2E'(0,1)$, $3d\,^2E''(0,1)$, and $3p\,^2E'(v_1=0, v_2=3, l_2=1)$ levels. If we adopt the simple approach (model I) of adding the vibrational origin frequencies (Table II) to the energy of the lowest ortho level of the vibrationless $3p$ and $3d$ states (Table III) we obtain the six predicted transition energies, 18 553, 19 317, 19 717, 19 818, and 20 009 cm^{-1} (listed under model I in Table I), tempting us to assign them to peaks (D), (E), (F), (G), and (H). Having already assigned peak (G) to symmetric-stretch excitation we must conclude that one of the predicted bending-excited transitions must be too weak to observe under the present conditions. The assignment of peak (D) to $3p^2E'(1,1)$ appears unavoidable, and $3p\,^2A_2''(0,1)$ is a good candidate for peak (E). Some of the remaining candidate levels might be weaker due to the large changes in quantum numbers, $\Delta G = 3$ for the $3d$ states and $\Delta v_2 = 3$ for the $3p$ states, and the upper level of the $3d$ pair could be made weaker by l uncoupling (all of which increases the splitting between the $3d$ levels).

Final analysis

So far we have considered only "electronic" and "vibrational" contributions to the transition energy. To make more careful estimates of the transition energies, we estimate the magnitude of the "rotational" contribution (model II). To do this we analyze the various H_3 states in terms of the "fractional parentage" of the various H_3^+ core states from which they can be constructed.

Herzberg *et al.*[5] indicate with the symbol R the rotational quantum number of the dominant H_3^+ core configuration for the $3d$ states of H_3^* and D_3^*; we are using N^+ to indicate the angular momentum of a H_3^+ rovibrational wave function. In a Hund's case (d) model, only one H_3^+ core configuration contributes. In Hund's case (b), we can calculate the relative contributions using angular momentum addition rules. The actual states are expected to be described by "intermediate" coupling, or a mixture of the pure Hund's cases. Following the work of Chang and Fano[28] and Pan and Lu[27] we write[25] the expansion of a Hund's case (b) wave function, $\Xi^{vLN}_{l\lambda+K^+}$, in terms of Hund's case (d) wave functions, $\gamma^{vlLN^+K^+}_{NM}$, as

$$\Xi^{vLN}_{l\lambda+K^+} = \sum_{N^+} \gamma^{vlLN^+K^+}_{NM}(-1)^{(L-\lambda)}(L\lambda, N-\lambda-K^+|LNN^+-K^+) \times [(1+\delta_{l0}\delta_{K^+0})/(1+\delta_{l0}\delta_{\lambda 0}\delta_{K^+0})]^{1/2}, \quad (1)$$

where $(L\lambda, N-\lambda-K^+|LNN^+-K^+)$ is a Clebsch–Gordon coefficient. This formula allows us to estimate the fractional parentage of the known vibrationless levels of H_3^* (given in Table III) and predicted bending-excited levels (given in Table IV).

Our model II consists of three steps. First, we construct a "rotationless" energy for each of the vibrationless $3p\,^2E'$, $3s\,^2A_1'$, $3p\,^2A_2''$, $3d\,^2E'$, $3d\,^2E''$, and $3d\,^2A_1'$ states by subtracting the estimated rotational energy of the underlying core from the various known energy levels. We have taken the core rotational energy to be the average of the Hund's case (b) and Hund's case (d) estimates, and have listed the uncertainty as half the difference between these estimates. The observed level energies, estimates for the rotational en-

ergies, and estimated rotationless level energies are tabulated in the final three columns of Table III. Second, we estimate a rovibrational core energy for the vibrationally excited core states, again taking the Hund's case (b) and Hund's case (d) average. Finally, we add this rovibrational core energy to the electronic rotationless energy to produce the calculated transition energy. The results of steps two and three are listed in Table IV.

Consider, for example, the $3d\,^2E'$ state, for which three low-lying levels are listed in Table III. The $N=0$ E' and $N=1$ A_2'' levels, which lie at 17 043.74 and 17 196.38 cm^{-1}, respectively, necessarily arise from single H_3^+ core rotational levels. Thus, when we subtract 169.27 cm^{-1} for the $(N^+=2,G=2)$ level and 315.29 cm^{-1} for the $(N^+=3,G=3)$ level (see Table II), we obtain the values 16 874.5 and 16 881.1 cm^{-1} as estimates for the rotationless energy of the $3d\,^2E'$ state. The lower-lying $N=2$ A_2' level at 17 001.17 cm^{-1} arises from a Hund's case (b) core mixture consisting of 80% $(N^+=1,G=0)$ and 20% $(N^+=3,G=0)$. If we add the energies of the corresponding H_3^+ states in the same proportions, we obtain 172.96 cm^{-1} as the Hund's case (b) rotational energy estimate. The Hund's case (d) energy estimate is 86.96 cm^{-1} from the lower-lying $(N^+=1,G=0)$ core level [there is a corresponding $N=2$ A_2' level of the $3d\,^2E''$ state that becomes 100% $(N^+=3,G=0)$ in Hund's case (d)]. Averaging these two estimates, we obtain the 130 ± 43 cm^{-1} core rotational energy and $16\,871\pm43$ cm^{-1} electronic rotationless energy listed in Table III. Despite the large uncertainty limits in the latter case, the agreement among the three calculations of the rotationless energy are in sufficient agreement that we can be relatively confident of the partitioning of electronic and rotational energies.

A similar approach was followed for estimating the rotationless energies for the other levels listed in Table III and for constructing the rovibrational energy estimates listed in Table IV. The final results are also listed in Table I. The level of agreement with the observed transition energies is quite satisfactory, leading to a confident assignment of all the peaks except for (H), for which we have two candidates (either of which could be weak, as mentioned above).

DISCUSSION

We now wish to discuss in more detail two points whose qualitative features merit attention even in the absence of quantitative support. The first point regards the splittings of the spectral features seen in Fig. 4. The origin of the splitting is attributed to rapid predissociation of the intermediate level. The qualitative explanation is as follows: since the cross section for photoionization of the intermediate is less than that for the bound–bound absorption step $3l\leftarrow 2p$, the leading edge of the laser pulse may have sufficient intensity to saturate the bound–bound transition, but insufficient intensity to photoionize the intermediates. Provided that the predissociation lifetime of the intermediate is much smaller than the width of the laser pulse, a significant portion of the intermediate state population can decay by predissociation before it is photoionized. The cross section for the discrete absorption step varies across the excitation line profile, while the two mechanisms for removal of the intermediate population (predissociation and bound–free photoionization) remain constant. At line center saturation is quite easily accomplished by the leading edge of the laser pulse and it is there that predissociation can effectively complete with ionization.

It seems, therefore, that the intermediates pumped in transitions D,G, and I [see Fig. 3(b)] predissociate on a time scale comparable to or shorter than the laser pulse width, while peaks (E), (F), and (H) are transitions through intermediates with longer lifetimes. Reference to Fig. 4 shows that the three transitions displaying the peak splitting effect are assigned to intermediate levels which possess a quantum of symmetric-stretch excitation; the remaining three transitions are assigned to intermediate levels having no symmetric-stretch excitation. This suggests to us that

TABLE IV. Ion core parentages in Hund's cases (b) and (d) for bending excited species with $N=1$ and overall symmetry A_2' of ortho H_3; comparison of estimated and observed transition energies.

State	(v_1, v_2, N, G)	Case (b)	Case (d)	E_{ELEC}	E_{ROVIB}	E_{CALC}[a]	E_{OBS}
$3pE'$	(0 3 1 0)	50%$(N^+=1,G=0)$ 50%$(N^+=2,G=0)$	100%$(N^+=1,G=0)$	12 912	7149 ± 48	20061 ± 48	19994 ± 1
$3dE''$	(0 1 1 3)	33%$(N^+=2,G=3)$ 67%$(N^+=3,G=3)$	100%$(N^+=3,G=3)$	17 179	2833 ± 44	20012 ± 44	19994 ± 1
$3dE'$	(0 1 1 3)	67%$(N^+=2,G=3)$ 33%$(N^+=3,G-3)$	100%$(N\pm=2,G=3)$	16 878 ± 3	2658 ± 44	19536 ± 44	19542.4 ± .4
$3pA_2'$	(0 1 1 0)	50%$(N^+=1,G=0)$ 50%$(N^+=2,G=0)$	100%$(N^+=2,G=0)$	16 709	2764 ± 49	19473 ± 49	19451.5 ± .2
$3pE'$	(1 1 1 0)	50%$(N^+=1,G=0)$ 50%$(N^+=2,G=0)$	100%$(N^+=1,G=0)$	12 912	5692 ± 48	18604 ± 48	18521.4 ± .4
$3pE'$	(0 1 1 0)	50%$(N^+=1,G=0)$ 50%$(N^+=2,G=0)$	100%$(N^+=1,G=0)$	12 912	2664 ± 48	15576 ± 48	15 548.8 ± 1[b]

[a]Model II (see the text).
[b]See *Note added in proof.*

the symmetric stretch vibrational mode induces predissociation more rapidly than the bending mode. This conjecture is supported by the lower ion count rates for the symmetric-stretch intermediates [Fig. 3(b)], indicating a stronger competition with the bound–free photoionization step. Effects similar to those shown here have been observed recently by Didier[29] in H_2 and by Haberland *et al.*[30] in He. (In the latter case, competition for bound–free photoionization was provided not by predissociation, but by the natural radiative decay of $1s3p\ ^3P$ intermediate levels). We note in addition that we have not observed splittings for the transitions to the vibrationless $3dE''$ or $3sA_1'$ intermediates, which certainly have stronger transition moments than their symmetric-stretch excited counterparts. This militates against considering the ac Stark effect as the origin of the line splittings.

Analysis of the intensities of the two-photon transitions is difficult both experimentally and theoretically. As described above, the first step of the two-photon detection scheme is easily saturated. Thus, the intensities of the peaks may reflect the cross section for photoionization, rather that the transition probability to the intermediate states. The strengths of the transitions resulting in excitation of the symmetric-stretch level could be estimated from a Franck–Condon analysis of the vibrational wave functions for the upper and lower potential energy surfaces. As in diatomic molecules, we expect vibrationally off-diagonal transitions only if the symmetric-stretch potentials differ in the upper and lower states.

Excitation of an odd number of bending quanta requires more thoughtful analysis. Consider the simplest case, the $3p\ ^2A_2''\cdot\chi_1 \leftarrow 2p\ ^2A_2''\cdot\chi_0$ transition, in which we have used the notations χ_1 and χ_0 to indicate the first-excited and ground-state bending vibrational wave functions. Since the vibrational wave functions are of different symmetry the optical dipole operator must be used to connect them. Thus we might write

$$\langle 3pA_2''\cdot\chi_1|\mu|2pA_2''\cdot\chi_0\rangle \simeq \langle 3pA_2''|2pA_2''\rangle\ \langle\chi_1|\mu|\chi_0\rangle$$

and would conclude that the Rydberg electron is a "spectator" to the transition, much as vibration is described as a spectator in the Franck–Condon principle. From this we conclude that the transition probability depends on the overlap between the nominal $3p$ and $2p$ orbitals, and is nonzero only to the extent that the electronic wave functions (or quantum defects) are different for the bending-excited and ground-vibrational states. In fact, the total rovibronic wave functions for the states we have labeled $3pA_2''$ and $2pA_2''$ contain small contributions from other rovibronic configurations; this will create additional sources of transition probability. These additional sources become essential for transitions such as $3pE'\chi_1 \leftarrow 2pA_2''\chi_0$. In this case, the initial and final electronic wave functions are also of different symmetry and cannot be connected by the dipole operator.

Further refinements will require a model hamiltonian, beginning with that used by Herzberg *et al.*,[5] which we will use to study the l uncoupling throughout the *np*, *nd*, and *nf* Rydberg series.[25] Particularly interesting will be development of means of estimating the extent of mixing between configurations of different l, based presumably on calculated permanent and dynamic electrostatic moments of H_3^+.

CONCLUSIONS

Using a two-step photoionization scheme in a fast–neutral-beam spectrometer, we have measured the positions of vibrationally excited levels of the $n = 3$ Rydberg manifold of H_3. We find symmetric-stretch vibrational frequencies of 3212.1 and 3168 cm^{-1} for the $3s\ ^2A_1'$ and $3d\ ^2E''$ states, respectively. In conjunction with results from photodissociation studies performed in this laboratory, we also infer a symmetric-stretch frequency for the $2pA_2''$ metastable level of 3254 ± 1.2 cm^{-1}. These values may be compared to the calculated frequency of 3178 cm^{-1} for the H_3^+ ion.[20]

We have assigned four transitions involving the asymmetric stretch or bending vibration. Direct determination of the fundamental bending frequencies is not possible from the available data, due to the yet unknown rotational energies of the bending excited molecule, but the simple model used to assign the spectrum shows that the bending vibrational frequencies are nearly equal to those of H_3^+.

In a similar study, we are probing higher Rydberg levels by utilizing one and two-color excitation schemes. This allows one to measure directly the vibrational frequencies in the H_3^+ ion,[21] as well as $n > 3$ states of H_3.

Note added in proof: The $3pE'(0,1,1,0)$ level, noted as being unobservable with the technique described herein, has been subsequently observed using a double-resonance technique ("V configuration") that relies on the dissociation of the $3p$ resonance to induce dimunition in the ionization of a high-lying Rydberg level.

ACKNOWLEDGMENT

This research was supported by the Air Force Office of Scientific Research under Contract No. F49620-87-K-0002.

[1]G. Herzberg, J. Chem. Phys. **70**, 4806 (1979).
[2]I. Dabrowski and G. Herzberg, Can. J. Phys. **58**, 1238 (1980).
[3]G. Herzberg and J. K. G. Watson, Can J. Phys. **58**, 1250 (1980).
[4]G. Herzberg, H. Lev, J. J. Sloan, and J. K. G. Watson, Can. J. Phys. **59**, 428 (1981).
[5]G. Herzberg, J. T. Hougen, and J. K. G. Watson, Can. J. Phys. **60**, 1261 (1982).
[6]F. M. Devienne, C. R. Acad. Sci. Paris B **267**, 1279 (1968).
[7]F. M. Devienne, C. R. Acad. Sci. Paris B **268**, 1303 (1969).
[8]T. Nagasaki, H. Doi, K. Wada, K. Higashi, and F. Fukazawa, Phys. Lett. A **38**, 3821 (1972).
[9]J. M. Gaillard, A. G. de Pinho, J. C. Poizat, J. Remillieux, and R. Saoudi, Phys. Rev. A **28**, 1267 (1983).
[10]G. I. Gellene and R. F. Porter, J. Chem. Phys. **79**, 5975 (1983).
[11]J. F. Garvey and A. Kuppermann, Chem. Phys. Lett. **107**, 4921 (1984).
[12]H. Helm, Phys. Rev. Lett. **56**, 42 (1986).
[13]J. F. Garvey and A. Kuppermann, J. Chem. Phys. **86**, 6766 (1987).
[14]H. Helm, Phys. Rev. A **38**, 3425 (1988).
[15]L. Lembo, D. L. Huestis, and H. Helm (in preparation).
[16]P. C. Cosby and H. Helm, Phys. Rev. Lett. **61**, 298 (1988).
[17]Ch. Nager and M. Jungen, Chem. Phys. **70**, 189 (1982).
[18]T. Oka, Phys. Rev. Lett. **45**, 531 (1980).
[19]J. K. G. Watson, S. C. Foster, A. R. W. McKellar, P. Bernath, T. Amano, F. S. Pan, M. W. Crofton, R. S. Altman, and T. Oka, Can. J. Phys. **62**, 1875 (1984).
[20]S. Miller and J. Tennyson, J. Mol. Spectrosc. **128**, 530 (1988).

[21]L. J. Lembo, A. Petit, and H. Helm, Phys. Rev. A (in press).
[22]*Atlas da Spectre de la Molecule de I/Iode*, edited by S. Gerstenkhorn and P. Luc (Editions du C.N.R.S., Paris, 1978).
[23]J. T. Hougen, J. Chem. Phys. 37, 1433 (1962).
[24]P. R. Bunker, *Molecular Symmetry and Spectroscopy* (Academic, New York, 1979).
[25]D. L. Huestis (in preparation).
[26]J. Tennyson and B. T. Sutcliffe, Mol. Phys. 51, 887 (1984).
[27]S. Pan and K. T. Lu, Phys. Rev. A 37, 299 (1988).
[28]E. S. Chang and U. Fano, Phys. Rev. A 6, 173 (1972).
[29]D. Normand and J. Morellec, J. Phys. B 21, L625 (1988).
[30]H. Haberland, M. Oschwald, and J. Broad, J. Phys. B 20, 3367 (1987).

Appendix D

OBSERVATION OF LOW-LYING RYDBERG STATES OF THE TRIATOMIC HYDROGEN MOLECULE

L. J. Lembo and H. Helm

Chem. Phys. Lett. 163, 425 (1989)

OBSERVATION OF LOW-LYING RYDBERG STATES OF THE TRIATOMIC HYDROGEN MOLECULE

L.J. LEMBO and H. HELM
Molecular Physics Laboratory, SRI International, Menlo Park, CA 94025, USA

Received 28 June 1989

A double-resonance scheme has been employed to locate vibrationless and symmetric-stretch-excited levels of the $nd\,^2E''$ and $s\,^2A_1'$ electronic states of triatomic hydrogen for the $n=4$–7 Rydberg manifolds. Symmetric-stretch frequencies follow from combination differences, and information on level widths and predissociation lifetimes is also obtained.

1. Introduction

The past decade has seen a proliferation of spectroscopic studies targeting the triatomic hydrogen molecule (H_3). These experiments have taken the form of emission studies, either in hollow-cathode discharges [1–4] or fast molecular beams [5–7], and fast-beam laser photoabsorption experiments [8–11]. The studies of Herzberg and coworkers were the first to identify rotational bands of H_3 and D_3 emitted from a hydrogen discharge [1–4]. These included visible bands resulting from $n=3$ to $n=2$ transitions, and infrared transitions among the $n=3$ states. Subsequent experiments succeeded in stimulating transitions in the $n=3$ to $n=2$ rotational bands using a hollow-cathode discharge placed inside a laser cavity [12]. With two tentative exceptions [4,7], all transitions observed in these experiments take place between levels with zero-vibrational excitation. Observation of transitions involving levels with $n>3$ seems equally difficult utilizing discharge techniques [13].

Fast-beam studies performed in this laboratory [8,10] and in Munich [11] have exploited the metastability of the rotationless ($N=0$) level of H_3 in the $2p\,^2A_2''$ electronic state in order to excite transitions to levels unobservable with the discharge techniques. Laser spectroscopy has been performed on single-photon transitions to vibrationless levels with $n>10$, detected using field-ionization techniques, and vibrationally excited levels with $n\geq 6$, detected by virtue of vibrational autoionization. More recently, we have extended the fast-beam studies and observed vibrationally excited levels in the $n=3$ manifold using two-step photoionization [14]. These studies have yielded measurements of the symmetric-stretch frequencies of the $3s\,^2A_1'$ and $3d\,^2E''$ electronic states. Here, we report an extension of this work to states with principal quantum number [4–7].

This includes the first observations of photoexcitation to the vibrationless levels of the $ns\,^2A_1'$ and $nd\,^2E''$ electronic states ($n=4$–7), as well as symmetric-stretch vibrationally excited levels of the $n=4$ and 5 manifolds. Together with previous observations of the symmetric-stretch level in the $3d\,^2E''$ state [14] and vibrationally autoionizing nd levels [8,15,16] for $n=6$–45, these observations result in the first complete characterization of a Rydberg series in H_3 from the lowest possible n-level up to $n=45$.

2. Experimental technique

The fast-beam laser spectrometer employed for these measurements has been described in detail elsewhere [8]. Briefly, a mass-selected beam of 1.5 keV H_3^+ ions traverses a cesium-vapor cell, where charge transfer creates a fast beam of neutral triatomic hydrogen in the metastable $2p\,^2A_2''$ level. A few cm downstream from the charge-transfer region,

0 009-2614/89/$ 03.50

this beam is comprised essentially of H_3 molecules populated in a distribution of rotationless levels that have a range of vibrational excitation [8]. One or more laser beams are directed coaxially to this molecular beam. Ions created as a result of this interaction are detected with a channel-electron multiplier. By varying the laser wavelength, photoabsorption spectra are accumulated under computer control, counting ions and background signal for each laser shot using a pair of gated scalers.

Fig. 1 shows an energy-level diagram of H_3 and depicts the ionization–dissociation double-resonance technique employed for these measurements. We use one excimer laser to pump two pulsed dye lasers, hereafter lasers I and II. The laser pulse durations are ≈ 15 ns; the pulse from laser I is (geometrically) delayed by ≈ 20 ns. Laser I is held at a fixed frequency and used to ionize a particular vibrational level of the rotationless $2p\,^2A_2''$ state; its ionization signal serves to monitor changes in the population of the selected level that are induced by laser II, which stimulates transitions from the $2p\,^2A_2''$ state to ns and nd levels in the $n=4$ to 7 electronic manifolds. To the extent that low-n levels populated by laser II either predissociate or else radiate to states other than the metastable level, the effect of laser II will be to deplete the lower $2p\,^2A_2''$ level and create a diminution in the ionization rate induced by laser I. The pulse energy of laser II is kept low enough so that it does not produce any ions on its own via two-step photoionization [14]. To study transitions from the vibrationless ($v_1=0$, $v_2=0$) metastable level, laser I is tuned to the R(0) line of the $40d\,^2E''(0,0) \leftarrow 2p\,^2A_2''(0,0)$ transition; this excitation is monitored by field ionization of the 40d level. Transitions from the symmetric-stretch-excited metastable level ($v_1=1$, $v_2=0$) are detected by labeling the $2p\,A_2''(1,0)$ level via excitation to the $6d\,^2E''(1,0)$ vibrationally autoionizing level. The twice symmetric-stretch-excited $2p\,^2A_2''(2,0)$ and the bending-excited $2p\,^2A_2''(0,1)$ level are also present in the metastable beam [8,16]; no attempt has yet been made to label these levels in the sort of double-resonance experiment described here.

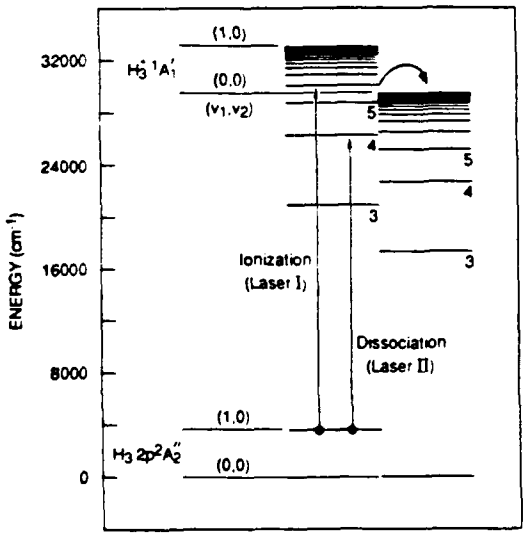

Fig. 1. Double-resonance scheme for the detection of $n=3$–7 vibrationless and symmetric-stretch-excited levels. The $2p\,^2A_2''$ population is monitored in ionization with laser I; here, laser I is shown labeling the symmetric-stretch-excited level: $(v_1, v_2) = (1,0)$. The photodissociation laser (II) pulse arrives prior to the laser I pulse.

The spectra are calibrated by feeding a small portion of the output of laser II into a grating monochromator and recording the wavelengths for each depletion resonance. In order to account for the substantial first-order Doppler shift (10^{-3}) of the 1.5 keV H_3 molecules, depletion spectra are taken with the neutral H_3 beam and laser II in the counter and copropagating configurations. The geometric mean of the transition frequencies so recorded equals the H_3-rest-frame transition frequency. Experimental uncertainty is limited by the monochromator accuracy; we estimate an uncertainty of ± 1 cm^{-1} for the rest-frame frequencies. This was verified by measuring the positions of the vibrationless $n=3$ levels and comparing them with Herzberg's results [1,4].

The appeal of the depletion technique, using two time-delayed laser beams, may be appreciated by comparison with the two-step ionization technique, described in ref. [14], used to observe the vibrationally excited levels in the $n=3$ manifold; in the latter technique one tunable laser is used to excite both the bound–bound transitions to the $n=3$ levels and the subsequent bound–free ionization step. The resulting spectrum is shown in the upper trace of fig. 2; the lower trace of fig. 2 shows the depletion spectrum taken for the same set of levels. Here, laser I labels the $2p\,^2A_2''(0,0)$ level. Electronic and vibrational assignments for the intermediates are indi-

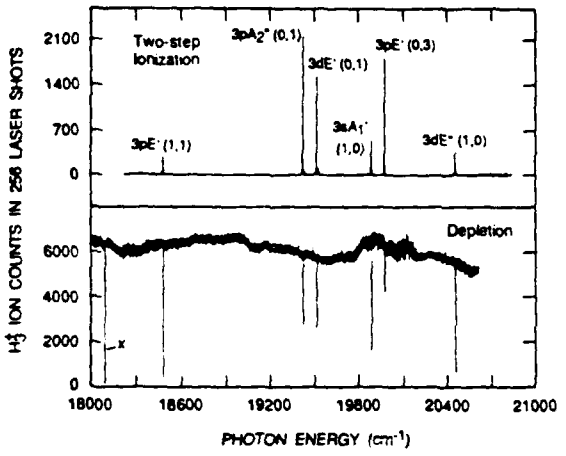

Fig. 2. Comparison of one-color two-step ionization (upper) and two-color depletion (lower) spectrum of vibrationally excited levels in the $n=3$ electronic manifold of H_3. The somewhat uneven ionization baseline reflects the experimental stability (neutral beam + laser I) over the required 25 h of data acquisition time.

cated. It is readily seen that "dips" occur in the depletion spectrum at the positions of the previously observed ionization peaks [#1]. The depletion dips are observed with laser II pulse energies of $\lesssim 100$ μJ; this is to be compared to the pulse energies of ≈ 4 mJ required for the creation of ions by two-step ionization. We find that despite the lower power, the size of the depletion dips can be greater than the corresponding ionization peaks by as much as a factor of 10. In fact, several of the depletion signals indicate that the $2p \rightarrow 3\ell$ transitions result in almost total depletion of the $2p\,^2A_2''$ level; this remains true for all of the transitions discussed in this paper.

A peculiarity of the two-step ionization technique (fig. 2, upper spectrum) is that predissociation of the intermediate ($n=3$) levels competes with the photoionization step, creating misleading relative intensities and apparent spectral-line splittings [14]. Based on the consistently lower intensities (see fig. 2) and spectral lineshapes for the symmetric-stretch-excited levels, we have suggested [14] that predissociation is relatively rapid for this mode of vibration. This is supported by the depletion spectrum in fig. 2, which shows that transitions to the symmetric-stretch levels are at least as strong as those to levels having no symmetric-stretch excitation (see fig. 2). In summary, the depletion scheme offers the advantage of detecting levels that are difficult to photoionize either because of rapid predissociation or small photoionization cross section.

[#1] The dip labeled "×" was not scanned in the previous ionization experiment [14]. It has been tentatively assigned to the 3p E'(0,2) level; the observed energy is 18139 ± 1 cm^{-1}.

3. Results

The double-resonance technique described above was used to observe vibrationless and symmetric-stretch-excited levels in the $n=4$–7 Rydberg manifolds. Fig. 3 shows typical spectra recorded for the $n=4$ levels. The lower trace was taken with laser I labeling the $2p\,^2A_2''(0,0)$ (i.e. vibrationless) level and shows depletion resonances that we identify as transitions to the $4s\,^2A_1'(0,0)$ and $4d\,^2E''(0,0)$ levels. Similarly, the upper trace was taken with laser I labeling the $2p\,^2A_2''(1,0)$ level and reveals the $4s\,^2A_1'(1,0)$ and $4d\,^2E''(1,0)$ (i.e. symmetric-stretch-excited) levels. These spectra were recorded with laser II pulse energies of ≈ 50 μJ and indicate further the ease with which these transitions deplete the lower $2p\,^2A_2''$ level.

In an earlier investigation, we measured the $2p\,^2A_2''(0,0)$ to $2p\,^2A_2''(1,0)$ interval to be 3255.4 ± 1 cm^{-1} [15]. Adding this value to the transition energies recorded in the upper trace of fig. 3 allows one

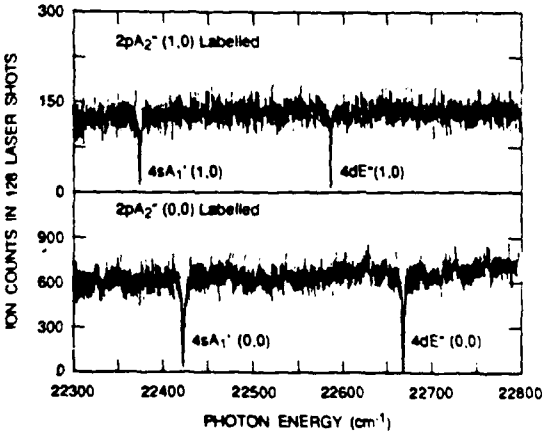

Fig. 3. Depletion spectra showing the $n=4$ symmetric-stretch-excited (upper) and vibrationless (lower) $4s\,^2A_1'$ and $4d\,^2E''$ levels. Photon energy scale refers to the molecular rest frame.

to reference both vibrationless and vibrationally excited Rydberg levels to a common level, namely, the vibrationless $2p\,^2A_2''$. In an identical fashion, we have measured the positions of vibrationless levels in the $n=5$–7 $s\,^2A_1'$ and $d\,^2E''$ states, and symmetric-stretch levels for $n=5$. The symmetric-stretch-excited $n=6$ and 7 levels lie above the lowest H_3 ionization threshold, and were observed in earlier studies via single-photon autoionization [15]. The energies of the vibrationless $n=3$ levels have been most accurately determined by Herzberg [1–4], and the symmetric-stretch $n=3$ levels by our own two-step ionization studies [14]. The energies of vibrationless and vibrationally excited $s\,^2A_1'$ and $d\,^2E''$ levels for $n=3$–7 are summarized in table 1. Additional depletion resonances were observed in this study; for most of them, no tentative assignments yet exist. Table 2 lists the photon energies at which these resonances occur along with the level in the $2p\,^2A_2''$ state from which they were observed. This latter bit of information is important since one cannot a priori rule out the possibility that the depletion resonance lies energetically below rather than above the labeled level.

3.1. Vibrational frequencies

Since all levels found in table 1 are accessed in single-photon transitions from a rotationless $2p\,^2A_2''$ level, they have a total angular momentum of $N=1$ (exclusive of spin). Combination differences of the level positions may be used to obtain the interval between the $N=1$ vibrationless and symmetric-stretch levels in the $n=3$–7 manifolds. These are given in the second column of table 3. Hereafter, we shall refer to this interval as the "symmetric-stretch frequency". The corresponding interval for the hypothetical $N=0$ states is usually understood implicitly to be "the" symmetric-stretch frequency, and will differ from the $N=1$ interval by twice the difference

Table 1
Positions of vibrationless and symmetric-stretch-excited $n=3$–7 electronic states. All levels have total angular momentum $N=1$

Electronic state	Vibration	Energy (cm^{-1}) [a]	Width (cm^{-1}) [e]
$2s\,^2A_1'$	(0,0)	−898 [b]	30 [b]
$3s\,^2A_1'$	(0,0)	16694.972 [b]	<0.005 [f]
	(1,0)	19907.1 ± 0.3 [c]	–
$3d\,^2E''$	(0,0)	17296.982 [b]	<0.005 [f]
	(1,0)	20465.4 ± 1.0 [c]	–
$4s\,^2A_1'$	(0,0)	22422.2 ± 1	0.7
	(1,0)	25631.0 ± 1	0.2
$4d\,^2E''$	(0,0)	22668.2 ± 1	–
	(1,0)	25841.6 ± 1	–
$5s\,^2A_1'$	(0,0)	25032.2 ± 1	1.2
	(1,0)	28222.6 ± 1	–
$5d\,^2E''$	(0,0)	25158.1 ± 1	–
	(1,0)	28328.3 ± 1	0.2
$6s\,^2A_1'$	(0,0)	26435.4 ± 1	–
	(1,0)	29618.8 ± 1 [d]	4
$6d\,^2E''$	(0,0)	26503.0 ± 1	–
	(1,0)	29676.4 ± 0.5 [d]	0.9
$7s\,^2A_1'$	(0,0)	27277.6 ± 1	–
	(1,0)	30456.5 ± 1.5 [d]	<1.0
$7d\,^2E''$	(0,0)	27317.4 ± 1	–
	(1,0)	30489.9 ± 5 [d]	<0.2

[a] *All energies relative to* ($N=0$, $K=0$) $2p\,^2A_2''(0,0)$ level. [b] From Herzberg's data. See refs. [1–4].
[c] Measured in two-step ionization studies [14]. [d] Observed in vibrational autoionization [8,15,16].
[e] Unless otherwise noted, linewidths are laser-bandwidth limited ($\lesssim 0.2\ cm^{-1}$). [f] Ref. [18].
[g] *In ref. [15], we reported a linewidth of 0.4* cm^{-1}; *subsequent measurements* have shown this to be power broadened. Lower laser power results in a laser-bandwidth limited lifetime, as listed here.

Table 2
Transition energies for depletion resonances not belonging to $ns\,^2A_1'$ or $nd\,^2E''$ series, $2p\,^2A_2''$ level from which they were observed, and assignment where possible

Transition energy (cm^{-1}) [a]	Lower level	Assignment
18138.7	$2p\,^2A_2''(0,0)$	$3p\,^2E''(0,2)$
22897.1	$2p\,^2A_2''(0,0)$	–
23102.0	$2p\,^2A_2''(0,0)$	$4d\,^2A_1'(0,0)$
25047.8	$2p\,^2A_2''(0,0)$	–
25114.5	$2p\,^2A_2''(0,0)$	–
24923.3	$2p\,^2A_2''(1,0)$	–
25167.6	$2p\,^2A_2''(1,0)$	–

[a] Uncertainty limits $\pm 1\ cm^{-1}$.

Table 3
Symmetric-stretch frequencies of $n=3$–7 electronic states in H_3, and of H_3^+

Electronic state	ν_1 (cm^{-1}) [a]	r_e (Å) [c]
$2p\,^2A_2''$	3255.4 ± 1 [b]	0.868
$3s\,^2A_1'$	3212.1 ± 0.3	0.871
$4s\,^2A_1'$	3208.8 ± 2	
$5s\,^2A_1'$	3190.4 ± 2	
$6s\,^2A_1'$	3183.4 ± 2	
$7s\,^2A_1'$	3178.9 ± 2	
$3d\,^2E''$	3168.4 ± 1	0.880
$4d\,^2E''$	3173.4 ± 2	
$5d\,^2E''$	3170.2 ± 2	
$6d\,^2E''$	3173.3 ± 2	
$7d\,^2E''$	3172.5 ± 2	
H_3^+	3176.1 ± 1 [b]	0.876

[a] With the exception of the $2p\,^2A_2''$ state, the quoted frequencies correspond to the energy difference between the $N=1$ rotational levels in the vibrationless and symmetric-stretch-excited state.
[b] From ref. [15]. [c] Ref. [13].

in rotational constants for the (0,0) and (1,0) levels. In the ground electronic state of the H_3^+ ion, this difference equals 2.12 cm^{-1} [18].

Also included in table 3 are the symmetric-stretch frequencies of the $2p\,^2A_2''$ state and of the ground state of the H_3^+ ion [15,16]. It can be seen that states of symmetry $d\,^2E''$ have frequencies lower than that of the ion, while the $2p\,^2A_2''$ and $s\,^2A_1'$ states have frequencies greater than that of the ion. This suggests that the $d\,^2E''$ Rydberg orbitals have an antibonding character, while the $2p\,^2A_2''$ and $s\,A_1'$ orbitals have a bonding character. This pattern correlates in a physically intuitive way with the experimental values for the equilibrium internuclear distances, r_e, in the $2p\,^2A_2''$, $3s\,^2A_1'$, $3d\,^2E''$, and the H_3^+ states. The experimental r_e values are listed in the final column of table 3; they are derived [13] from analyses of the rotational band structures observed by Herzberg's group [1,4] and by Oka [19]. States whose vibrational frequencies are greater than that of the ion have smaller r_e's than that of the ion, an independent indicator of tighter bonding. Conversely, the $3s\,^2A_1'$ state, whose vibrational frequency is smaller than that of the ion, has an r_e which is larger than the ion's. The correlation is depicted graphically in fig. 4.

Another interesting pattern to be observed in the symmetric-stretch frequencies is their dependence on the principal quantum number, n. Without surprise, the symmetric-stretch frequencies within the $ns\,^2A_1'$ and the $nd\,^2E''$ series generally approach the H_3^+ frequency as n increases; the $2p\,^2A_2''$ frequency shows the largest difference of all relative to H_3^+. This trend simply indicates the decreasing interaction between the Rydberg orbital and ion core with increasing principal quantum number. Fig. 5 plots the symmetric-stretch frequencies of all states versus the principal quantum number of the Rydberg electron; frequencies belonging to a given series are connected by line segments, and the H_3^+ frequency is drawn as the dashed horizontal line. This seems a quite plausible asymptote for the $ns\,^2A_1'$ series; the fluctuations

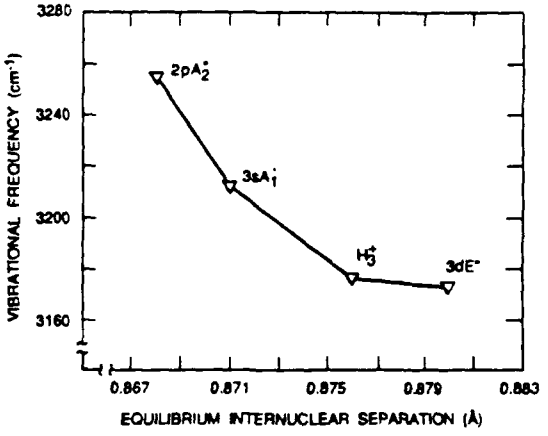

Fig. 4. Symmetric-stretch frequencies of selected H_3 and H_3^+ states plotted against equilibrium internuclear distances derived from rotational band spectra. Frequencies are seen to decrease monotonically with increasing r_e.

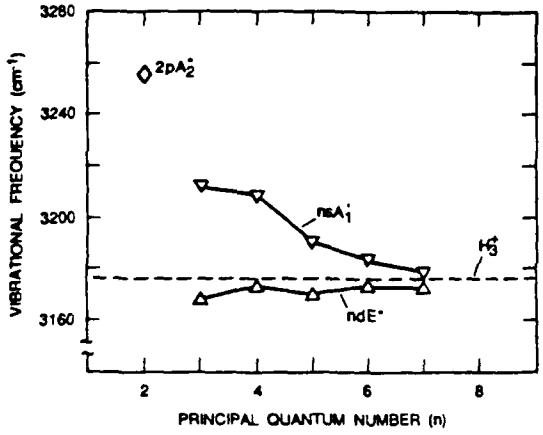

Fig. 5. Vibrational frequencies versus principal quantum number of H_3 Rydberg electron. Frequencies for states belonging to a given series are connected by line segments. Dashed, horizontal asymptote value of H_3^+ frequency.

in the $nd\,^2E''$ series cannot be taken too seriously, as they are within the estimated $\pm 2\ cm^{-1}$ experimental uncertainty.

3.2. Level lifetimes

The widths of the depletion signals contain some information regarding the lifetimes of these levels. We have estimated natural widths for the observed levels, making allowance both for the laser bandwidth ($0.2\ cm^{-1}$) and for the depletion broadening of molecules in the fast beam. The extent of depletion broadening in the fast beam is modeled on the assumption of a lower-state $2p\,^2A_2''$ population, N, that decays with time according to

$$N(t) = N_0 \exp[-R(\nu)\, t]\,, \qquad (1)$$

where $R(\nu)$ is the frequency-dependent laser-induced transition rate to the dissociating level. $R(\nu)$ is taken to be Lorentzian, and we assume that the upper level dissociates so rapidly that the molecule is lost from the fast beam once a transition is induced to the upper level.

Since each molecule sees the laser pulse for some effective time, τ_p, the extent of depletion is given by

$$D(\nu) \equiv 1 - \frac{N(\tau_p)}{N_0} = 1 - \exp[-R(\nu)\,\tau_p]\,, \qquad (2)$$

where

$$R(\nu) = R_0 \frac{1}{1 + (\nu - \nu_0)^2/\gamma_N^2}\,. \qquad (3)$$

The resulting depletion signal has a fwhm linewidth, γ_D, that depends on the natural width γ_N, and the transition strength $R_0\tau_p$. It is a simple matter to calculate that

$$\frac{\gamma_D}{\gamma_N} = \left(\frac{R_0\tau_p}{\ln 2 - \ln[1 + \exp(-R_0\tau_p)]} - 1\right)^{1/2}. \qquad (4)$$

One can also see from eq. (2) that the amount of depletion at line center is given by

$$D(\nu_0) = \exp(-R_0\tau_p)\,. \qquad (5)$$

Taken together, eqs. (4) and (5) have been used to estimate the extent of depletion broadening given the experimental values of $D(\nu_0)$, the "dip strength". We expect the experimental depletion profile to be a convolution of the laser power spectrum and the depletion-broadened signal for an ideal laser; we assume that the experimental linewidth equals the simple addition of the laser bandwidth and the depletion-broadened level width. As an example, the 4s(0,0) level was probed using two different laser intensities. One spectrum showed a depletion depth at line center of 30% and a width of $1.0\ cm^{-1}$. Subtracting the laser linewidth gives a depletion-broadened width of $0.8\ cm^{-1}$. When $D(\nu_0) = 0.3$, eqs. (4) and (5) indicate that $\gamma_D/\gamma_N = 1.1$, giving an estimate of $0.7\ cm^{-1}$ for the natural width of the 4s(0,0) level. A spectrum taken at a higher laser-II intensity showed a depletion depth of 85% and a width of $1.5\ cm^{-1}$. The correction prescription yields a natural width of $0.8\ cm^{-1}$, in agreement with the estimate from the lower intensity spectrum. This width corresponds to a lifetime of ~ 7 ps, confirming that in this case predissociation is the dominant decay mechanism.

Estimates for experimental level widths are listed in the final column of table 1. For most of the observed levels, the widths were limited by the laser bandwidth. It is interesting to note that the vibrationless $4s\,^2A_1'$ and $5s\,^2A_1'$ levels predissociate more rapidly than their symmetric-stretch-excited counterparts. Electronic states of A_1' symmetry are coupled to the dissociative $2p\,^2E'$ state by the bending vibration, which is of symmetry E', and by rotational

(Coriolis) coupling. The symmetric-stretch mode cannot couple the $ns\,^2A_1'$ and $2p\,^2E'$ states, so the addition of a quantum of symmetric-stretch excitation to the $ns\,^2A_1'$ levels cannot change the mechanism of predissociation. It is possible, therefore, that this pattern of linewidths results from the dependence of Franck–Condon factors on the degree of symmetric-stretch excitation. It is also noteworthy that the $2s\,^2A_1'$ and $4s\,^2A_1'$ levels are shorter-lived than either the $3s\,^2A_1'$ or the $5s\,^2A_1'$.

We call attention also to one property of the autoionizing $n=6$ ($v_1=1$) levels observed in this work: the $6s\,^2A_1'(1,0)$ level decays by vibrational autoionization with a rate four times greater than the $6d\,^2E''(1,0)$ level. This comparison is to be expected, since autoionization proceeds via Rydberg-electron/core interactions, and an "s" electron is more likely to be found near the core than a "d" electron.

In summary, we have used an optical–optical double-resonance technique and demonstrated it to be a sensitive method for detecting low-n Rydberg levels of H_3. Vibrationless and symmetric-stretch $ns\,^2A_1'$ and $nd\,^2E''$ levels were detected for $n=4$–7. Symmetric-stretch frequencies were inferred from spectroscopic combination differences; these frequencies approach that of H_3^+ as n increases and correlate in the expected manner with the rotational constants measured by other workers. These frequencies should serve as an additional, more sensitive test than energy-level positions for theoretical calculations of potential-energy surfaces for the various Rydberg states.

Acknowledgement

This research was supported by the Air Force Office of Scientific Research under Contract No. F49620-87-K-0002. We thank Dr. David L. Huestis for many helpful discussions and Professor Nis Bjerre for communicating his unpublished results for the $3s\,^2A_1'$ and $3d\,^2E''$ lifetimes.

References

[1] I. Dabrowski and G. Herzberg, Can. J. Phys. 58 (1980) 1238.
[2] G. Herzberg and J.K.G. Watson, Can. J. Phys. 58 (1980) 1250.
[3] G. Herzberg, H. Lew, J.J. Sloan and J.K.G. Watson, Can. J. Phys. 59 (1981) 428.
[4] G. Herzberg, J.T. Hougen and J.K.G. Watson, Can. J. Phys. 60 (1982) 1261.
[5] H. Figger, M.N. Dixit, R. Maier, W. Shrepp, H. Walther, I.R. Peterkin and J.K.G. Watson, Phys. Rev. Letters 52 (1984) 906.
[6] H. Figger, Y. Fukuda, W. Ketterle and H. Walther, Can. J. Phys. 62 (1984) 1274.
[7] A.B. Raksit, R.F. Porter, W.P. Garver and J.J. Leventhal, Phys. Rev. Letters 55 (1985) 378.
[8] H. Helm, Phys. Rev. Letters 56 (1986) 42; Phys. Rev. A 38 (1988) 3425.
[9] S.F. Selgren and G.I. Gellene, Chem. Phys. Letters 146 (1988) 485.
[10] P.C. Cosby and H. Helm, Phys. Rev. Letters 61 (1988) 298.
[11] A. Dodhy, W. Ketterle, H.P. Messmer and H. Walther, Chem. Phys. Letters 151 (1988) 133.
[12] H. Figger, H. Moller, W. Shrepp and H. Walther, Chem. Phys. Letters 90 (1982) 90.
[13] J.K.G. Watson, to be published.
[14] L.J. Lembo, H. Helm and D.L. Huestis, J. Chem. Phys. 90 (1989) 5299.
[15] L.J. Lembo, A. Petit and H. Helm, Phys. Rev. A 39 (1989) 3721.
[16] W. Ketterle, H.-P. Messmer and H. Walther, Europhys. Letters 8 (1989) 333.
[17] N. Bjerre, private communication.
[18] S. Miller and J. Tennyson, J. Mol. Spectry. 128 (1988) 530.
[19] T. Oka, Phys. Rev. Letters 45 (1980) 531.

Appendix E

PHOTOIONIZATION AND DISSOCIATION OF THE TRIATOMIC HYDROGEN MOLECULE

H. Helm, L. J. Lembo, P. C. Cosby, and D. L. Huestis

Lecture Notes of Physics, Vol #339, Fundamentals of Laser Interactions
(Springer Verlag, 1989), P. 264

PHOTOIONIZATION AND DISSOCIATION OF THE TRIATOMIC HYDROGEN MOLECULE

H. Helm, L. J. Lembo, P. C. Cosby and D. L. Huestis
Molecular Physics Laboratory
SRI International, Menlo Park, CA 94025

ABSTRACT

Rotationless triatomic hydrogen molecules are synthesized in a fast molecular beam. Laser excitation of the molecules allows study of electric field induced ionization as well as autoionization of the ns, np, nd, and nf Rydberg series of H_3. Two photon ionization and double resonance techniques are applied to determine vibrational frequencies of trihydrogen.

Experimental analysis of the electron-core interaction shows that selective optical excitation of core rotation and core vibration can be achieved concurrent with excitation of the Rydberg electron.

Predissociation of low principal quantum number Rydberg states is observed to lead to the formation of both H_2 + H as well as H + H + H fragments.

INTRODUCTION

Triatomic hydrogen presents topics for experimental and theoretical investigation that are interesting from a variety of points of view. As the simplest polyatomic molecule it should have received extensive experimental attention, yet its electronic emission spectrum was first identified only ten years ago [He79]. From a chemist's perspective H_3 consists of H_2 with an extra hydrogen atom, or the unstable transition state in the most fundamental of chemical reactions,

$$H + H_2 \rightarrow H_2 + H \ .$$

The unstable nature of the ground state of H_3 easily explains the difficulties in its quantitative experimental investigation.

From a physicist's perspective we might think of H_3 as the combination of the exceptionally stable molecular ion H_3^+ with an extra electron. In our investigations we take this perspective literally. We begin with a beam of H_3^+ molecular ions, to which we attach a single electron by charge transfer in a Cs vapor cell. Most of the resulting H_3 neutrals are predissociated by the vibrational continuum of the ground electronic state. The few that remain are in a single rotational level of a single electronic state and survive only because they have a symmetry that is not present in the ground-state continuum [GP83,He86]

We detect the existence of these levels by laser photoabsorption, leading either to photodissociation, in which case the H_2 + H or H + H + H fragments are detected in coincidence by a position-sensitive detector, or by reionization, in which case reformed H_3^+ ions are detected. The resulting spectra are remarkably simple, appearing more like that of the hydrogen atom, than that of the hydrogen molecule. The objective of our studies is to quantitatively investigate the interactions among the relatively uncoupled electronic, vibrational, and rotational motions of H_3.

In this lecture we first develop the symmetry classification of molecular wavefunctions, and the selection rules that govern radiative transitions and configuration interaction in this molecule. We then discuss experimental examples of different types of interactions between the Rydberg electron and the H_3^+ core, and our observations of predissociation, autoionization, and field ionization.

SYMMETRY CLASSIFICATION

The "overall symmetry" classification of rovibronic wavefunctions for symmetric-top molecules is used to label the rovibrational levels of H_3^+ and D_3^+ and the rotational levels of the vibrationless excited states of H_3 and D_3 [CP77,Ho62,Bu79,HHW84]. These overall symmetry labels are the same as for the representations of the normal symmetry point group of the nonrotating molecule, but the rotational wavefunction also makes a contribution, since changing the numbering of the nuclei requires a reanalysis of the Euler angles. To develop selection rules for radiative transitions and for perturbations there are two things to accomplish (1) rovibronic wavefunctions must be combined with appropriate nuclear spin wavefunctions to achieve the correct Fermi-Dirac or Bose-Einstein permutation symmetry and (2) the parities of the levels must be established.

As might be expected, some levels have rovibronic wavefunctions that are antisymmetric with respect to nuclear exchange, which for H_3 must be combined with symmetric nuclear spin wavefunctions. These are called ortho levels, having a total nuclear spin of I = 3/2, and spatial symmetry labels A_2' and A_2'', with and even odd inversion parity, respectively. Since we cannot construct an antisymmetric nuclear spin wavefunction out of three spin 1/2 nuclei, exchange-symmetric rovibronic wavefunctions are forbidden (these would be labeled A_1' and A_1'', and are allowed for D_3). A third kind of rovibronic wavefunction is neither exchange-symmetric nor antisymmetric. These are to be combined in a direct-product sense with the similarly asymmetric I = 1/2 nuclear spin wavefunctions, resulting in so called para levels, with labels E' and E".

Symmetry Classification of Rovibronic Levels

To describe the symmetry properties of the rovibronic levels of H_3 we construct a basis set by multiplying together wavefunctions for the angular parts of degenerate vibration $\left(\chi_{v\ell} \right)$ and motion of a single electron $\left(Y_{L\lambda} \right)$ in the body-fixed frame and rotation of the entire molecule in the laboratory frame $\left(D^{(N)}_{KM} \right)$. Thus we write

$$\Psi^{vLN}_{\ell\lambda K} = \chi_{v\ell} \cdot Y_{L\lambda} \cdot D^{(N)}_{KM}$$

The vibrational-projection quantum number ℓ indicates the vibrational angular momentum, and ranges over v,v-2,...-v, where v is the total number of vibrational quanta in the ν_2 (bending or asymmetric stretch) mode (see [Bu79] pp196-200). The electronic orbital angular momentum quantum number L is expected to be rather well defined for the outer electron in Rydberg states of H_3^*. For the discussion below we only need to know if it is even or odd. For H_3^+ we can take $L = \lambda = 0$.

Classification of the states is accomplished using Hougen's three-part symmetry operations [Ho62],

$$Op = {}^1Op \cdot {}^2Op \cdot {}^3Op ,$$

where we each of the three operators, ^1Op, ^2Op, and ^3Op, is chosen from the from the same symmetry group, D_{3h} in the case of H_3. The first type of operator, ^1Op, affects only body fixed coordinates, i.e. $\chi_{v\ell}$ and $Y_{L\lambda}$. The second, ^2Op, affects only the angles of the $D^{(N)}_{KM}$. The third, ^3Op, affects only the center-of-mass coordinates in the laboratory frame. Hougen describes how to apply the operators C_n (n = 3 for H_3), σ_h, and σ_v on the rotation matrices $D^{(N)}_{KM}$. He also

says that ${}^1C_n$ rotates by $-2\pi/n$ while ${}^2C_n$ rotates by $+2\pi/n$. We can easily work out the transformation properties of $\chi_{v\ell}$ and $Y_{L\lambda}$ in the body-fixed frame (supposing that the phases of $\chi_{v\ell}$ can be chosen to be the same as for $Y_{v\ell}$). Thus we can write the results of multiplying the group operators as

$$C_n \, \psi^{vLN}_{\ell\lambda K} = e^{-2\pi i(\ell+\lambda-K)/n} \, \psi^{vLN}_{\ell\lambda K} = e^{-2\pi iG/n} \, \psi^{vLN}_{\ell\lambda K}$$

$$\sigma_h \, \psi^{vLN}_{\ell\lambda K} = (-1)^{v+L-\ell-\lambda+K} \, \psi^{vLN}_{\ell\lambda K} = (-1)^{v+L-G} \, \psi^{vLN}_{\ell\lambda K}$$

$$\sigma_v \, \psi^{vLN}_{\ell\lambda K} = (-1)^{N+\ell+\lambda-K} \, \psi^{vLN}_{-\ell-\lambda-K} = (-1)^{N+G} \, \psi^{vLN}_{-\ell-\lambda-K} \, ,$$

where we have introduced the quantity $G = \ell+\lambda-K$, which Hougen calls the "convenient" quantum number. G corresponds to the projection onto the principal axis of the angular momentum associated with the mechanical rotation of the H_3 frame. It is therefore related to the nuclear-exchange symmetry of the level. We are now ready to begin classifying the total symmetry of our rovibronic wavefunctions.

C_3: If G is 0 or a multiple of 3, the wavefunction has a character of +1 under rotation. This means that it belongs to one of the one-dimensional representations: A_1', A_1'', A_2', or A_2''. If G is not a multiple of 3, then the representation is either E' or E".

σ_h: The operation of σ_h allows us to decide between symmetric reflection in the plane (A_1', A_2', and E' for v+L-G even) and antisymmetric reflection (A_1'', A_2'', and E" for v+L-G odd).

σ_v: Finally, we use σ_v to decide on the subscript for the one-dimensional representations (i.e. for G = 3t, t=0,1,2,...). If ℓ, λ, and K are all simultaneously zero then $\psi^{vLN}_{\ell\lambda K}$ and $\psi^{vLN}_{-\ell-\lambda-K}$ are identical, and the character for σ_v is $(-1)^N$ (+1 means A_1' or A_2'', -1 means A_1'' or A_2') otherwise we form linear combinations.

$$\left(\psi^{vLN}_{\ell\lambda K} + \eta \, (-1)^{(N+G)} \, \psi^{vLN}_{-\ell-\lambda-K} \right) / \sqrt{2}$$

and get both +1 and -1 (i.e. the value of η chosen) as characters. Thus two representations are obtained, either both A_1' and A_2', or both A_1'' and A_2''.

Nuclear-spin Labeling

Following equations (2-9), (7-204), (7-206), and (7-251) of Bunker [Bu79] we identify Hougen's σ_v operator as the overall-inversion or parity operator E^*. Similarly, Hougen's product $\sigma_h \cdot \sigma_v$ is identified as exchanging two protons. We follow Townes and Schawlow [TS55 p69-71] and construct a nuclear spin basis set consisting of three $m_I = 1/2$ states (G = 0, 1, 2) of the form

$$\Phi^G_{nspin} = \left(\beta\alpha\alpha + e^{-2\pi iG/3}\ \alpha\beta\alpha + e^{-4\pi iG/3}\ \alpha\alpha\beta \right)/\sqrt{3} \ .$$

A similar set of nuclear-spin basis functions can be constructed for $m_I = -1/2$ by replacing all the α's by β's and vice versa. By applying the nuclear raising and lowering operators (I_+ and I_-) we can show that these wavefunctions give $I_{total} = 3/2$ for G = 3t and $I_{total} = 1/2$ for G = 3t+1 and 3t+2, these two spins corresponding to ortho and para respectively.

We then construct normalized, combined rovibronic/nuclear-spin wavefunctions for both the ortho and para states of H_3 of the form

$$\Xi^{vLN}_{\ell\lambda K} = \left(\Phi^{vLN}_{\ell\lambda K} \Phi^{\ell+\lambda-K}_{nspin} - (-1)^{v+L+N}\ \Phi^{vLN}_{-\ell-\lambda-K} \Phi^{-\ell-\lambda+K}_{nspin} \right)$$
$$\times \left[(2N+1)/8\pi \left(1+\delta_{\ell 0}\delta_{\lambda 0}\delta_{K0} \right) \right]^{1/2} \ .$$

Such a wavefunction will transform into itself when we apply the C_3 operator (C_3 corresponds to cyclic permutation of all three nuclei, with respect to which the total wavefunction must be symmetric). Similarly, applying the operator $\sigma_h\sigma_v$ results in interchange of the $\ell+\lambda-K$ term with the $-\ell-\lambda+K$ term with the appropriate sign that it always is antisymmetric, thus satisfying Fermi-Dirac nuclear permutation rules. For $G = \ell - \lambda - K = 3t$ it has spatial symmetry classification A_2' if v + L - G is even and A_2'' if v + L - G is odd. Similarly, for G = 3t+1 and 3t+2, the spatial symmetries are E' and E" for v + L - G even and odd, respectively. The wavefunction vanishes identically for quantum numbers that prevent construction of an antisymmetric combination, i.e. v + L + N even and $\ell = \lambda = K = 0$.

Transformation of Ordinary Objects from the Laboratory Frame

The angular part of the wavefunction for a single particle that is uncorrelated with the molecular frame, say a photon or free electron, can be expressed in the laboratory frame as a spherical harmonic, $Y_{JM}(lab)$. Following Chang and Fano [CF72] we can rewrite

it, using rotation matrices, as a combination of spherical harmonics in the body-fixed frame,

$$Y_{JM}(\text{lab}) = \sum_{\lambda} Y_{J\lambda}(\text{body}) \cdot D^{(J)}_{\lambda M}$$

Such an object has $v = \ell = 0$, $L = N = J$, $G = 0$. We can immediately apply Hougen's symmetry operators, establishing that the symmetry classification is A_1' or A_1'' if J is even or odd, respectively.

Optical Selection Rules

A particularly interesting case is the dipole transition operator, which has J=1, and thus is of symmetry A_1'', and can induce the transitions $A_1' \leftrightarrow A_1''$, $A_2' \leftrightarrow A_2''$, and $E' \leftrightarrow E''$. Thus without even knowing about the existence of nuclear spin labeling we have divided the energy levels into three distinct classes, within which optical transitions are possible, but between which optical transitions are strictly forbidden.

The states of H_3^+

We construct normalized rovibrational wavefunctions (including nuclear spin) for the ground electronic state of H_3^+, with total angular momentum N^+ and figure-axis projection K^+, of the form

$$\theta^{vN^+}_{\ell K^+ M} = \left[\chi_{v\ell} \cdot D^{(N^+)}_{K^+ M} \cdot \phi^{\ell - K^+}_{\text{nspin}} - (-1)^{v+N^+} \chi_{v-\ell} \cdot D^{(N^+)}_{-K^+ M} \cdot \phi^{-\ell + K^+}_{\text{nspin}} \right] \times \left[(2N^+ + 1)/8\pi \left(1 + \delta_{\ell 0} \delta_{K^+ 0} \right) \right]^{1/2} .$$

Wavefunctions for H_3 in Hund's Case (d)

We follow Chang and Fano [CF72] in combining a core state of H_3^+ (with quantum numbers v, ℓ, N^+, K^+, and M) with a Rydberg electron (with laboratory angular quantum numbers L and m) using angular momentum addition to obtain states of well defined total rovibronic angular momentum N:

$$\gamma^{v\ell LN^+K^+}_{NM} = \sum_{m} Y_{Lm}(\text{lab}) \cdot \theta^{vN^+}_{\ell K^+ M-m} \, (Lm, N^+ M-m \mid LN^+ NM) .$$

We use the frame transformation introduced above to write this Hund's case (d) wavefunction in terms of Hund's case (a/b) wavefunctions,

$$\gamma^{v\ell LN^+K^+}_{NM} = \sum_{\lambda} E^{vLN}_{\ell \lambda + K^+} \left[(2N+1)/8\pi \left(1 + \delta_{\ell 0} \delta_{\lambda 0} \delta_{K^+ 0} \right) \right]^{-1/2} \times \left[(2N^+ + 1)/8\pi \left(1 + \delta_{\ell 0} \delta_{K^+ 0} \right) \right]^{1/2} (L\lambda, N^+ K^+ \mid LN^+ N\lambda + K^+) ,$$

and to write Hund's case (a/b) wavefunctions in terms of Hund's case (d) wavefunctions,

$$\Xi^{vLN}_{\ell\lambda\lambda+K^+} = \sum_{N^+} \gamma^{v\ell LN^+K^+}_{NM} (-1)^{(L-\lambda)} (L\lambda, N-\lambda-K^+ | LNN^+-K^+) \times \left[\left(1+\delta_{\ell 0}\delta_{K^+0}\right)/\left(1+\delta_{\ell 0}\delta_{\lambda 0}\delta_{K^+0}\right)\right]^{1/2} .$$

Metastability

All of the excited states of H_3 lie in the vibrational continuum of the repulsive ground state, which correlates asymptotically to $H_2(X^1\Sigma_g^+)$ + H(1s). At the equilibrium geometry of H_3^+ this state is called $\bar{X}$ 2p $^2E'$, which we identify as L = 1, λ = 1. The symmetries of the levels of the $\bar{X}$ are classified, as functions of angular momentum, N, and bending vibration, v, as follows:

N = 0 We must have K=0. Thus v + L - G is always even, and the possible states have symmetry A_2' and E' (plus A_1' for D_3).

N > 0 K can be either even or odd, thus v + L - G is correspondingly either even or odd, giving states of symmetry A_2' and E' or A_2'' and E" (plus A_1' or A_1'' for D_3), respectively.

Thus we conclude that all of the excited states of H_3 and D_3 are predissociated for N > 0, since all possible symmetries are present in the ground state. For an excited state with L odd, predissociation is mediated by rotation, while for L even it is mediated by bending vibration.

Any states that are metastable with respect to predissociation are limited to N=0, and must have one of the symmetries A_2'' or E" (plus A_1'' for D_3). Since K = 0, v + L - G = v + L - ℓ - λ must be odd, which allows us to establish that L - λ must be odd, since v - ℓ is always even. The low-lying choices are only L = 1, λ = 0, and L = 2, λ = 1, which reduces to the single electronic state, $\bar{B}$ 2p $^2A_2''$, if we insist that the state also be radiatively metastable. This state is predicted to be immune to predissociation for all rotationless vibrational levels.

EXPERIMENTAL RESULTS

Formation of H_3^*

We form the metastable species of H_3 by electron transfer from a stationary alkali target (Cs or Rb) to a mass selected H_3^+ ions in a fast beam. As mentioned above only a small fraction of charge transfer products are metastable [JB84]. Typically 10^7 to 10^9 metastable molecules are produced per second in a 1 mm diameter beam traveling at energies of several keV. Experimental schematics for the laser photoionization and photodissociation spectrometers have been presented in recent publications [LHH89a,HC87].

Photodissociation in the Visible

The lowest photoexcitation transitions from the $\tilde{B}$ 2p $^2A_2''$ are to the 3s $^2A_1'$ and 3d$^2E''$ states at 16694 and 17297 cm^{-1} respectively, as reported by Herzberg *et al*. [DH80,HHW84]. In our experiments, the initial state is unique, having N"=0, thus the one-photon absorption spectrum can have only a single rotational branch with N'=1. These same transitions are easily observed by collecting H_2 + H photodissociation products, as shown as peaks labeled $3s\nu_0$ and $3d\nu_0$ in Figure 1 [CH88]. The energy analysis capability of the position-

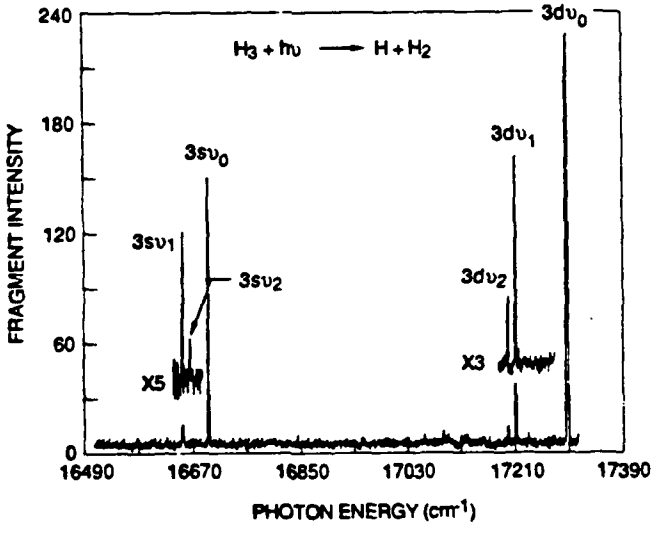

Figure 1: Observed production of photofragments from H_3 as a function of the photon energy of the exciting laser. Only photofragments produced with center-of-mass energies W > 4 eV are recorded for this spectrum. The spectrum at other energy releases is similar, but with a substantial background due to spontaneous dissociation fragments.

sensitive detector allows us to show that predissociation of these two states leads to substantially different distributions of vibrational energy in the H_2 fragment. For the 3s state, H_2 is observed in vibrational levels from v=0 to v>12. For the 3d state, however, a significance preference is observed for the formation of H_2 with v=5-9. In addition to predissociation to H_2 + H products, both the 3s and 3d states are observed to predissociate into three atoms, H + H + H. Also shown in Figure 1 are transitions from vibrationally excited $\tilde{B}$ 2p $^2A_2''$ initial states to 3s and 3d states with the corresponding vibrational excitation (labeled $3s\nu_1$, $3s\nu_2$, $3d\nu_1$, $3d\nu_2$). These indicate that vibrationally excited metastables are present in the beam (their relative abundance depends on the ion source conditions) and provides the first direct information about the vibrational frequencies of the excited states of H_3.

Field Ionization in the Ultraviolet

The vibrational structure described above provides an indication of the role to be played by the H_3^+ core in making more interesting the pseudo-atomic H_3^* absorption spectrum. We can explore this core structure in somewhat more detail by gradually promoting the outer electron to higher principal quantum numbers in the Rydberg series nd ← 2p, and detecting the photoabsorption by field ionization. The resulting spectrum is shown in Figure 2, in which nd levels from

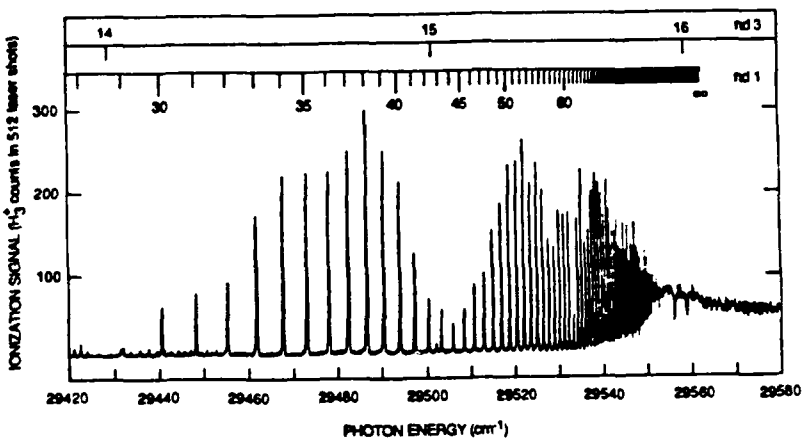

Figure 2: Photoabsorption of the lowest metastable level of H_3, detected by field ionization of the excited d-electron Rydberg series. Series members converging to the N^+=1, K^+=0 level of H_3^+ are marked at the top of the figure as nd1. A series of interlopers, nd3, converging to the rotational level N^+=3, K^+=0 is also indicated. Three additional window resonances appear within 30 cm^{-1} of the threshold.

n = 28 to n = 100 have been assigned [He88]. Field ionization has also been used by Dodhy et al. [DKM89] to detect nd states for n as low as 14. All *n* values from *n* = 3 to *n* = 100 have been detected by double-resonance ionization-depleting spectroscopy [LHH89b]. Extrapolation of this series has enabled the accurate determination of the ionization potential of the rotationless $\tilde{B}$ 2p $^2A_2''$ state as 29562.58 ± 0.5 cm^{-1}. The intensity modulations shown in Figure 2 are significant, although weakly dependent on laser power, and show the influence of having multiple Rydberg series converging to different rotational states of the H_3^+ core. A particular example is the broad dip in signal near n = 42, which appears to correspond to an n = 15 interloper from the N^+ = 3 level of H_3^+. Attempts to model this spectrum suggest that the actual situation is not quite so simple.

Vibrational Autoionization

Just to the red of the spectrum shown in Figure 2, additional photoionization peaks appear that reveal photoabsorption into levels that ionize spontaneously without an external field. These are shown in Figure 3, and as indicated by the labels, are the higher members of the ns ← 2p and nd ← 2p Rydberg series from the vibrationally excited metastables. These peaks appear in the ionization spectrum because the upper levels lie energetically above that of the vibrationless H_3^+

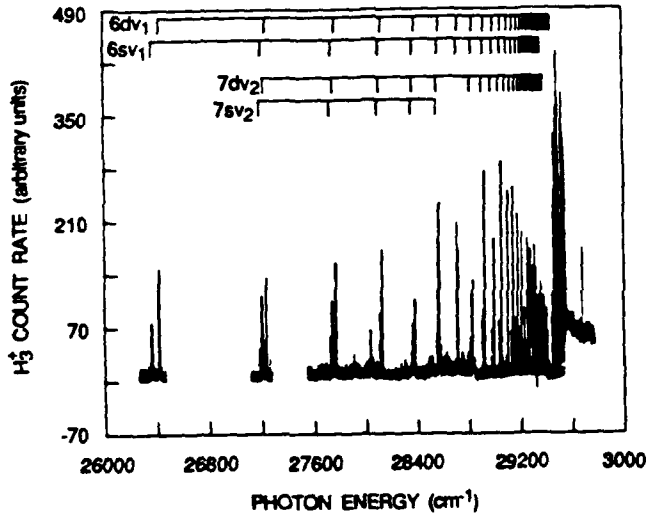

Figure 3. Vibrational autoionization of s- and d-electron Rydberg series converging to the bending excited core level (ν_2) and symmetric stretch excited core level (ν_1) of H_3^+.

core plus a free electron. The autoionization mechanism is depicted in Figure 4. Note that n = 6 in the symmetric-stretch (ν_1) series and n = 7 in the bending vibration (ν_2) series are the lowest members that are subject to vibrational autoionization.

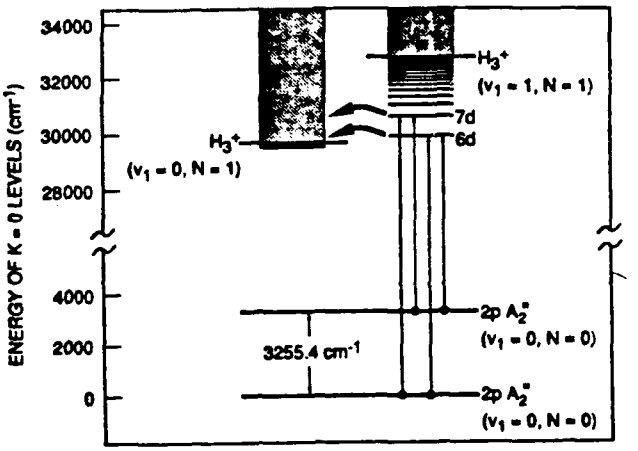

Figure 4. Energy level diagram of H_3 showing diagonal and off-diagonal excitation to the vibrationally autoionizing 6d and 7d Rydbergs with symmetric stretch excitation.

Two-Photon Excitation of np and nf Rydberg Series

The great strength of the 3s ← 2p and 3d ← 2p transitions suggests using these transitions in double-resonance experiments. In this paragraph we discuss the use of the 3s and 3d states as intermediates for two-photon excitation of the np and nf Rydberg series that are of the same symmetry as the 2p initial state. Two-step excitation also allows us to reach higher total angular momentum, i.e. N=0,1,2, and to influence the relative strengths of the transitions by choosing intermediate states with different core properties. In Figure 5 we indicate schematically the excitation pathways used. The 3s intermediate state favors excitation of np final states. The resulting field-ionization spectrum is shown in the lower trace in Figure 6. Since there are two one-photon accessible 3d states, called 3dE" and $3dA_1'$, and since these two states have core rotational character of predominantly $N^+ = 1$ and $N^+ = 3$, respectively, we can bias the absorption spectrum. As shown in the upper two traces in Figure 6, choosing the 3dE" intermediate leads to a field-ionization spectrum labeled nf1, by which we mean an nf Rydberg orbital outside an $N^+ = 1$ H_3^+ core. Similarly, choosing the $3dA_1'$ intermediate leads to a substantially different spectrum, called nf3.

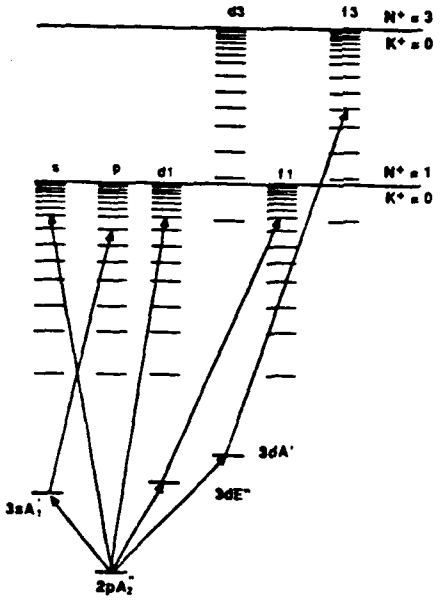

Figure 5. Energy level diagram of N=1 Rydbergs built on the lowest rotational cores of ortho-H_3. Direct and stepwise excitation paths to these Rydbergs from the metastable $\tilde{B}$ 2p $^2A_2$" state are indicated.

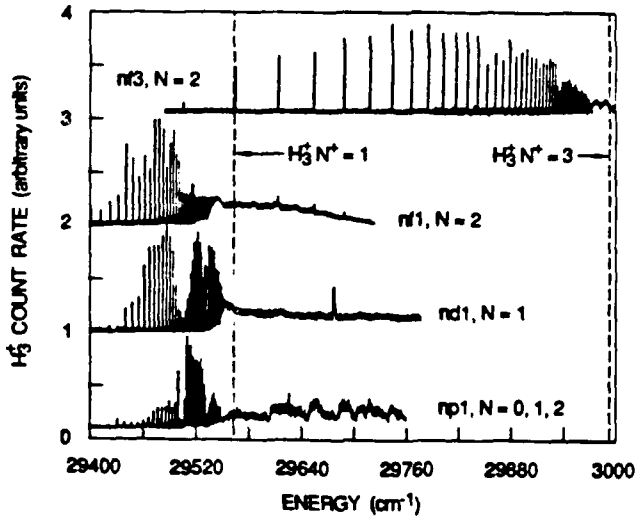

Figure 6: Excitation spectra into the field-ionized and rotationally-autoionized regions of the lowest p-, d-, and f- Rydberg series.

Interestingly, some of the peaks appear in both spectra. The narrow peaks in the right hand part of the trace labeled nf1, above the $N^+ = 1$ ionization limit (dashed line), agree in position with the peaks in the nf3 trace and manifest the weak admixture of the $N^+ = 3$ core in the $3dA_1'$ intermediate state. Above the $N^+ = 1$ threshold the spectra result as a consequence of rotational autoionization.

Vibrationally Off-Diagonal Transitions

Finally, we have examined the spectral region between the n = 3 and n = 4 members of the Rydberg series. Absorptions are detected by one- or two-color photoionization, or by ionization depletion of another transition. Some of the transitions observed are shown schematically in Figure 7 and as a spectrum in Figure 8. The peaks

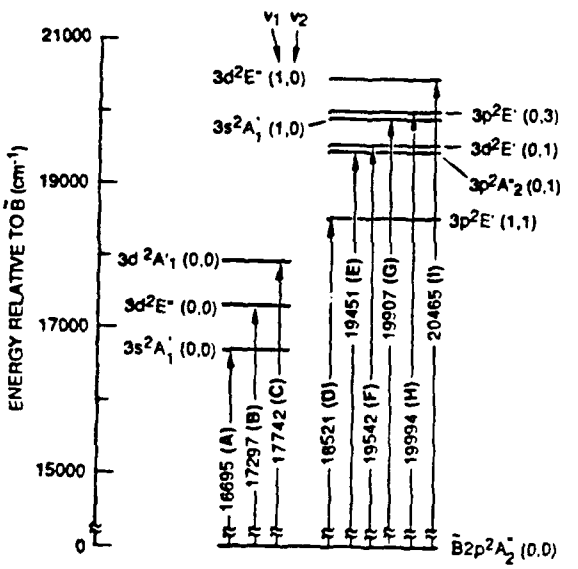

Figure 7: A selection of diagonal and off-diagonal excitations observed into the n=3 manifold of H_3

labeled "G" and "I" correspond to simultaneous excitation of the electron, 3s ← 2p or 3d ← 2p, and of the symmetric vibration mode, ν_1. Peaks "D", "E", "F", and "H" result from excitation of the bending vibrational mode, ν_2. But here the simultaneous electronic excitation is unusual. Only electronic transitions that previously were forbidden by parity, i.e. 3p ← 2p, are now possible. This is because the bending vibrational wavefunction changes the overall parity of the

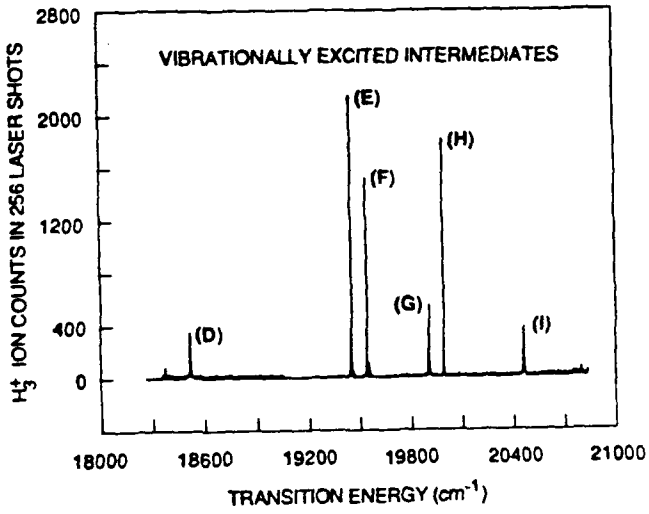

Figure 8: One-photon resonant two-photon ionization spectra involving rovibronic transitions marked in Figure 7.

state. Such vibronically allowed transitions have also been observed in other polyatomic molecules and provide a detailed and specific probe of the electron-core interactions.

Summary

We have seen that the $\tilde{B}$ 2p $^2A_2''$ state of H_3 is metastable only for $N = 0$, but for any v. It is easily produced by charge transfer and is straightforward to investigate using photodissociation and photoionization. It shows a very simple, atomic-like absorption spectrum, with relatively weak, but revealing, interactions between the outer Rydberg electron and the vibrational and rotational motions of the underlying H_3^+ core.

Acknowledgments

This research was supported by the Air Force Office of Scientific Research and the National Science Foundation.

References

Bu79 P. R. Bunker, Molecular Symmetry and Spectroscopy, (Academic Press, NY, 1979).

CF72 E. S. Chang and U. Fano, Phys. Rev. A 6, 173 (1972).

CH88 P. C. Cosby and H. Helm, Phys. Rev. Lett. 61, 298 (1988).

CP77 C. D. Carney and R. N. Porter, J. Chem. Phys. 66, 2758 (1977).

DH80 I. Dabrowski and G. Herzberg, Can. J. Phys. 58, 1238 (1980).

DKM89 A. Dodhy, W. Ketterle, H.-P. Messmer, and H. Walther, Chem. Phys. Lett. 151, 133, (1988).

GP83 G. I. Gellene and R. F. Porter, J. Chem. Phys. 79, 5975 (1983).

HC87 H. Helm and P. C. Cosby, J. Chem. Phys. 86, 6813 (1987).

He79 G. Herzberg, J. Chem. Phys. 70, 4806 (1979).

He86 H. Helm, Phys. Rev. Lett. 56, 42 1986).

He88 H. Helm, Phys. Rev. A 38, 3425 (1988).

HHW84 G. Herzberg, J. T. Hougen, and J.K.G. Watson, Can. J. Phys. 60, 1238 (1984).

Ho62 J. T. Hougen, J. Chem. Phys. 37, 1433 (1962).

JB84 J. R. Peterson and Y. K. Bae, Phys. Rev. A 30, 2807 (1984).

LHH89a L. J. Lembo, H. Helm, and D. L. Huestis, J. Chem. Phys. (in press).

LHH89b L. J. Lembo, D. L. Huestis, and H. Helm, to be published.

LPH89 L. J. Lembo, A. Petit, and H. Helm, Phys. Rev. A (in press).

TS55 C. H. Townes and A. L. Schawlow, Microwave Spectroscopy (McGraw Hill, NY, 1955; Dover, NY, 1975).

Appendix F

AUTOIONIZATION OF H_2 INDUCED BY A DOUBLY EXCITED TRIPLET STATE

N. Bjerre, S. R. Keiding, L. J. Lembo, and H. Helm

Phys. Rev. Lett. 60, 2465 (1988)

Autoionization of H_2 Induced by a Doubly Excited Triplet State

Nis Bjerre and Søren R. Keiding
Institute of Physics, University of Aarhus, 8000 Aarhus C, Denmark

and

Lawrence J. Lembo and Hanspeter Helm
Molecular Physics Department, SRI International, Menlo Park, California 94025
(Received 4 January 1988)

A fast beam of H_2 molecules in the metastable $c\,^3\Pi_u^-$ state is photoionized with visible laser light in the region 540–670 nm. Very strong photoionization from high vibrational levels is observed with a conversion of up to ten vibrational quanta into electronic energy. This extreme non-Franck-Condon behavior is attributed to avoided crossings between the doubly excited $2p\sigma_u 2p\pi_u Q_1\,^3\Pi_g$ state and the singly excited $1snd\,^3\Pi_g$ Rydberg states with $n \geq 3$.

PACS numbers: 33.80.Eh

The photoionization of molecular hydrogen has been extensively studied in recent years. For the singlet states, a variety of schemes for multiphoton excitation from the ground state has been developed.[1–4] The spectroscopy of the triplet states usually starts from the metastable $c\,^3\Pi_u^-$ state, which can be populated in electron impact excitation of a slow molecular beam[5,6] or by resonant charge exchange in alkali vapor of a fast beam of H_2^+.[7] The latter technique is used in the present work.

All the bound triplet states observed so far are singly excited Rydberg states in the sense that their configuration is well described as an H_2^+ core in the electronic ground state with a loosely bound outer electron. When photoionization proceeds via such a Rydberg state, it usually follows rather strict propensity rules in the vibrational quantum number: Vibrational autoionization of pure Rydberg states becomes less and less efficient with increasing Δv.[8,9] Therefore it is quite remarkable that we in the present experiment observe strong one-photon ionization with a change of as much as ten vibrational quanta.

Recently, a non-Franck-Condon behavior was observed in multiphoton ionization via the $C\,^1\Pi_u$ state.[10,11] This was explained by Chupka[12] and by Hickman[13] as resulting from excitation of a repulsive doubly excited state which on its way towards dissociation has a number of avoided crossings with the potential curves of H_2^+ and the high-n Rydberg states. This results in competition between dissociation and autoionization with a change of several vibrational quanta. The extreme non-Franck-Condon photoionization observed in the present work results from excitation directly into a system of avoided crossings between the doubly excited $2p\sigma_u 2p\pi_u Q_1\,^3\Pi_g$ state and the singly excited $1snd\,^3\Pi_g$ states.

The present experiments were carried out on a fast neutral-beam apparatus at SRI International[7] and on a similar apparatus at the University of Aarhus. There was excellent agreement between the results obtained in the two laboratories. An H_2^+ beam of 1.4–2 keV undergoes resonant charge transfer in Cs vapor producing a fast neutral beam of H_2 in the metastable $c\,^3\Pi_u^-$ state. The beam is excited in a collinear geometry with about 500 mW of visible light from a cw dye laser with a bandwidth of 1 cm^{-1}. The ions formed in the 0.8-m laser/beam interaction region are deflected onto a Channeltron detector. The laser beam is modulated with a mechanical chopper and the modulated ion signal from the Channeltron is recorded on a computer. The strong lines in the spectrum represent more than 10 times as many ions as the spontaneous and electric-field- and collision-induced ionization of the metastable molecules. Even the modest cw laser power saturates the strong optical transitions, indicating that they are vibrationally and electronically allowed.

Figure 1 shows a portion of the spectrum. The full spectrum consists of three groups (like the one shown), separated by regions with only few and weak lines. The three groups fall near 640, 600, and 560 nm. A fourth group of lines appears to begin at 670 nm at the very red end of our laser range. Most of the spectrum is not yet assigned, but a few lines have been identified in terms of an unambiguous assignment of the lower-state vibrational and rotational quantum numbers. The lines represent transitions from $v''=9$–12 in the $c\,^3\Pi_u^-$ state; the three groups contain transitions to the same upper levels from different lower-state vibrational levels.

For most of the lines in the spectrum, the width is limited by the 1-cm^{-1} bandwidth of the dye laser. An exception is the $R1$ and $P3$ lines (Fig. 1) which are about 4 cm^{-1} wide, indicating a lifetime of 1.3 ps for the autoionizing upper level. We have also scanned one of the $R7$ lines using a single-frequency dye laser. The homogeneous linewidth corresponds to a lifetime of 70 ps. These lifetimes are much shorter than the fluorescence lifetimes, and so predissociation is the only process that

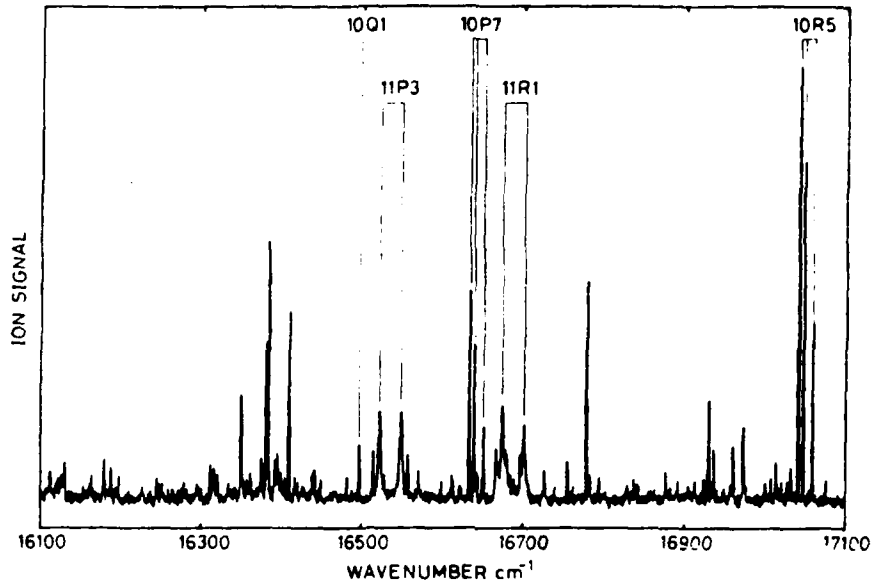

FIG. 1. Portion of the photoionization spectrum of H_2 $c\,^3\Pi_u^-$. The transitions are labeled by v'', ΔN, and N''; P, Q, and R denote $\Delta N = -1$, 0, and 1, respectively.

can possibly compete efficiently with autoionization.

The vibrational and rotational splittings observed for the $c\,^3\Pi_u^-$ state agree very well with the *ab initio* calculations of Kołos and Rychlewski[14] as indicated in Table I. We use the theoretical vibrational splittings to define the energy scale relative to $v=1$, $N=1$ in the $c\,^3\Pi_u^-$ state. The ionization potential of this level has been measured accurately[15] and defines the energy levels relative to H_2^+ and the dissociation limits. The assigned transitions and their upper state energy levels are listed in Table II along with the relevant energies of the dissociation limits and of H_2^+. Most of the assigned transitions must autoionize into $v^+ \leq 2$ of H_2^+. Accordingly, the photoionization from $v''=12$ in the $c\,^3\Pi_u^-$ state has $\Delta v \geq 10$.

Also listed in Table II are energy levels for selected *nd* Rydberg states obtained from a computer simulation based on a model similar to that of Herzberg and Jungen[16] and Eyler and Pipkin.[17] The model neglects all couplings but the rotational coupling between states of the same n and v. The energy levels of the nonrotating molecule are calculated separately for each n with quantum defects derived from the quadrupole moment and polarizability of H_2^+. The rotational coupling is then represented in terms of the effective Hamiltonian previously used for the $3d$ states of HD.[18] The simulation indicates that some of the upper-state levels are almost degenerate with Rydberg levels of intermediate n and v. These near degeneracies explain the appearance of "multiplets" like the $R5$ lines (Fig. 1) with closely spaced upper levels of the same N. The degeneracies may guide the molecule through the higher Rydberg states towards autoionization, but they do not account for the very large Δv observed.

TABLE I. Molecular constants for the $c\,^3\Pi_u^-$ state. Experimental values are from this work, and theoretical values are from Ref. 14.

v	ΔG (Expt.)	ΔG (Theor.)	B_v (Expt.)	B_v (Theor.)
9	1300	1298.7	18.26	18.23
10	1175	1175.6	16.83	16.84
11	1046	1046.1	15.36	15.38
12			13.79	13.82

TABLE II. Assigned transitions and energy levels. Transitions are labeled by v'', ΔN, and N''. Energy levels are in inverse centimeters relative to $c\,^3\Pi_u^-$ $v''=1$, $N''=1$.

Transition	$\tilde{\nu}$ (cm^{-1})	E(upper)	Rydberg level (n,v,N)	E
$11Q1$	15325.4			
$10Q1$	16497.4	32309		
$9Q1$	17794.6			
$12R5$	14910.9			
$11P7$	15540.4			
$11R5$	15910.4		(6,4,6)	33299
$10P7$	16633.6	33313	(9,3,6)	33293
$10R5$	17041.3		(12,3,6)	33294
$9P7$	17854.4			
$9R5$	18298.2			
$12P3$	15496.1			
$12R1$	15632.3	33658	(8,4,2)	33683
$11P3$	16522.7			
$11R1$	16674.4			
H_2^+, $v^+=2$, $N^+=0$		31392		
H_2^+, $v^+=3$, $N^+=0$		33334		
H(1s) + H(3s,p,d)		36330		

To account for the strong photoionization, we seek a bound upper state with a potential curve that deviates markedly from that of H_2^+ and the normal Rydberg states. To give a good Franck-Condon factor, the outer turning point in the vibration must be in the region $R = (4.5\text{-}6)a_0$, where the outer turning points for $v'' = 9\text{-}12$ in the $c\,^3\Pi_u^-$ state occur. The upper state must have $^3\Pi_g$ or $^3\Delta_g$ symmetry, since $\Delta N = \pm 1$ transitions, which are observed, are not allowed from the $c\,^3\Pi_u^-$ state to $^3\Sigma_g^+$ states.

By analogy with the recent work on singlet H_2,[10-13] we propose that the photoionization observed here involves a doubly excited state. According to Guberman's calculations,[19] the lowest doubly excited triplet state is the $Q_1\,^3\Pi_g$ state. These calculations were optimized for $R = 1.4a_0$ and seem to have problems in correlation with the correct dissociation limits. Therefore, we choose to describe the $Q_1\,^3\Pi_g$ state in terms of its dominant electronic configuration: a $2p\pi$ electron on an H_2^+ core in the excited state $(2p\sigma)\,^2\Sigma_u^+$. In a diabatic treatment, this doubly excited state correlates with the $n = 2$ limit [i.e., $H(1s) + H(2s,p)$] as illustrated in Fig. 2. Similarly, a diabatic treatment of the singly excited $1snd$ configurations gives rise to a series of $^3\Pi_g$ states, each of which correlates with the dissociation limit of the same principal quantum number. However, in the adiabatic picture, these states undergo avoided crossings with the doubly excited state near $R = 4a_0$. As a result of these crossings the $nd\,^3\Pi_g$ states change character into $(n-1)d\,^3\Pi_g$ over the interval $3a_0 < R < 6a_0$ and they correlate with the $n-1$ dissociation limit. This change of character corresponds to a change of 1 in the quantum defect. The well-known barrier in the $i\,^3\Pi_g$ state[14] results from the crossing of the potential curves of the $3d$ state and the $Q_1\,^3\Pi_g$ state. Beyond the top of the barrier, the $i\,^3\Pi_g$ state assumes the character of the doubly excited state[14] because no d states correlate to the $n = 2$ dissociation limit.

The potential curves in Fig. 2 were derived by our setting up a Hamiltonian in a basis of the $nd\,^3\Pi_g$ states and the $Q_1\,^3\Pi_g$ state. The doubly excited state is coupled to the nd states by a matrix element that varies with n as $n^{-3/2}$.[12] The magnitude of the matrix element is adjusted as a function of R such that the lowest adiabatic state reproduces the potential curve of the $i\,^3\Pi_g$ state.

The next higher $^3\Pi_g$ state, $2\,^3\Pi_g$, has the properties required to account for the photoionization with large Δv. At short internuclear distances, this state is a normal singly excited Rydberg state with $n = 4$. The levels $v = 0\text{-}2$ were observed by Eyler and Pipkin.[17] The avoided crossing with the doubly excited state creates a kink in the $2\,^3\Pi_g$ potential near $R = 4a_0$. The potential goes quickly towards larger R and the electronic wave function changes character from $n = 4$ via a mixture of all n's into $n = 3$. The energies of the upper states observed at consistent with $v' = 7,8$ in the $2\,^3\Pi_g$ state.

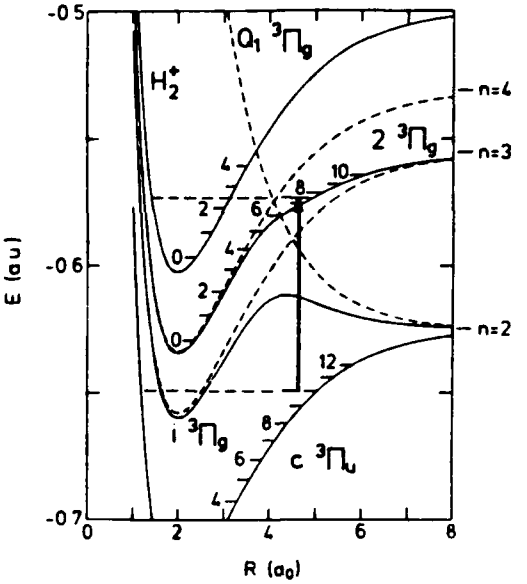

FIG. 2. Potential energy curves for H_2 and H_2^+: dashed line, diabatic states; solid line, adiabatic states. The adiabatic potential curve of the $2\,^3\Pi_g$ state observed in photoionization has the character of the $n = 4$ diabatic state at short R. It develops a kink near the diabatic crossing with the doubly excited state, and assumes the diabatic character of the $n = 3$ state at large R.

These levels have their outer turning points in the vibration at the flat portion of the potential so that the maximum of the vibrational wave function occurs just at the avoided crossing with the doubly excited $Q_1\,^3\Pi_g$ state. The photoionization involves a "loss" of several vibrational quanta in the excitation step followed by the conversion of about five vibrational quanta into electronic energy, resulting in H_2^+ with $v^+ = 2\text{-}3$. A more detailed analysis may shift the position of the crossing and consequently change the present assignment of v' in the $2\,^3\Pi_g$ state. We note that the lowest doubly excited Δ state arises from the $n = 3$ limit. As a consequence, the $nd\Delta$ states do not show any anomalous behavior below the $n = 3$ limit, but rather follow a smooth potential energy curve like that of H_2^+. Hence, there is no ambiguity about the assignment of $2\,^3\Pi_g$ as the intermediate state in the observed photoionization.

The avoided crossings may also lead to dissociation if the coupling to states of lower n dominates. The competition between autoionization and dissociation is probably important in the determination of the relative intensities of the transitions in the ionization spectrum. Using a double resonance technique,[20] we have observed dissociation of the high vibrational levels in both the $3d\,j\,^3\Delta_g$ state and the $2\,^3\Pi_g$ state. This will be the subject of a separate publication.

Quantitative representation of the level energies and the competition between ionization and dissociation can possibly be achieved with use of multichannel quantum-

defect theory. This approach was recently applied by Ross and Jungen[21] to calculate accurate level energies in the system of avoided crossings that give rise to the $^1\Sigma_g^+$ double-well states in H_2.

The present experiment illustrates the dramatic effect of a doubly excited state on the dynamics of autoionization and opens new possibilities for the study of the competition between the various decay channels open to a simple molecule in electronically and vibrationally highly excited states.

This work was supported by the National Science Foundation under Grant No. NSF PHY87-06332 and the U.S. Air Force Office of Scientific Research under Contract No. F49620-87-K-0002, as well as by a NATO travel grant. We appreciate helpful discussions with Dr. D. L. Huestis, Dr. T. Andersen, and Dr. K. Taulbjerg.

[1] H. Rottke and K. H. Welge, J. Opt. Soc. Am B **1**, 485 (1984).

[2]N. Bjerre, R. Kachru, and H. Helm, Phys. Rev. A **31**, 1206 (1985).

[3]S. T. Pratt, P. M. Dehmer, and J. L. Dehmer, Chem. Phys. Lett. **105**, 28 (1984).

[4]J. H. M. Bonnie, J. W. J. Verschuur, H. J. Hopman, and H. B. van Linden van den Heuvell, Chem. Phys. Lett. **130**, 43 (1986).

[5]E. E. Eyler and F. M. Pipkin, Phys. Rev. Lett. **47**, 1270 (1981).

[6]R. D. Knight and L.-g. Wang, Phys. Rev. Lett. **55**, 1571 (1985).

[7]R. Kachru and H. Helm, Phys. Rev. Lett. **55**, 1575 (1985).

[8]P. M. Dehmer and W. A. Chupka, J. Chem. Phys. **65**, 2243 (1976).

[9]E. E. Eyler, Phys. Rev. A **34**, 2881 (1986).

[10]M. A. O'Halloran, S. T. Pratt, P. M. Dehmer, and J. L. Dehmer, J. Chem. Phys. **87**, 3288 (1987).

[11]E. Y. Xu, T. Tsuboi, R. Kachru, and H. Helm, Phys. Rev. A **36**, 5645 (1987).

[12]W. A. Chupka, J. Chem. Phys. **87**, 1488 (1987).

[13]A. P. Hickman, Phys. Rev. Lett. **59**, 1553 (1987).

[14]W. Kołos and J. Rychlewski, J. Mol Spectrosc. **66**, 428 (1977).

[15]E. E. Eyler, R. C. Short, and F. M. Pipkin, Phys. Rev. Lett. **56**, 2602 (1986).

[16]G. Herzberg and Ch. Jungen, J. Chem. Phys. **77**, 5876 (1982).

[17]E. E. Eyler and F. M. Pipkin, Phys. Rev. A **27**, 2462 (1983).

[18]S. R. Keiding and N. Bjerre, J. Chem. Phys. **87**, 3321 (1987).

[19]S. L. Guberman, J. Chem. Phys. **78**, 1404 (1983).

[20]L. J. Lembo, D. L. Huestis, S. R. Keiding, N. Bjerre, and H. Helm, to be published.

[21]S. Ross and Ch. Jungen, Phys. Rev. Lett. **59**, 1297 (1987).

Appendix G

DOUBLE-RESONANCE STUDY OF PREDISSOCIATION OF THE $\beta^3\Delta g$ STATE OF H_2

L. J. Lembo, D. L. Huestis, S. R. Keiding, N. Bjerre, and H. Helm

Phys. Rev. A 38, 3447 (1988)

Double-resonance study of predissociation of the $j\,^3\Delta_g$ state of H_2

L. J. Lembo and D. L. Huestis
Molecular Physics Department, SRI International, Menlo Park, California 94025

S. R. Keiding and N. Bjerre
Institute of Physics, University of Aarhus, 8000 Aarhus C, Denmark

H. Helm
Molecular Physics Department, SRI International, Menlo Park, California 94025

(Received 18 March 1988)

A photoionization-photodissociation double-resonance technique has been employed to excite transitions from selected rovibrational levels of the metastable $c\,^3\Pi_u^-$ state to the rapidly predissociated $j\,^3\Delta_g$ state of H_2. The photodissociation resonances arise from the configuration interaction between the $j\,^3\Delta_g$ and $i\,^3\Pi_g$ states, and exhibit the asymmetry of Fano-Beutler profiles. These resonances have widths that decrease with increasing v' from 29 to 10 cm^{-1}; calculated predissociation widths show the same vibrational trend but are consistently 30% smaller. Results have been obtained for the rovibrational energy spacings of high-v levels within each state, and are in good agreement with theory. Photon energies for the c-to-j state transitions are slightly larger than those predicted theoretically.

I. INTRODUCTION

Despite its apparent simplicity, a great deal of interest and uncertainty still remain concerning the structure and spectrum of the hydrogen molecule. This is especially true for the high vibrational levels of the excited electronic states. The triplet manifold in particular has recently become the subject for numerous experimental investigations.[1–9] The ability to study the triplet system of H_2 hinges upon the existence of the metastable $2p\pi\ c\,^3\Pi_u^-$ state[10] (see Fig. 1). For spectroscopic studies the c-state molecules are commonly formed by electron-impact excitation[2,3,5,9] of a thermal hydrogen beam or by charge transfer of a fast H_2^+ beam at keV energies.[4,6–8]

Spectroscopic investigations employing the fast-beam technique have used primarily two means of monitoring photoabsorption from the $c\,^3\Pi_u^-$ state. These are (1) detection of neutral atomic fragments[4] resulting from direct photodissociation, predissociation, and bound free photon emission; and (2) detection of H_2^+ ions,[6] resulting from direct photoionization and from autoionization. Using either detection scheme a rich spectrum is obtained, due in part to the broad rotational and vibrational distributions of the parent H_2^+ ions used to form the metastable hydrogen beam. Strong coupling between continuum and bound states results in large linewidths for many of the transitions. Consequently, transitions from neighboring lower-state levels often overlap in the wavelength spectrum, making the contribution of individual levels difficult to resolve.

An example of this spectral overlap problem appears in excitation of the $3d\delta\ j\,^3\Delta_g$ state. Levels of this state lying above the potential barrier of the $3d\pi\ i\,^3\Pi_g$ state ($v > 5$) are rapidly predissociated by the continuum of the $i\,^3\Pi_g$ state (see Fig. 1). The spectral overlap is partially resolved in experiments which measure the kinetic energy of the dissociation fragments as a function of excitation wavelength.[7,11] Such studies have very clearly demonstrated the modification of the i-state continuum by the presence of the rapidly predissociated j-state levels. The technique has, however, not yet been employed to isolate

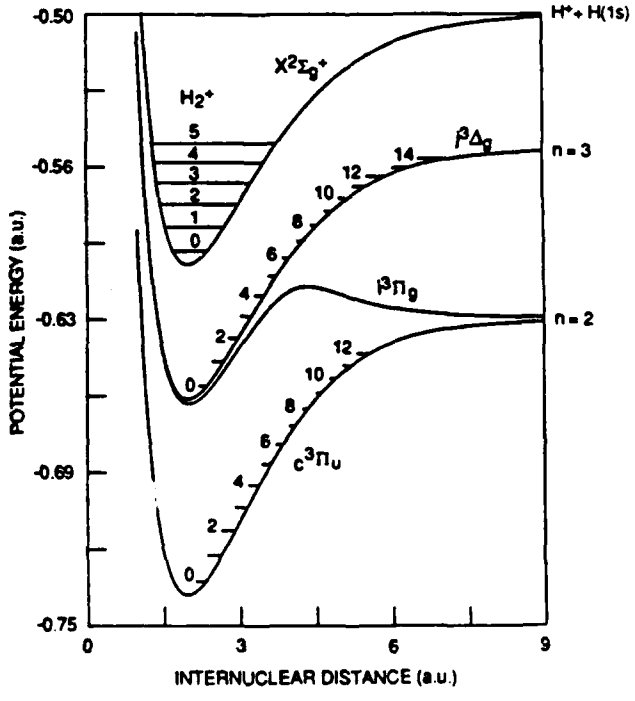

FIG. 1. Pertinent potential curves of H_2 and H_2^+.

excitation profiles of individual j-state levels.

In the present study, we introduce a double-resonance technique that monitors all photoabsorptions from selected $c\ ^3\Pi_u^-$ (v'',N'') levels by detecting a reduction in the ionization rate on a transition to an autoionizing level. We report the application of this method to the study of photodissociation transitions to high vibrational levels of the $j\ ^3\Delta_g$ state lying above the potential barrier of the $i\ ^3\Pi_g$ state. This technique provides straightforward rovibrational assignments of both the upper and lower levels of the transitions and allows the identification of weak and broad transitions that would otherwise remain unresolved. The double-resonance dissociation spectra allow one to resolve the weakly asymmetric Fano-Beutler photodissociation line shapes.

II. EXPERIMENTAL ARRANGEMENT

The experiments described below were performed on two similar fast-neutral-beam spectrometers, one at SRI and one at the University of Aarhus. Detailed descriptions of the fast-neutral-beam apparatus used in these studies have appeared elsewhere.[6,12] A beam of H_2^+ ions, extracted from an electron-impact or hot-filament discharge ion source, is accelerated to an energy of 1–2 keV and mass-selected. The H_2^+ ions are directed into a cesium-vapor cell, where near-resonant charge transfer populates the metastable c state and results in typical neutral-beam currents of 50 pA. This beam is then coaxially excited in an ultra-high vacuum region, using the double-resonance scheme to be described below. Ions created as a result of the laser excitation are either deflected directly into a channel-electron multiplier, or energy analyzed before being detected. Ion counts are registered with gated scalers interfaced to a PDP11 microcomputer via a CAMAC dataway.

Figure 2 depicts the optical arrangement for double-resonance probing of the neutral beam. One laser (henceforth designated laser I) was a broadband (1 cm^{-1}) tunable cw dye laser operating at a power of 100–500 mW over the wavelength range investigated in these studies. Laser I is tuned to acquire the photoionization spectrum of the c state. Figure 3 shows a typical ionization spectrum of the $H_2\ c\ ^3\Pi_u^-$ state, obtained by monitoring the resulting photoions. As discussed in more detail in a separate paper,[13] these ionization resonances are single-photon transitions from high vibrational levels of the c state to autoionizing resonances lying above the first ionization limit of H_2. For the double-resonance experiments, a narrow-band cw ring laser (laser II) operating between 200 and 500 mW was tuned to a fixed frequency, corresponding to one of the ionization resonances in Fig. 3, in order to label a particular rovibrational level of the c state. While monitoring the ionization signal produced by laser II, the broadband laser (laser I) was frequency scanned over the wavelength range 5400 to 6400 Å.

The two laser beams are chopped at different frequencies, combined with a polarizing beamsplitter, and then steered into the fast-beam chamber. Ion counts are recorded by two counters (henceforth designated counters 1 and 2), each gated with a digital-delay generator to detect ions for the two different excitation conditions necessary for the acquisition of double-resonance spectra; this gating scheme is shown in Fig. 4. Each gating cycle consists of four 4.5 msec intervals, each separated by a dead time of ~1 msec, during which the mechanical chopper is blocking or unblocking the continuous-wave lasers. Counter 1 is gated to record ions which are created while either laser I or II is on separately. Counter 2 records ions which are created from neutral molecules which see both lasers simultaneously, and from neutrals which see neither laser; the latter dark interval records ions created primarily as a result of collisional and field ionization, and is necessary in order to insure

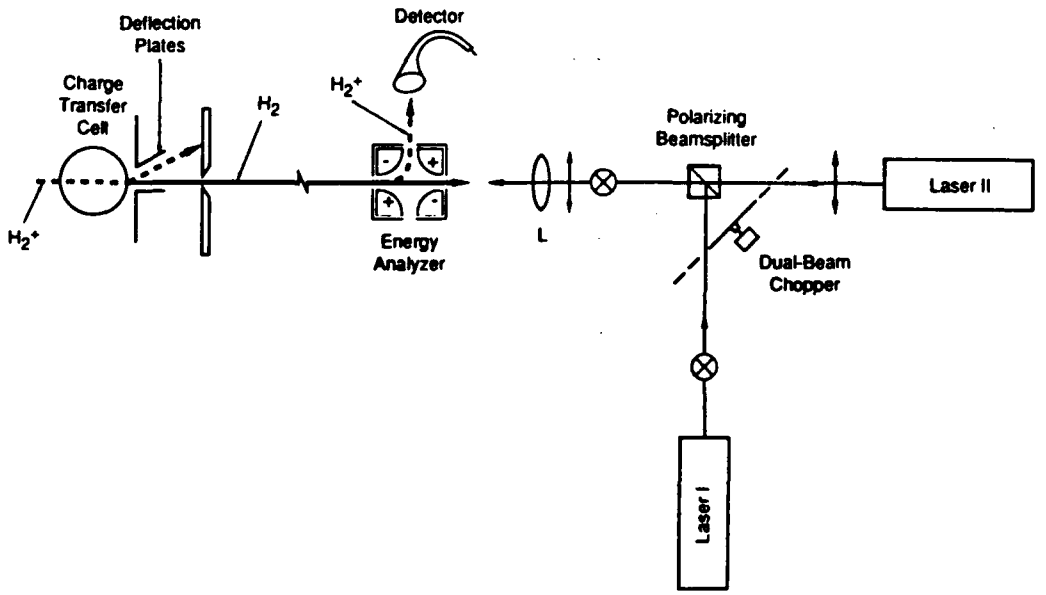

FIG. 2. Experimental arrangement. Depicted here are a portion of the fast-beam apparatus and the optical setup used for double-resonance excitation of the fast H_2 beam.

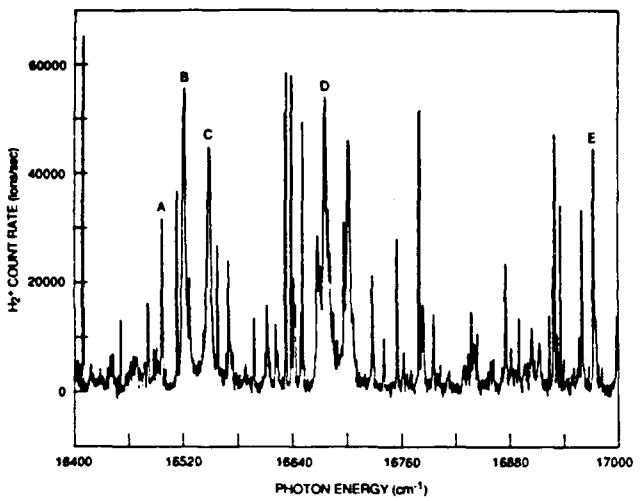

FIG. 3. Typical cw ionization spectrum of H_2 $c\,^3\Pi_u^-$. Gated scalers and mechanical chopping of the laser are employed to achieve background subtraction.

proper background subtraction. As laser I is frequency tuned, the data-acquisition system thus records two spectra (spectra 1 and 2) corresponding to the ion counts accumulated by the two counters for each laser-I wavelength.

Spectrum 1 will consist of the simple addition of the spectra which would be accumulated by either laser alone: a wavelength-dependent ionization spectrum from laser I, such as that shown in Fig. 3, and the constant ionization induced by the fixed-frequency laser II. In the absence of competition by the two lasers for the same molecules, spectrum 2 would be identical with spectrum 1. However, when laser I and laser II are on at the same time (spectrum 2) and both attempt to excite molecules out of the same lower state, the total ionization rate will be less than the corresponding rate recorded in spectrum 1, when the molecular beam is exposed to the two lasers at different times. The difference of spectra 1 and 2 (hereafter the double-resonance or depletion spectrum) should, therefore, display features that indicate any transition (e.g., ionizing or dissociative) whose lower c-state level is the same as that for the ionization resonance to which laser II has been tuned. The experimental double-resonance spectra were found to display three types of depletion resonances competing with ionization from the labeled c-state level. One class are photoionization transitions; these double resonances were used to clarify the assignment of the photoionization spectra.[13] A second class are transitions to states for which both dissociation and ionization channels are open; these transitions will be discussed in a future paper. A third class are transitions to the rapidly predissociated levels of the j state; in what follows, we specifically discuss these results.

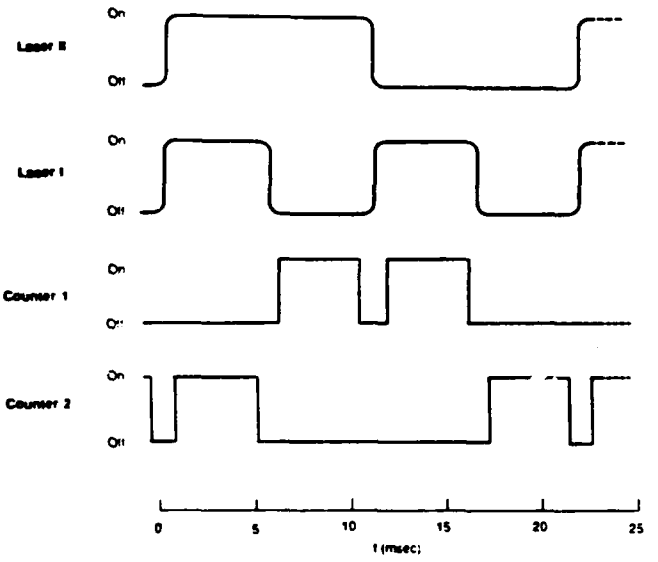

FIG. 4. Duty cycles for the two gated scalers and laser beams. Separate spectra are recorded from the ion counts registered by counters 1 and 2; their difference indicates competition of the two lasers for the same molecules.

III. RESULTS AND DISCUSSION

A. Rovibrational-level assignments

Figures 5(a) and 5(b) show two portions of a typical double-resonance scan. This particular scan was ob-

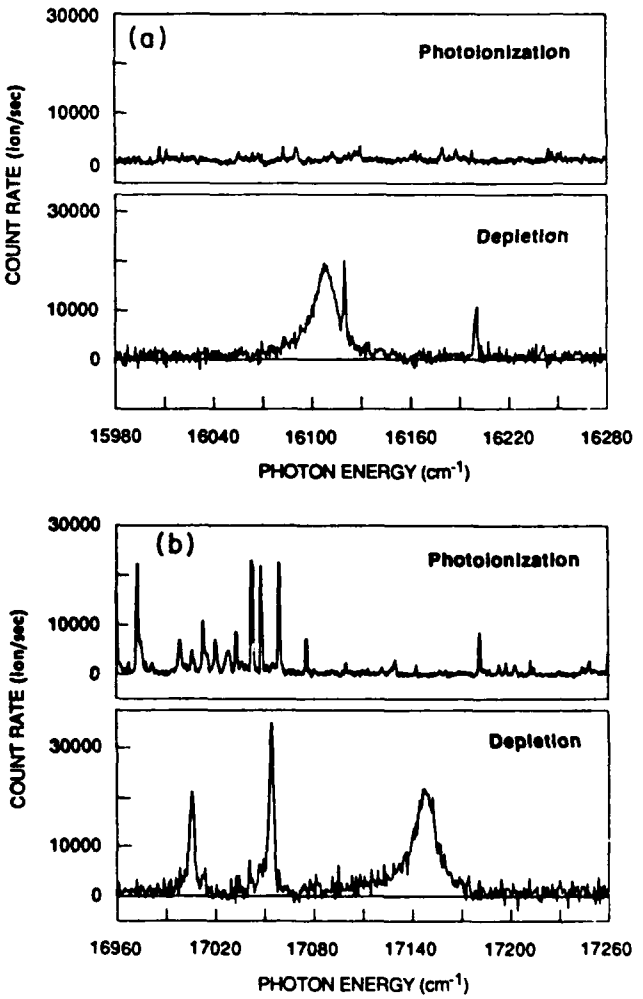

FIG. 5. Associated ionization and double-resonance spectra recorded with laser II tuned to the resonance labeled A in Fig. 3.

tained with laser II tuned to the ionization transition at 16497.4 cm^{-1} (peak *A* in Fig. 3). The ionization spectra, obtained with laser I alone, are shown in the top traces of the figure; the corresponding double-resonance (depletion) spectra, obtained by subtracting spectrum 2 from spectrum 1 are shown in the lower traces. In this experiment, laser II produced typically 6×10^4 H_2^+ ions per second at the labeled photoionization transition; laser I depleted up to 60% of this signal at the strongest double resonance. There are two broad (15 cm^{-1}) and four narrow (~2 cm^{-1}) features indicating depletion of the labeled *c*-state level. The broad features in Fig. 5 resemble other depletion resonances observed with laser II tuned to the ionization resonances labeled *B*, *C*, and *D* (Fig. 3). In no case do these broad resonances have analogous counterparts in the corresponding ionization spectrum.

As will be shown below, these broad resonances represent excitation of the rapidly predissociated $j\,^3\Delta_g$ state, depicted in the potential diagram of Fig. 1. The level diagram in Fig. 6 helps to illustrate the situation; shown here are the observed dissociation transitions from $N''=1$ to $N'=2$. Altogether, nine ionization transitions

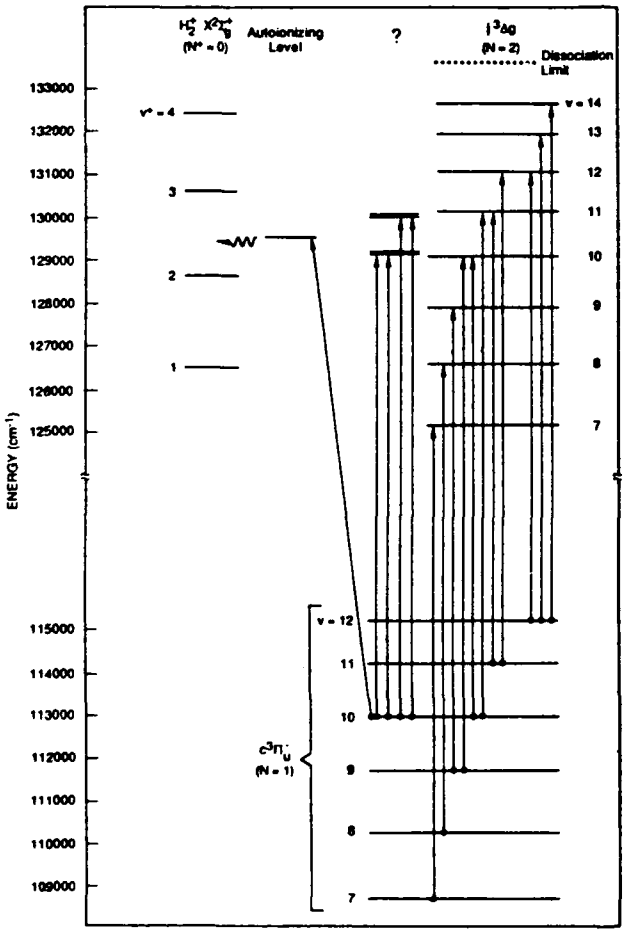

FIG. 6. Energy-level diagram for some of the observed transitions. Dissociation transitions are represented by vertical lines; the inclined line represents the ionization transition corresponding to peak *A* in Fig. 3. Energy scale referenced to $v=0$ level of the (ground) $X\,^1\Sigma_g^+$ state.

were used for the current double-resonance experiments; their transition energies are listed in Table I. The ionization transitions used to generate the double-resonance signals in Fig. 5 is also shown in Fig. 6 in order to indicate the general location of the open ionization channels.

The assignment of the broad dissociation transitions is made possible by accurate Born-Oppenheimer potential curves for the *c* and *j* states. Kolos and Rychlewski[14] have calculated the potential-energy curve and rovibrational energies for the *c* state. Rychlewski[15] has published energies for the *j* state, but as he has kindly pointed out,[16] the potential curve as listed in his Table I is in error at the internuclear separation $R=1.2$ a.u. This error also affects the vibrational energies listed in his Table IV. Using the corrected[16] energy $V(R=1.2)=-0.584\,371\,73$ a.u. and a numerical eigenvalue-search routine,[17] we have calculated a new set of rovibrational energies for the *j* state. The reliability of our numerical method was checked by calculating the rovibrational energies of the *c* state; the resulting values agree with those of Kolos and Rychlewski[14] to within 0.5 cm^{-1}. Table II lists the results of our calculations for the *j* state. Energies are given for the lowest possible rotational levels ($N=2$) of a Δ ($\Lambda=2$) state, assuming an effective potential energy curve given by the expression

$$V_{\text{eff}}=V+\frac{\hbar}{2\mu R^2}[N(N+1)-\Lambda^2]\,. \tag{1}$$

Rotational constants are also given, having been calculated for the hypothetical rotationless ($N=\Lambda=0$) state.

The assignments for the dissociation transitions are based on analyses such as those discussed here in detail for Fig. 5. The difference in the experimental transition energies of the broad resonances in Fig. 5 is 1042±2 cm^{-1}, and must equal the energy spacing of the two rapidly dissociating upper-state levels. This upper-state spacing is consistent with the theoretical spacing of 1041.8 cm^{-1} between the $N'=2$ levels of $v'=10$ and $v'=11$ of the $j\,^3\Delta_g$ state, as predicted by our calculations. The energies of the two broad dissociation transitions in Fig. 5 are within 10 cm^{-1} of the theoretically predicted energy differences between the $v''=10, N''=1$ level of the *c* state[14] and the corresponding aforementioned upper *j*-state levels. If the two broad transitions are assigned to these rotational levels of the *c* and *j* states, they are identified as *R*(1) transitions from an $N''=1$ level to $N'=2$ levels of the *j* state. Since the *j* state is a Δ state, there is only one rotational transition allowed from any $N''=1$ level; the absence of rotational structure in the double-resonance spectra is consistent with this assignment.

The results shown in Fig. 5 are not by themselves definitive proof for the proposed assignment. However, the other transitions listed in Table I and shown graphically in Fig. 6 share common upper as well as lower-state levels and produce similar agreement with theoretical predictions on the two electronic states involved. When considered in this broader context, no doubt remains concerning the assignment of *c*- and *j*-state levels.

Table III summarizes the comparison between theoretical and experimentally inferred energy spacings for rovi-

TABLE I. Observed transition energies and widths, in cm^{-1}. Γ_i denotes the autoionization linewidth, Γ_d denotes the predissociation linewidth.

Lower state $c\,^3\Pi_u^-$		Ionization transition E[a]	Γ_i	Upper state $j\,^3\Delta_g$		Depletion transition E	Γ_d
v''	N''			v'	N'		
7	1	18 172[b]	<1	7	2	16 539±1	29±1
8	1	17 796[b]	<1	8	2	16 392±1	24±1
9	1	16 383.5[b]	<1	9	2	16 249±1	20±1
				10	2	17 403±1	15±1
				10	2	16 109±1	16±1
				11	2	17 149±1	15±1
10	1	16 497.4 (*A*)	<1	?[c]	?[c]	16 120±1	1.7±0.5
				?[c]	?[c]	16 200±1	2.2±0.5
				?[c]	?[c]	17 006±1	3.5±0.5
				?[c]	?[c]	17 054±1	2.9±0.5
11	1	16 674.4 (*D*)	4±1	11	2	15 976±1	15±1
				12	2	16 894±1	15±1
11	3	16 549.6 (*C*)	5±1	12	3	16 813±3	20±4
				12	4	16 910±3	45±5
11	3	16 522.7 (*B*)	4±1	12	3	16 813±3	24±4
?	?	16 972.9 (*E*)	<1	?[c]	?[c]	16 887±1	4±1
				12	2	15 852±1	14±1
12	1	15 658[b]	4±1	13	2	16 642±1	11±1
				14	2	17 295±1	10±1

[a] (*A*)–(*E*) denote those lines labeled in Fig. 3.
[b] Ionization resonance outside the spectra region shown in Fig. 3.
[c] Transitions to $n=4$ manifold.

TABLE II. Dissociation energies of lowest rotational levels ($N=\Lambda=2$) and rotational constants of $j\,^3\Delta_g$ state, calculated using corrected (Ref. 16) Rychlewski potential for H_2 using a reduced mass value of 0.503 626 5. All values in cm^{-1}.

v	D_v	B_v
0	21 184.9	29.4
1	18 975.5	27.8
2	16 892.6	26.4
3	14 932.9	24.9
4	13 091.9	23.5
5	11 367.6	22.2
6	9757.3	20.8
7	8259.8	19.5
8	6874.5	18.2
9	5601.9	16.8
10	4443.2	15.4
11	3401.4	14.0
12	2480.6	12.5
13	1687.2	10.9
14	1030.5	9.17
15	522.9	7.18
16	181.2	4.86

brational levels of the *c* and *j* states. It is seen that comparison with theory is excellent for the *c*-state spacings; the theoretical *j*-state spacings are consistently larger than the experimental ones, although the agreement is within 5 cm^{-1}.

The $j \leftarrow c$ transition energies listed in Table I also constitute a direct measurement of the $j\,^3\Delta_g$ level energies relative to the lower *c*-state levels. These experimental values are listed in Table IV and compared with the theoretical calculations; the experimental *c*-state energies, inferred from the transition-energy differences, are listed for completeness. The zero of energy is taken to be the $v''=9, N''=1$ level of the $c\,^3\Pi_g$ state. The theoretical energies of the *j* state are calculated based on the Born-Oppenheimer difference of 15 241.3 cm^{-1} between the $n=2$ and 3 limits of the $H + H(nl)$ system, i.e., based on the infinite-mass Rydberg. This infinite-mass Rydberg approximation is one contribution to the adiabatic corrections to the Born-Oppenheimer potential curves; it amounts to a correction of $+8$ cm^{-1} in the difference between the *c*- and *j*-state dissociation limits.

The final column of Table IV notes the discrepancy between the theoretical and experimental level energies. The agreement of the experimental *c*-state energies with

TABLE III. Comparison of theoretical and experimentally inferred energy spacings. Δ indicates the difference between theory and experiment.

	States	Energy spacings (cm^{-1}) Theory[a,b]	Experiment
$c\,^3\Pi_u^-$	$(v=9,N=1)$ to $(v=10,N=1)$	1296.6	1294±2
	$(v=10,N=1)$ to $(v=11,N=1)$	1172.0	1173±2
	$(v=11,N=1)$ to $(v=11,N=3)$	153.8	152±2[c]
	$(v=11,N=1)$ to $(v=12,N=1)$	1043.0	1042±2
$j\,^3\Delta_g$	$(v=9,N=2)$ to $(v=10,N=2)$	1158.6	1154±2
	$(v=10,N=2)$ to $(v=11,N=2)$	1041.8	1040±2
	$(v=11,N=2)$ to $(v=12,N=2)$	920.8	918±2
	$(v=12,N=2)$ to $(v=13,N=2)$	793.4	790±2
	$(v=13,N=2)$ to $(v=14,N=2)$	656.8	653±2
	$(v=12,N=2)$ to $(v=12,N=3)$	74.3	72±4
	$(v=12,N=3)$ to $(v=12,N=4)$	97.6	97±4

[a] *c*-state values from Kolos and Rychlewski (Ref. 14).
[b] *j*-state values calculated using corrected potential curve of Rychlewski (Refs. 15 and 16).
[c] Inferred from double-ionization resonance experiments.

theory merely reflects the already noted congruity between the theoretical and experimental rovibrational energy differences recorded in Table III. Similarly, the trend in Δ for the *j*-state levels mirrors the cumulative differences between the theoretical and experimental energy spacings for that state.

While we consider the agreement between theoretical and experimental *j*-state energies to be very good, the discrepancies are nevertheless greater than the experimental uncertainties. The origin of this residual difference is uncertain. The effect of the adiabatic corrections is unknown for the triplet states under consideration, but for the analogous states in the H_2 singlet manifold, adiabatic corrections are known to decrease the *C*-to-*J* state band origin by 93 cm^{-1}.[14,18] Near the *j*-state dissociation limit, one might expect the effect of these adiabatic corrections to be dominated by the aforementioned reduced-mass correction; this would lower the theoretical *j*-state energies in Table IV by 8 cm^{-1}, which actually increases the discrepancy with theory.

The *j*-state levels under consideration here lie in the dissociation continuum of the two remaining 3*d* states, $3d\pi$ ($i\,^3\Pi_g$) and $3d\sigma$ ($g\,^3\Sigma_g^+$); this results in *j*-state level shifts caused by *l* uncoupling. The effect of *l* uncoupling in the 3*d* complex is sketched in Sec. III B; suffice it here to note that our calculations indicate that these shifts are also insufficient to explain the discrepancy between theoretical and experimental *c*-to-*j* state transition energies.

The assignment of the narrow transitions that appear

TABLE IV. Comparison of experimental and theoretical energies. All energies in cm^{-1}.

	State		Theory[a,b]	Experiment	Δ
	v''	N''			
$c\,^3\Pi_u$	9	1	0	c	c
	10	1	1296.59	1294±2	3±2
	11	1	2468.54	2467±3	2±3
	11	3	2619.44	2619±3	0±3
	12	1	3511.53	3509±3	3±3
	v'	N'			
$j\,^3\Delta_g$	9	2	16234.2	16249±1	−14±1
	10	2	17392.8	17403±2	−10±2
	11	2	18434.6	18443±2	−8±2
	11	3	18517.9	18524±4	−6±4
	12	2	19355.5	19361±3	−5±3
	12	3	19429.?	19432±5	−2±5
	12	4	19527.4	19529±5	−1±5
	13	2	20148.8	20151±4	−2±5
	14	2	20805.6	20804±4	2±4

[a] *c*-state values from Kolos and Rychlewski (Ref. 14).
[b] *j*-state values calculated using corrected potential curve of Rychlewski (Refs. 15 and 16).
[c] Experimental values derived assuming this level to agree exactly with theory.

in Fig. 5 and similar spectra is more complex. The upper-state levels accessed in the narrow transitions in Fig. 5 are depicted in the column designated "?" of Fig. 6. We attribute these to $Q(1)$ and $R(1)$ transitions to the $n=4$ $^3\Pi_g$ state. For the vibrational levels involved here, the $n=4$ manifold is strongly perturbed by the lowest doubly excited $^3\Pi_g$ and $^3\Sigma_g$ states, and we have observed both ionization and dissociation for the discrete levels in the $n=4$ states. A detailed discussion of this system will be part of a future publication.

We wish to point out that the assignments for the $c\,^3\Pi_u$-state levels, obtained here from assignment of the predissociated j-state levels, is consistent with the independent assignment of the ionization transitions.[13]

B. The effects of configuration interaction

The appearance of broad dissociation resonances such as those seen in Fig. 5 results from the configuration interaction between bound and continuum states.[19] Specifically, the bound j-state levels and the continuum of the $i\,^3\Pi_g$ state (see Fig. 1) perturb each other via rotational coupling; the pertinent matrix element is given by the $J_{\pm}L_{\mp}$ interaction terms arising from the nuclear kinetic energy Hamiltonian. If the transition moment to the continuum state is negligible, excitation of the predissociated j-state resonances should result in symmetric Lorentzian profiles with a width given by Fermi's golden rule:[20]

$$\Gamma(v,N)=2\pi\,|\,V_E\,|^2\rho(\epsilon)\,, \tag{2}$$

where

$$V_E=[N(N+1)-2]^{1/2}\langle\phi_\Pi\,|\,L_-\,|\,\phi_\Delta\rangle \times\langle\chi_\Pi(N,\epsilon)\,|\,-\hbar^2/2\mu R^2\,|\,\chi_\Delta(N,v)\rangle \tag{3}$$

and $\rho(\epsilon)$ is the i-state continuum density of states:[7]

$$\rho(\epsilon)=\left[\frac{2}{h}\right](2\mu/\epsilon)^{1/2} \tag{4}$$

and the coupling matrix element is taken from Ref. 21. In Eqs. (2)–(4) the χ's are vibrational wave functions and the ϕ's are electronic wave functions; E is the energy of the v,N j-state level, while ϵ denotes the kinetic energy of the dissociation fragments. The continuum wave function $\chi_\Pi(N,\epsilon)$ is normalized to have unity modulus asymptotically.

In addition to causing predissociation of the j-state levels, the rotational interaction induces a shift in the position of the j-state level. This shift is given by Fano[19] as

$$F(E_0)=P\int dE'\,|\,V_{E'}\,|^2/(E_0-E')\,. \tag{5}$$

Where P denotes the principal part for the integral and $V_{E'}$ the rotational interaction matrix element [Eq. (3)] between the unperturbed discrete j-state level of energy E_0 and the continuum i-state eigenfunction of energy E'. For use in Eq. (5), the continuum wave function appearing in the matrix element $|\,V_{E'}\,|$ must be energy-normalized.[19] We have used Eq. (5) to estimate the l-uncoupling shift induced by the i state on the $v'=10$ level of the j state. The result is a 2-cm^{-1} increase in the theoretical energy of this j-state level; this small shift is unable to account for the discrepancy between theory and experiment noted in Table IV and discussed in the previous section.

If the "discrete" j- and the i-state continuum have comparable transition moments from the c state, an asymmetric excitation ("Fano-Beutler") profile will result. Examples of this are common in ionization studies but relatively rare in dissociation studies. The asymmetry arises from an interference of optical transitions to the continuum and bound states, which become inextricably mixed as a result of the configuration interaction. The resonance shape will depend upon the relative strength of the aforementioned transitions, and contains information regarding the relative phases of the wave functions describing the initial c-state level, the unperturbed i-state continuum, and the bound j-state level.

Asymmetric resonances of this type have been observed previously in dissociation.[22,7] In these previous studies, resonances often overlap, due in part to the rovibrational distribution of the lower states involved. The double-resonance technique employed here helps to overcome this difficulty. The asymmetry characteristic of the effects being discussed is evident in Figs. 5 and 7, where we show the profiles of various $R(1)$ transitions. The resonances appear superimposed on a nonzero background value of the double-resonance signal. This indicates transitions to the i-state continuum far from the discrete j-state level, and must be present whenever configuration interaction causes an asymmetric line shape to appear. It should be noted that in addition to the $N'=2$ continuum of the $i\,^3\Pi_g$ state, the $N'=1$ continua of the i state and the $g\,^3\Sigma_g^+$ state, which are free from interaction with the $j\,^3\Delta_g$ state, contribute to this nonzero background.

Quantitatively, the asymmetry in the excitation profile

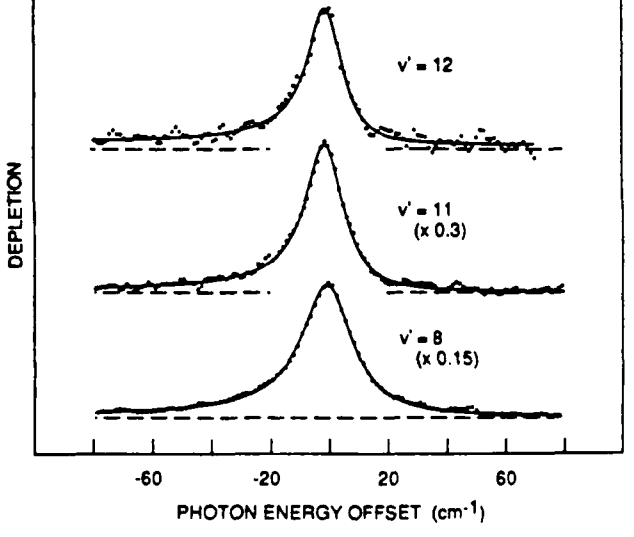

FIG. 7. Photodissociation line profiles for selected $N'=2$ levels of the $j\,^3\Delta_g$ state, $v'=8,11,12$. Experimental data are shown as points. Solid curve represents best fit of Eq. (3). q parameters obtained from best fit are listed in Table V.

$f(\epsilon)$ is characterized by the dimensionless Fano q parameter which characterizes the generalized line-shape function $f(\epsilon)$:

$$f(\epsilon)=\frac{(q+\epsilon)^2}{1+\epsilon^2} . \tag{6}$$

In (6) the reduced energy parameter is

$$\epsilon=\frac{E-E_0'}{\frac{1}{2}\Gamma} , \tag{7}$$

where E_0' is the perturbed resonance energy, $E_0+F(E)$, and Γ is the configuration-interaction-induced linewidth given by Eq. (2). The asymmetry parameter q depends on the relative transition strength to the discrete and continuum states.[19] Perfectly symmetric resonances will occur only in the limits where the optical transition couples the initial state exclusively to the continuum ("window resonances") or exclusively to the perturbed discrete state (symmetric Lorentzian), and are characterized by q values of 0 to ∞, respectively. For the system under consideration here, transition moments tend to favor excitation of the discrete state, resulting in profiles that are only weakly asymmetric.

The experimental dissociation profiles shown in Fig. 7 were fit to a line shape describing the superposition of a Fano profile onto a constant background:

$$AF(\epsilon)+B , \tag{8}$$

where the constant B represents excitation to continuum states that are not coupled to the j state. These fits are included in Fig. 7 as full lines. The best-fit q values for the Fano-profile terms are listed in Table V. The line shape represented by Eq. (8) falls to a minimum when the Fano profile equals zero; this occurs at a photon-energy offset of $\frac{1}{2}\Gamma q$ cm^{-1}. For all profiles shown, this minimum occurs at photon energies greater than those included in the figure. Since the ratio of peak height to background for a Fano profile is approximately equal to q^2, the minima would be difficult to discern visually given the q values listed in Table V. In addition, the noise levels in this experiment would not permit an accurate measurement of the continuum strength. In cases such as these, the asymmetry parameter q therefore serves as a useful alternative measure for the strength of excitation of the continuum.

The final column of Table I lists the Γ parameters resulting from a best fit to Eq. (8) for each of our experimental profiles. The uncertainty limits are statistical limits. For a given vibrational level, Eq. (3) shows that the predissociation widths are expected to increase with the rotational quantum number N in close proportion to $N(N+1)$. Table I shows that the j-state resonances for $v'=12$ have measured widths which display this predicted trend for the rotational levels $N'=2$, 3, and 4.

We also see from Table I that the observed widths of the $N'=2$ levels decrease with increasing values of v. This dependence arises essentially from the fact that the $\langle\,|R^{-2}|\,\rangle$ matrix element appearing in Eq. (3) decreases monotonically with increasing v. With the i-state potential of Kolos and Rychlewski[14] and the corrected Rychlewski j-state potential, we have generated the appropriate vibrational wave functions and used Eqs. (2)–(4) to calculate the expected theoretical $i\leftarrow j$ predissociation widths. These results are listed in Table VI along with the experimental widths from Table I from all observed $N'=2$ levels of the j state. The theoretical results reproduce the trend in Γ with v rather well, and the magnitudes of the theoretical widths are within 30% of the experimental ones.

TABLE V. Best-fit Fano q parameters for resonances displayed in Fig. 7.

Lower level $c\,^3\Pi_u^-$	Upper level $j\,^3\Delta_g$	q
$v=8, N=1$	$v=8, N=2$	-16 ± 3
$v=10, N=1$	$v=11, N=2$	-13 ± 2
$v=12, N=1$	$v=12, N=2$	-11 ± 3

TABLE VI. Theoretical and experimental j-state dissociation widths for all observed $N'=2$ levels. R represents the ratio $\Gamma_{\text{theory}}/\Gamma_{\text{expt}}$.

v	Γ_{theory}	Γ_{expt}	R
7	18	29±1	0.6
8	16	24±1	0.7
9	14	20±1	0.7
10	13	15±1	0.8
11	11	15±1	0.7
12	10	14±1	0.7
13	8	11±1	0.7
14	7	10±1	0.7

IV. CONCLUSIONS

We have studied dissociative levels of the $j\,^3\Delta_g$ state of molecular hydrogen through the use of an optical-optical double-resonance technique. Using one laser to label rovibrational levels in the metastable $c\,^3\Pi_u^-$ state by exciting a photoionization transition, we have observed transitions to the dissociative j-state levels via their depletion of the labeled c-state level. We have identified transitions from high-v levels of the c state, previously observed at lower resolution in photofragmentation studies, to high-v levels of the j state heretofore unobserved. Rovibrational energy spacings within either electronic state are in good agreement with the calculations of Kolos and Rychlewski[14] for the $c\,^3\Pi_u$ state, and our calculations for the $j\,^3\Delta$ state using the corrected form of Rychlewski's potential. The $j\leftarrow c$ transition energies are all within 20 cm^{-1} of the theoretical ones.

The dissociation resonances observed in this experiment reveal weakly asymmetric Beutler-Fano profiles, characteristic of the coupling between and simultaneous

excitation to the bound levels of the $j\,^3\Delta_g$ state and the continuum of the $i\,^3\Pi_g$ state. The observed widths of these resonances are within 30% of those predicted by theory. Studies identical to those described herein have been initiated in the isotopic species HD; these results should serve to complement and further elucidate those reported here for H_2.

ACKNOWLEDGMENTS

This research was supported by the National Science Foundation under Grant No. NSF PHY-8706332, the U. S. Air Force Office of Scientific Research under Contract No. F49620-87-K-0002, as well as a NATO travel grant.

[1]W. Lichten, T. Wik, and T. A. Miller, J. Chem. Phys. **71**, 2441 (1979).

[2]E. E. Eyler and F. M. Pipkin, Phys. Rev. Lett. **47**, 1270 (1981).

[3]E. E. Eyler and F. M. Pipkin, Phys. Rev. A **27**, 2462 (1983).

[4]H. Helm, D. P. de Bruijn, and J. Los, Phys. Rev. Lett. **53**, 1642 (1984).

[5]R. D. Knight and L. Wang, Phys. Rev. Lett. **55**, 1572 (1985).

[6]R. Kachru and H. Helm, Phys. Rev. Lett. **55**, 1575 (1985).

[7]D. P. de Bruijn and H. Helm, Phys. Rev. A **34**, 3855 (1986).

[8]N. Bjerre and H. Helm, Chem. Phys. Lett. **134**, 361 (1987).

[9]E. E. Eyler, R. C. Short, and F. M. Pipkin, Phys. Rev. A **56**, 2602 (1987).

[10]W. Lichten, Phys. Rev. **120**, 848 (1960).

[11]H. Helm and P. C. Cosby, J. Chem. Phys. **86**, 6813 (1987).

[12]H. Helm, in *Invited Papers of the Fourteenth International Conference on the Physics of Electronic and Atomic Collisions, Palo Alto, 1985*, edited by D. C. Lorents, W. E. Meyerhof, and J. R. Peterson (North-Holland, Amsterdam, 1986).

[13]N. Bjerre, S. Keiding, L. Lembo, and H. Helm, Phys. Rev. Lett. **60**, 2465 (1988).

[14]W. Kolos and J. Rychlewski, J. Mol. Spectrosc. **66**, 428 (1977).

[15]J. Rychlewski, J. Mol. Spectrosc. **104**, 253 (1984).

[16]J. Rychlewski (private communication).

[17]J. LeRoy, University of Waterloo, Chemical Physical Research Report No. CP-110, 1979 (unpublished).

[18]P. Quadrelli and K. Dressler, J. Mol. Spectrosc. **86**, 316 (1981).

[19]U. Fano, Phys. Rev. **124**, 1866 (1961).

[20]L. Schiff, *Quantum Mechanics* (McGraw-Hill, New York, 1968).

[21]M. Mizushima, *The Theory of Rotating Diatomic Molecules* (Wiley, New York, 1975), p. 143.

[22]M. Glass-Moujean, J. Breton, and P. M. Guyon, Chem. Phys. Lett. **63**, 591 (1979).